Friction, Wear and Noise of Short-cut Aramid Fibre Reinforced Elastomers in Sliding Contacts

Muhammad Khafidh

Friction, Wear and Noise of Short-cut Aramid Fibre Reinforced Elastomers in Sliding Contacts

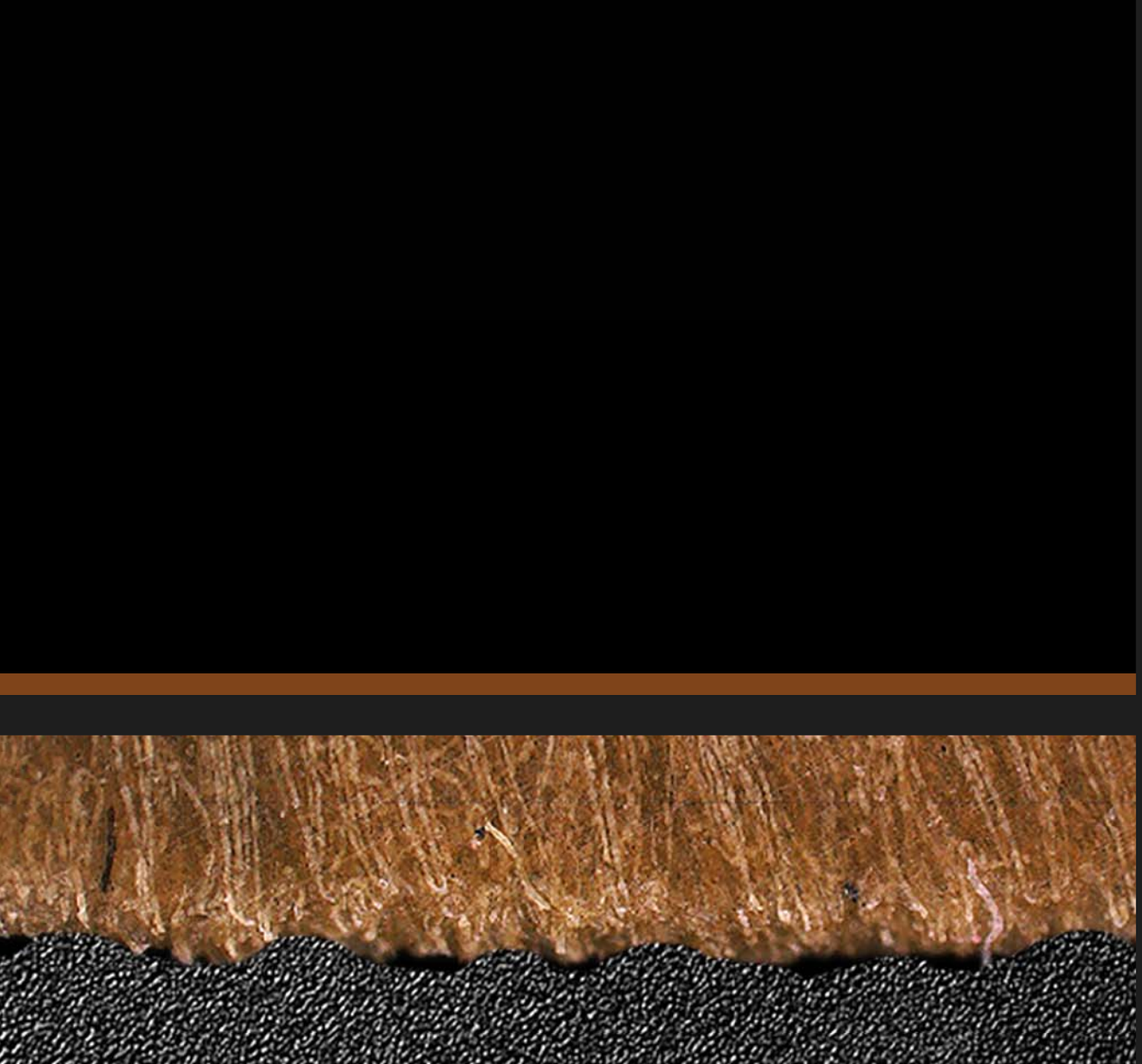

Muhammad Khafidh

Friction, Wear and Noise of Short-cut Aramid Fibre Reinforced Elastomers in Sliding Contacts

Muhammad Khafidh

De promotiecommissie is als volgt samengesteld:

Voorzitter en secretaris:
Prof.dr. G.P.M.R. Dewulf — Universiteit Twente

Promotor:
Prof.dr.ir. D.J. Schipper — Universiteit Twente

Assistent Promotoren:
Dr.ir. M.A. Masen — Imperial College London
Dr.ir. J. Jamari — University of Diponegoro

Leden
Prof.dr.ir. J.W.M. Noordermeer — Universiteit Twente
Prof.dr.ir. A. de Boer — Universiteit Twente
Prof.dr.ir. L.E. Govaert — Technische Universiteit Eindhoven
Prof.dr.ir. R.P.B.J. Dollevoet — Technische Universiteit Delft
Dr. P.J. de Lange — Teijin Aramid B.V.

Muhammad Khafidh
Friction, wear and noise of short-cut aramid fibre reinforced elastomers in sliding contacts

Ph.D. Thesis, University of Twente, Enschede, The Netherlands, January 2019
ISBN: 978-90-365-4682-9
DOI: 10.3990/1.9789036546829
Cover design: Aditya Jati Istanto, images are created by welcomia/Freepik
Printed by Gildeprint, Enschede, The Netherlands

FRICTION, WEAR AND NOISE OF SHORT-CUT ARAMID FIBRE REINFORCED ELASTOMERS IN SLIDING CONTACTS

PROEFSCHRIFT

ter verkrijging van
de graad van doctor aan de Universiteit Twente,
op gezag van de rector magnificus,
prof.dr. T.T.M. Palstra,
volgens besluit van het College voor Promoties
in het openbaar te verdedigen
op donderdag 24 Januari 2019 om 12.45 uur

door

Muhammad Khafidh

geboren op 27 Juni 1990
te Kab. Semarang, Indonesia

Dit proefschrift is goedgekeurd door:

Promotor	: Prof.dr.ir. D.J. Schipper
Assistent promotoren	: Dr.ir. M.A. Masen
	Dr.ir. J. Jamari

The studies described in this thesis are part of the Research Programme of the Dutch Polymer Institute, P.O. Box 902, 5600 AX Eindhoven, The Netherlands, project nr. #782.

꧋ꦩꦤꦼꦧ꧀ꦢꦮꦩꦫ꧈ꦲꦶꦏꦸ꧈

ꦱꦼꦤꦮꦤꦩꦏꦸꦥꦂꦏ꧉

Acknowledgements

I would like to start my acknowledgments by saying '*Alhamdulillah*'. I would have been able to complete this thesis without the support and contribution of many people. I would like to thank all those who supported and encouraged me to finish my PhD journey.

First of all, I am grateful to my promoter, Prof.dr.ir. D.J. Schipper. Dik, thank you for your guidance and patience during my study. I would not have completed this thesis without your help and assistance. Moreover, I would like to thank dr. M. Masen for the useful discussion and his support during experiments in Imperial College London. I also would like to thank dr. Jamari for introducing me to the Surface Technology and Tribology group at the University of Twente.

I would like to acknowledge the graduation committee members: G.P.M.R. Dewulf, D.J. Schipper, M.A. Masen, J. Jamari, J.W.M. Noordermeer, A. de Boer, L.E. Govaert, R.P.B.J. Dollevoet and P.J. de Lange for reading my final thesis draft and giving me their comments and valuable advice to improve the quality of my thesis.

This thesis was carried out under the project of FINE-FIT (Fibre in Elastomer for Improved Tribology). I would like to express my gratitude to DPI (Dutch Polymer Institute) for the financial support of this project. I would also like to thank Prof.dr.ir. J.M.W. Noordermeer and dr. N. Vleugels for our excellent discussions and collaboration. Nadia, thanks for your help in making the composites and all of our discussions about elastomer. The project partners, Denka from DPI, Peter from Teijin Aramid, Richard from SKF, Auke and Waldo from AkzoNobel are gratefully acknowledged too.

I am indebted to Walter, Erik, Ivo and Dries for their help and assistance during my experimental work. I am thankful to Belinda, Shivam, Yibo, Ida, Hilwa, Melkamu, Mattijs, Michel, Mohammad, Yuxin, Gangqian, Yinglei, Emile, Lydia, Tanmaya, Can, Xavi, Dariush, Milad, Mattijn, Rob, Faizan, Liangyong, Pak Budi, Pak Rifky, Pak Taufiq, Pak Muchammad, Mas Eko and all of my colleagues at Tribology group, University of Twente. Thanks for your help during my study. I give thanks also to my colleagues at Universitas Islam Indonesia, Pak Risdy, Pak Ridlwan, Pak Pur, Pak Adji, Pak Paryana, Pak Faizun, Bu Yus, Mbak Indah, Mas Adi and Mas Faris.

My sincere thanks also go to all members of IMEA, PPIE and all of my Indonesian friends in the Netherlands. I am happy to have made new friends and family away from my homeland. They have truly provided me a second home.

Special thanks go to Bapak and Ibu. Their support, love and unconditional prayers always strengthen me in all conditions. I dedicate this thesis to them. And to my family in Indonesia, Mbak Nunik, Mbak Endah, Mas Nur, Mas San, Dek Moni, Ayah and Ibu Semarang, thanks for your endless support.

Last, but certainly not least, I would like to thank my wife and my little "diamond", Dek Siti and Hira. Both of you are the special gift from God during my PhD journey. Thanks for always being at my side and the happiness you bring to my life. Your love, sacrifice, and patience are precious to me. Hopefully, both of you had lovely memories and experiences during our stay in the Netherlands.

Summary

Many types of elastomer based products are found in daily life, such as tyres, v-belts and wiper blades. In applications, several reinforcing materials are usually added into the elastomers to increase their mechanical and tribological properties. The examples of these reinforcing materials are carbon black, silica and fibres. Short-cut aramid fibre is a relatively new high-performance material that can be used to reinforce elastomers. However, the interaction between fibre and elastomer matrix is still a problem to be solved. Moreover, friction, wear and friction-induced noise of short-cut aramid fibre reinforced elastomers is not well known. Understanding friction, wear and friction-induced noise will lead to a better design, so that the lifetime of the elastomers can be prolonged.

This research is conducted within the project FINE-FIT (Fibres IN Elastomer For Improved Tribology), which is a collaboration between the Surface Technology and Tribology (STT) group and the Elastomer Technology and Engineering (ETE) group at the University of Twente. An optimized formulation of composites to improve the interaction between the fibres and elastomer matrix was investigated by the ETE group, while the investigation of the tribological behaviour of short-cut aramid fibre reinforced elastomers was conducted by the STT group. The short-cut aramid fibre reinforced elastomers used in this thesis are based on the optimized formulation of the ETE group.

Tribological phenomena of elastomers during sliding friction were studied, such as the contact area, the formation of a modified surface layer and the occurrence of a wavy wear track. The size and shape of the contact area of elastomers during sliding change in comparison with the static condition. The contact area depends on the sliding velocity and the mechanical properties of the elastomers, such as storage modulus.

During sliding contact, the composition and the mechanical properties of the elastomer surface may change. These surface alterations will lead to a change of the tribological behaviour of elastomers. The existence of a modified surface layer is influenced by the competition between formation and wear, which depends on the contact pressure, sliding velocity and sliding distance. Another phenomenon during sliding friction is a macro surface irregularity at the wear track, called a wavy wear track. In application, the wavy wear track needs to be avoided because it will reduce the performance of the sliding system and generate vibrations and noise. The occurrence of the wavy wear track depends on the mechanical properties of the elastomer, the operating conditions (such as sliding velocity and force), the inertia mass of the counter surface frame and the circumferential length of the wear track.

Friction, wear and friction-induced noise of short-cut aramid fibre reinforced elastomers were investigated by using two types of short-cut aramid

fibres, namely non-coated fibre (NF) and epoxy-coated fibre (EF). The wear mechanism during sliding contact greatly influences the frictional behaviour of the composites. For a long sliding distance, the presence of fibres on the wear track reduces the coefficient of friction and friction-induced noise drastically. The presence of fibres on the wear track causes the composites to follow Amontons' law when the applied contact pressures are below a certain threshold value. Once the contact pressure is higher than the threshold value, Amontons' law is no longer valid. The threshold contact pressure of composites containing EF is higher than those containing NF. Furthermore, the effect of fibre direction and fibre amount in the composites on friction and wear were studied. Elastomers reinforced with silica and short-cut aramid fibres were also studied to investigate the effect of short-cut aramid fibres. The coefficient of friction and wear of elastomers containing EF is lower than those containing NF.

During sliding contact, noise generation due to sliding friction between the composites and counter surface was investigated. Adding short-cut aramid fibres into the elastomers reduces the friction-induced noise in comparison with the unreinforced elastomers. The friction-induced noise was found to increase with increasing sliding velocity and contact pressure. Moreover, the friction-induced noise of the composites containing EF is lower than those containing NF. The presence of fibres on the wear track reduces the friction-induced noise. The increase of noise is caused by vibrations of the pin holder and motor noise. The noise can be reduced by two ways: (1) reduce the amplitude of friction force and (2) reduce the level of friction force.

Samenvatting

Veel producten op basis van elastomeren (rubber) zijn te vinden in het dagelijks leven, zoals banden, v-riemen en ruiten wisserbladen. Bij toepassingen worden gewoonlijk stoffen aan de elastomeren toegevoegd om hun mechanische en tribologische eigenschappen te verbeteren. Voorbeelden van deze toewegingen zijn carbon black, silica en vezels. Korte aramidevezels worden recentelijk gebruikt om elastomeren te versterken. De interactie tussen de vezels en de elastomeermatrix is echter nog steeds een onderwerp van onderzoek. Bovendien zijn het wrijvings en slijtage gedrag alsmede wrijving-geïnduceerd geluid van korte aramidevezel-versterkte elastomeren niet goed bekend. Het begrijpen van de wrijving, slijtage en wrijving-geïnduceerd geluid zal leiden tot een beter ontwerp, zodat o.a. de levensduur van de elastomeren kan worden verlengd.

Dit onderzoek wordt uitgevoerd binnen het project FINE-FIT (Fiber IN Elastomer for Improved Tribology), een samenwerking tussen de Surface Technology and Tribology (STT) -groep en de Elastomer Technology and Engineering (ETE) -groep aan de Universiteit Twente. Een geoptimaliseerde formulering van composieten om de interactie tussen de vezels en de elastomeermatrix te verbeteren, werd onderzocht door de ETE-groep, terwijl het onderzoek naar het tribologisch gedrag van korte aramide vezels versterkt rubber werd uitgevoerd door de STT-groep. De korte aramide vezels versterkte elastomeren die zijn gebruikt in dit proefschrift zijn gebaseerd op de geoptimaliseerde formulering van de ETE-groep.

Tribologische fenomenen van elastomeren tijdens glijdende wrijving werden bestudeerd, zoals het contactgebied, de vorming van een gemodificeerde oppervlaktelaag en het optreden van een golfvormige slijtspoor. De afmeting en vorm van het contactgebied van elastomeren tijdens het glijden veranderen in vergelijking met de statische contact situatie. Het contactoppervlak is afhankelijk van de glijsnelheid en de mechanische eigenschappen van de elastomeren, zoals de dynamische opslagmodulus.

Tijdens glijdend contact kunnen de samenstelling en de mechanische eigenschappen van het elastomeeroppervlak veranderen. Deze oppervlakte veranderingen zullen leiden tot een verandering van het tribologische gedrag van elastomeren. Het bestaan van een gemodificeerde oppervlaktelaag wordt beïnvloed door de competitie tussen formatie en slijtage van dezelaag, die afhangt van de contactdruk, glijsnelheid en glijafstand. Een ander verschijnsel tijdens glijdende wrijving is de onregelmatigheid in het macro-oppervlak van het slijtspoor, dat een golfvormige slijtspoor wordt genoemd. Bij het toepassen van elastomeren in producten moet het golfvormige slijtspoor vermeden worden omdat dit de prestatie van het glijdendsysteem zal verminderen en trillingen en geluid opwekken. Het optreden van een golfvormig slijtspoor hangt af van de mechanische eigenschappen van het elastomeer, de operationele condites (zoals glijsnelheid en kracht), de massa

traagheid van het frame van het tegenoppervlak en de omtrekslengte van de slijtspoor.

Wrijving, slijtage en wrijving-geïnduceerd geluid van korte aramidevezel versterkte elastomeren werden onderzocht met behulp van twee soorten korte aramide vezels, namelijk niet-gecoate vezels (NF) en epoxy-gecoate vezels (EF). Het slijtagemechanisme tijdens glijdend contact beïnvloedt in grote mate het wrijvingsgedrag van de composieten. Voor een lange glijafstand vermindert de aanwezigheid van de aramide vezels in het slijtspoor de wrijvingscoëfficiënt en het wrijvingsgeïnduceerde geluid drastisch. De aanwezigheid van vezels in het slijtagespoor zorgt ervoor dat de composieten de wrijvinss wet van Amontons volgen wanneer de toegepaste contactdrukken onder een bepaalde drempelwaarde liggen. Zodra de contactdruk hoger is dan de drempelwaarde, is de wet van Amontons niet meer geldig. De drempelcontactdruk van composieten die EF bevatten, is hoger dan die met NF. Verder werd het effect van vezelrichting en vezelhoeveelheid in de composieten op wrijving en slijtage bestudeerd. Elastomeren versterkt met silica en kort gesneden aramidevezels werden ook bestudeerd om het effect van korte aramide vezels te onderzoeken. De wrijvingscoëfficiënt en slijtage van elastomeren die EF bevatten, is lager dan die met NF.

Tijdens het glijdend contact werd de geluidsontwikkeling als gevolg van glijdende wrijving tussen de composieten en een stalen tegenoppervlak onderzocht. Het toevoegen van kort gesneden aramidevezels in de elastomeren vermindert de door wrijving geïnduceerde geluid significant in vergelijking met de niet-versterkte elastomeren. Het wrijvingsgeïnduceerd geluid neemt toe met toenemende glijsnelheid en contactdruk. Bovendien is het door wrijving geïnduceerd geluid van de composieten die EF bevatten lager dan die welke NF bevatten. De aanwezigheid van vezels in het slijtagespoor vermindert het wrijvingsgeïnduceerd geluid. De toename van het geluid wordt veroorzaakt door trillingen van de pinhouder en motorgeluid. Het geluid kan op twee manieren worden gereduceerd: (1) verminder de amplitude van de wrijvingskracht en (2) verminder het niveau van wrijvingskracht.

Nomenclature

Roman symbols

a_x	Radius of contact area in x-direction	[m]
a_y	Radius of contact area in y-direction	[m]
A	Contact area	[m²]
A_{static}	Contact area in the static case	[m²]
$A_{dynamic}$	Contact area during sliding	[m²]
D	Diameter of the contact area	[m]
E^*	Effective elastic modulus	[Pa]
E'	Storage modulus	[Pa]
E''	Loss modulus	[Pa]
f_n	Frequency of indenter system in normal direction	[s^{-1}]
F_{def}	Friction force due to deformation	[N]
F_N	Normal force	[N]
G	Shear modulus	[Pa]
I_1, I_2	Numerical contour integrals	[Pa^{-1}]
k_n	Normal stiffness of the elastomer	[N/m]
m_w	Dead weight mass	[kg]
m_f	Inertia mass of the indenter frame	[kg]
P	Mean contact pressure	[Pa]
p_0	Measured sound pressure	[Pa]
p_1	Reference sound pressure	[Pa]
r	Distance between the contacting area and the centre of elastomer	[m]
R	Radius of the counter surface	[m]
t	Time	[s]
SPL_{fric}	Sound pressure level due to friction	[dB]
SPL_l	Sound pressure level under loading condition	[dB]
SPL_u	Sound pressure level under unloading condition	[dB]
T	Temperature	[K]
v	Velocity	[m/s]
n	Number of the wavy wear pattern	[-]
Δx_n	Wavy wear pattern length	[m]

Greek symbols

μ	Coefficient of friction	[-]
ε	Tensile stess	[Pa]

ω	Frequency	[Hz]
σ	Tensile strain	[%]
$\bar{\phi}$	Normalized creep compliance	[-]
τ_i	Relaxation time	[s]
τ	Frictional shear stress	[Pa]
ξ_f	Damping factor of the indenter frame	[-]
δ	Indentation depth	[m]
υ	Poisson's ratio	[-]
λ_i	Retardation time of the creep compliance coefficient	[s]

Abbreviations

BR	Butadiene rubber
CBS	N-cyclohexyl2-benzothiazole sulfenamide
DMA	Dynamic mechanical analyser
DPG	Diphenyl guanidine
EF	Epoxy coated short-cut aramid fibre
EPDM	Ethylene propylene diene rubber
NF	Non-coated fibre short-cut aramid fibre
NXT	S-(3-(triethoxysilyl)propyl)-octanethioate
phr	Parts per hundred rubber
SBR	Styrene-butadiene rubber
SEM	Scanning electron microscope
SPL	Sound pressure level
TESPT	*Bis*-(triethoxysilylpropyl)-tetrasulfide

Contents

PART II

Paper A : **M. Khafidh**, M.A. Masen, D.J. Schipper. The formation of a modified surface layer on elastomeric materials. Submitted to Tribology Letters.

Paper B : **M. Khafidh**, B. Setiyana, M.A. Masen, J. Jamari, D.J. Schipper. Understanding the occurrence of the wavy wear track on elastomeric materials. Wear, 2018, 412-413, 23-29.

Paper C : **M. Khafidh**, M.A. Masen, D.J. Schipper, N. Vleugels, J.W.M. Noordermeer. Friction and wear mechanism of short-cut aramid fiber reinforced elastomers. Submitted to Wear.

Paper D : **M. Khafidh**, M.A. Masen, D.J. Schipper, N. Vleugels, J.W.M. Noordermeer. The validity of Amontons' law of fiber reinforced elastomers: the effect of epoxy coated fibers. Submitted to Friction.

Publications (not included in the thesis):

Paper E : **M. Khafidh**, N.V. Rodiguez, M.A. Masen, D.J. Schipper. The dynamic contact area of elastomers at different velocities. Tribology-Materials, Surfaces & Interfaces, 2016, 10, 70-73.

Paper F : **M. Khafidh**, M.A. Masen, D.J. Schipper, N. Vleugels, J.W.M. Noordermeer. Tribological behavior of short-cut aramid fiber reinforced SBR elastomers: the effect of fiber orientation. Journal of Mechanical Engineering and Sciences, 2018, 12, 3700-3711.

Paper G : N.V. Rodiguez, **M. Khafidh**, M.A. Masen, D.J. Schipper. Adhesive friction in tribo-systems with elastomeric materials. To be submitted to Tribology International.

Conference contributions:

1. N.V. Rodiguez, **M. Khafidh**, M.A. Masen, D.J. Schipper. The contact area of elastomers as a function of the sliding velocity. Presented at Malaysian International Tribology Conference (MITC), November 16-17, 2015, Penang, Malaysia.
2. **M. Khafidh**, M.A. Masen, D.J. Schipper, N. Vleugels, J.W.M. Noordermeer. Tribological behaviour of short aramid fiber reinforced S-SBR elastomers: the effect of fibre orientation. Presented at International Conference on Mechanical and Manufacturing Engineering (ICME), August 1-3, 2016, Yogyakarta, Indonesia.
3. **M. Khafidh**, M.A. Masen, D.J. Schipper, N. Vleugels, J.W.M. Noordermeer. Friction of short-cut aramid fiber reinforced elastomer. Presented at 6th World Tribology Congress (WTC), September 17-22, 2017, Beijing, China.
4. **M. Khafidh**, M.A. Masen, D.J. Schipper, N. Vleugels, J.W.M. Noordermeer. Friction and wear mechanism of short-cut aramid fiber reinforced elastomer. Presented at TurkeyTrib'18 International Conference on Tribology, April 18-20, 2018, Istanbul, Turkey.

PART I

Chapter 1 Introduction

Elastomers are polymers which have intermediate behaviour between the response of a viscous liquid and an elastic solid at room temperature. Generally, they have very weak inter-molecular forces, resulting in a low Young's modulus in comparison with other materials. Elastomeric materials are widely used in daily applications, such as tyres, wiper blades, hoses and v-belts. However, a single elastomer usually cannot fulfil all the required properties that are needed in such applications. There are various methods to improve the mechanical properties of the elastomers; one of the methods is adding reinforcing materials (such as carbon black, silica and fibres) into the elastomers. In addition to the mechanical properties, tribological behaviour (such as friction and wear) of the elastomers is an important aspect due to their influence on the performance and lifetime of the elastomers. Therefore, a better understanding of the tribological behaviour of elastomers will lead to sustainable materials because of a prolonged lifetime. This study discusses the friction, wear and friction-induced noise of elastomers reinforced by short-cut aramid fibres during sliding contact. The study is based on two different types of systems. The first system is elastomers reinforced by solely short-cut aramid fibres. The second system is composed of elastomers reinforced by short-cut aramid fibres and silica. Moreover, an epoxy coated short-cut aramid fibre (EF) is used to investigate the effect of an epoxy coating to the adhesion between the fibre and the elastomer matrix in comparison with that for an uncoated short-cut aramid fibre (NF). Furthermore, the effect of epoxy coating on friction, wear and friction induced noise is investigated.

1.1 Viscoelastic properties of elastomers

The mechanical properties of elastomers vary, depending on their temperature. At low temperatures, elastomers become hard and behave more like an elastic material. This condition is usually called glassy region. At high temperature, elastomers become softer and behave in a viscous manner, and they will lose their mechanical properties. This condition is called flow region. At temperatures between the glassy and flow region,

elastomers have an intermediate behaviour between elastic and viscous materials, called viscoelastic behaviour. This region is usually called elastomeric region. The transition temperatures between the glassy, elastomeric and flow regions are different for every type of elastomer.

When a stress is applied to an elastic material, it deforms and goes back entirely to the initial position when the stress is released. For a viscous material, it will strain linearly with time when a stress is applied. Due to the viscoelastic properties, elastomers have instantaneous elastic response and linearly time-dependent viscous response when a stress is applied. Further, elastomers have different properties at different loading frequencies. The mechanical properties are relatively low at low frequencies and increase with increasing frequency. The mechanical properties of elastomers become high at very high frequencies. These mechanical properties of elastomers are frequency-dependent because of their viscous behaviour. The other time-dependent phenomena of the elastomeric materials are as follows:

a. Hysteresis
   As mentioned before, a viscoelastic material will not completely go back to its original position when the applied stress is released. Hysteresis is defined as the dissipated energy under loading and unloading stress applied to an elastomer, see Figure 1.1(a).
b. Stress relaxation
   Under a constant applied strain, the stress of the elastomer reaches a maximum and it will diminish with time, see Figure 1.1(b). This phenomenon is called stress relaxation.
c. Creep
   The strain of elastomeric materials increases with time when a constant stress is applied, see Figure 1.1(c). The ratio between the strain varies with time and the constant stress is called creep compliance.

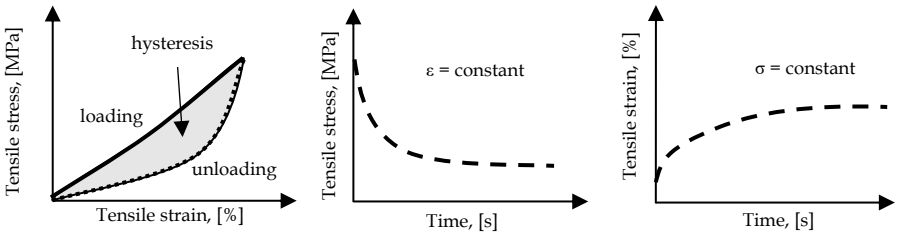

Figure 1.1: Time-dependent phenomena of elastomeric materials: (a) Hysterisis; (b) stress relaxation; and (c) creep.

1.2 Fibre reinforced elastomers

A composite material is defined as a combination of two or more constituent materials. The materials act together to fulfil the required characteristics in the applications. A fibre reinforced elastomer is an example of a composite. Fibres are used because they can improve the mechanical properties of the elastomers. Several types of fibres have been used to reinforce elastomers, such as natural fibres (sisal [1], cellulose [2], and silk [3]) and synthetic fibres (nylon [4], glass [5], and aramid[6]).

Based on the length, fibres can be divided into long (continuous) fibres and short-cut fibres. The advantages of long and continuous fibres that they are easy to orient and process, whereas the short-cut fibres are more difficult to orient. However, the short-cut fibres are easy to work with and offer an increase in stiffness and strength of the composite [7]. In the present study, short-cut aramid fibres are used. The term "short-cut" means that the length of the fibre is a few millimetres. Aramid is the generic term for aromatic poly(amide) fibres. Since these fibres have flexible characteristics and a high modulus, they are often added to the composite structures to improve the mechanical properties.

The improvement of the mechanical properties of short-cut aramid fibre reinforced elastomers depends on several factors: 1) fibre volume fraction, 2) fibre length and distribution, 3) fibre orientation, 4) the properties of the elastomer and fibre, and 5) the fibre-elastomer interface strength [8]. In a previous research, Vleugels [9] investigated the optimum formulation of the short-cut aramid fibre reinforced elastomers to obtain optimum mechanical properties. It is concluded that the bond between the fibre and elastomer matrix can be strengthened when the fibres are coated with epoxy in combination with a coupling agent in the elastomer. As a result, the mechanical properties of epoxy coated fibre (EF) reinforced elastomers are higher than those of non-coated fibre (NF) reinforced elastomers. The materials used in the present study are based on the optimized formulation of short-cut aramid fibre reinforced elastomers done by Vleugels [9].

1.3 Tribology of fibre reinforced elastomers

Tribology is defined as the science of interacting surfaces in relative motion. The tribo-systems that contain elastomers are relevant to a large number of applications, such as tyres and conveyor belts. Friction and wear are the tribological phenomena that influence the performance of the elastomer based products. They are not material properties but are system-dependent, being influenced by the materials in contact and the operating conditions. The operating conditions play an essential role in the friction and wear phenomena, such as normal force, sliding velocity, type of

motion, sliding distance, and temperature. Understanding the friction and wear phenomena will provide a longer and more sustainable lifetime of elastomers.

Sliding friction in elastomeric materials can be found in daily activities, such as tyre-road and shoes-road friction. In general, two components contribute to sliding friction, namely deformation and adhesive friction [10]. The deformation friction originates from the internal damping in the bulk of an elastomer when the oscillating forces are exerted from the counter surface onto the elastomer surface. The deformation friction will be more pronounced on a rough counter surface and a soft material with high contact pressure [11]. Mechanical properties of the bulk elastomer determine the deformation friction [12], whereas the adhesive friction comes from the attractive forces between the contacting bodies [13]. The adhesive friction will be dominant when the contacting surfaces are smooth and the sliding velocity is low [11, 14]. The adhesive friction is greatly influenced by the mechanical properties of the surface of the material. Unfortunately, the surface properties of the contacting materials are not constant. They change during sliding contact and therefore lead to a change in tribological behaviour.

When an elastomer is in contact with a rigid counter surface in relative motion, the rigid counter surface may damage and remove a certain part of the elastomer surface. The removal of material during contact in relative motion is defined as wear. Together with friction, wear is an essential factor which has to be controlled to prolong the lifetime of the elastomer. The sliding friction between an elastomer and a rigid counter surface may also generate noise. Noise becomes an important issue in industry because it may have a direct impact on customers' perception of the quality of products. Therefore, many attempts have been conducted to minimize the noise during the usage of products [15-17]. During sliding contact, noise can be generated either in the structure of the system or the contacting surfaces. The structural noise is generated by the vibration of the system as a consequence of friction, whereas the noise generation in the contacting surfaces is caused by stick-slip phenomenon [18]. The noise generation in the contacting surfaces of elastomer-based products can be found in daily life, such as tyre noise in car parks and during turning and/or braking.

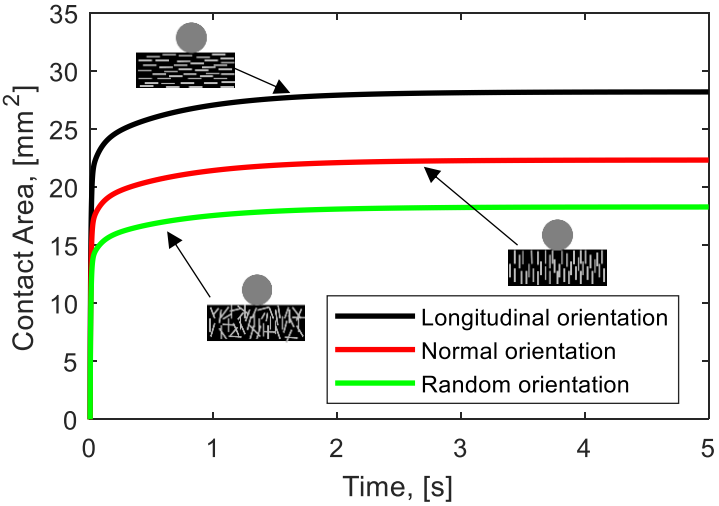

Figure 1.2: Contact area as a function of time for three types of reinforcement directions.

Adding fibres in an elastomer not only changes the mechanical properties of the elastomer but also changes the tribological behaviour, such as contact area, friction and wear. Moreover, orientation of the fibres in the composite influences the behaviour of the composite. When the fibres are oriented in random direction, the composite has isotropic material behaviour, whereas an anisotropic material behaviour will be observed when the fibres are oriented in a certain direction. Figure 1.2 shows the contact area as a function of time for three types of reinforcement directions, namely random orientation, normal orientation (the fibres are oriented perpendicular to the elastomer surface) and longitudinal orientation (the fibres are oriented parallel to the elastomer surface). The contact area between a rigid ball and an elastomeric composite flat was calculated by using the contact model of viscoelastic-anisotropic material available in the literature [19]. In the calculation, the elastic modulus of the composite containing randomly oriented fibres are assumed to increase in all directions, while the elastic modulus of the composites containing longitudinally and normally oriented fibres increases in only one direction. The results show that the contact area of the composite containing randomly oriented fibres is the smallest one because the mechanical properties increase in all directions. While the contact area of the composite containing fibres in the z-direction is lower than that in the x-direction. The contact area increases with increasing time due to the effect of time-related properties of the elastomeric materials. At a certain time, the contact area will be constant.

Studies regarding the short-cut aramid fibre reinforced elastomers with respect to friction and wear have been conducted by some researchers [6, 20, 21]. Khasani [6] studied the abrasive wear of elastomer reinforced with 1 phr (parts per hundred rubber) short-cut aramid fibres. The results showed that the wear of the fibre reinforced elastomer is slightly lower than that of the unreinforced elastomer. The low amount of short-cut aramid fibres improve the hysteresis and the abrasion resistance of a truck tread composite [20]. Later, Rodriguez [21] showed that by adding short-cut aramid fibres in the elastomer reduces the coefficient of friction in comparison with that of the unreinforced elastomer at the same normal force. Although several studies of short-cut aramid fibre reinforced elastomers have been conducted, the wear processes of short-cut aramid fibre reinforced elastomer and their relation to friction and friction-induced noise are still not fully understood. In this thesis, the friction, wear and friction-induced noise mechanism that occur in short-cut aramid fibre reinforced elastomers are examined.

1.4 Objectives of this research

In this thesis, the tribological behaviour between elastomers in contact with a rigid counter surface was studied. Elastomers based on a butadiene rubber (BR) and a styrene butadiene rubber (SBR) reinforced by short-cut aramid fibres were used. Two types of short-cut aramid fibres were used, namely non-coated fibre (NF) and epoxy coated fibre (EF). The objectives of this thesis can be described as follows:

a. Investigation of the tribological phenomena of elastomers during sliding contact.
b. Investigation of the friction mechanism in short-cut aramid fibre reinforced elastomers during sliding contact.
c. Investigation of the wear mechanism in short-cut aramid fibre reinforced elastomers during sliding contact.
d. Investigation of the friction-induced noise in short-cut aramid fibre reinforced elastomers during sliding contact.

1.5 Outline of this thesis

This thesis is divided into two parts, the first part is a summary of the whole work and consists of five chapters. Chapter 1 introduces the fibre reinforced elastomers and their tribological phenomena. Chapter 2 focuses on the material compositions used in this study and the mechanical properties of the composites. The evaluation of the friction component that is dominant in the present study is also described in

this chapter. In Chapter 3, the tribological phenomena of elastomers during sliding contact is investigated, such as contact area, wavy wear track and formation of a modified surface layer. Both experimental and analytical approaches are used. The study of friction and wear of short-cut aramid fibre reinforced elastomer with and without silica is shown in Chapter 4. The wear mechanisms of short-cut aramid fibre reinforced elastomers and their relation to friction and friction-induced noise are also explained. A summary of conclusions and recommendations for future research are given in Chapter 5.

The second part presents some publications in research papers. The relationship between the first and second part is outlined in Figure 1.3.

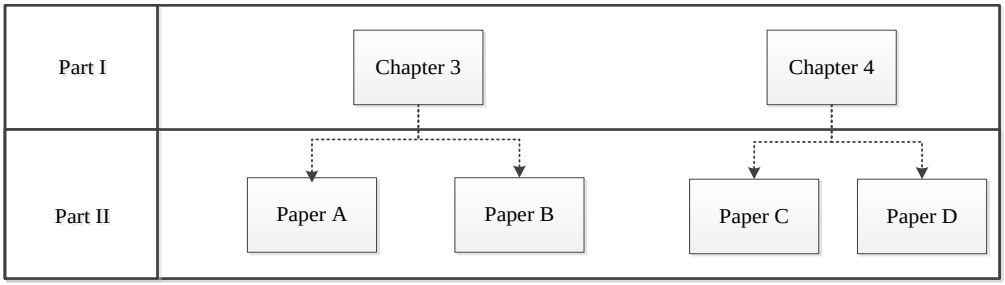

Figure 1.3: The schematic outline of the thesis and the relationship of the chapters and the papers.

Chapter 2 Materials and Mechanism of Sliding Friction

In this chapter, the elastomers used in this study are explained. Two types of elastomers are used based on a styrene butadiene rubber (SBR) and a butadiene rubber (BR) reinforced by short-cut aramid fibres. Two types of short-cut aramid fibres are used, namely non-coated short-cut aramid fibre (NF) and ones coated with an epoxy coating (EF). Silica fillers are added into the composites to investigate the effect of epoxy coating for more realistic practical application. Tensile and hysteresis tests are performed to investigate the mechanical properties of the composites. A pin-on-disc tribometer is used to evaluate the frictional behaviour of the composites. During sliding contact, the total friction is composed of a deformation and an adhesive friction. The contribution of each type of friction in the total friction at the present tribo-system is also discussed.

2.1 Composition of elastomers

The materials used in this study were elastomers based on SBR and BR vulcanized with sulfur and with two types of reinforcing materials, namely highly dispersible silica and short-cut aramid fibre. The initial length of the short-cut aramid fibres is approximately 3 mm, and their diameter is 10-12 μm; they were supplied by Teijin Aramid B.V, Arnhem, The Netherlands. Two types of poly-p-phenylene-terephtalamide (aramid) fibres were used, namely NF and EF.

The interfacial strength between a short-cut aramid fibre and an elastomer matrix can be influenced by two elements: an adhesive coating and a coupling agent which can interact with this coating [9]. An epoxy coating on the fibre's surface was used, which can chemically react with a coupling agent. Two formulations were used to analyse the effect of epoxy coated fibre in the composites. To improve the fibre-matrix interfacial interaction a silane coupling agent S-3-(triethoxysilylpropyl)-octanethioate (NXT) was used in formulation 1. The first formulation is based on the optimized formulation used by Vleugels [9]. The composite's ID of formulation 1

used in this thesis is "SBR." Furthermore, a high silica elastomer formulation was taken to investigate the effect of short-cut aramid fibre for more realistic practical application. Formulation 2 is based on a silica-reinforced passenger car tyre tread, called "Green Tyre" [22]. The coupling agent used in this formulation was *Bis*-(triethoxysilylpropyl)-tetrasulfide (TESPT). The composite's ID of formulation 2 is "SBR-BR." Details of the formulation in parts per hundred rubber (phr) are given in Table 2.1.

Table 2.1: Material formulations of the composites.

Ingredients	SBR [in phr]	SBR-BR [in phr]	Supplier
SBR, Buna VSL VP PBR 4045 HM	100	-	Arlanxeo, Leverkusen, Germany
SBR, Buna VSL 5025-2 HM	-	97.3*	Arlanxeo, Leverkusen, Germany
BR, KBR 01	-	30.0	Kumho, Seoul, S-Korea
Silica Ultrasil VN3	-	80.0	Evonik Industries AG, Essen, Germany
Zinc oxide (ZnO)	2.5	2.5	Sigma Aldrich, St. Louis, United States
Stearic acid (SA)	1.5	2.5	Sigma Aldrich, St. Louis, United States
TDAE oil	-	6.7	Hansen & Rosenthal, Hamburg, Germany
Twaron aramid fibre	15 NF/EF	20 NF/EF	Teijin Aramid B.V, Arnhem, The Netherlands
Bis-triethoxysilylpropyl-tetrasulfide (TESPT)	-	7.0	Evonik Industries AG, Essen, Germany
S-3-triethoxysilylpropyl-octanethioate (NXT)	6.0	-	Momentive, New York, United States
6PPD stabilizer	-	2.0	Flexsys, Brussels, Belgium
TMQ stabilizer	-	2.0	Flexsys, Brussels, Belgium
Sulfur	2.8	1.4	Sigma Aldrich, St. Louis, United States
N-Cyclohexyl Benzothiazole	3.4	1.7	Flexsys, Brussels, Belgium

Sulfenamide (CBS)			
Di-Phenyl Guanidine (DPG)	4	2.0	Flexsys, Brussels, Belgium

* Containing 37.5 wt% oil.

2.2 Mechanical properties of elastomers

The orientation of fibres has a significant impact on the mechanical properties of the composites. Fibres in the composites are oriented during the production process by using a two-roll mill. Although not all the fibres can orient in the desired direction, usually a high degree of fibre orientation is achieved by a repetitive milling process. For the composites containing randomly oriented fibres, the mixing process is done only with an internal mixer without a two-roll mill process. Three types of fibre orientations were prepared for tensile measurements, namely *x*, random and *z*-orientation. The fibre reinforced elastomer in *z*-orientation means that the fibres are oriented longitudinally to the applied force, while the fibre reinforced elastomer in *x*-orientation means that the fibres are oriented transverse to the applied force, see Figure 2.1. The tensile measurements of the vulcanized composites were performed on a 3343 series Tensile Tester from Instron according to ISO 37 Type 2 dumbbell size. A crosshead speed of 500 mm/min was employed.

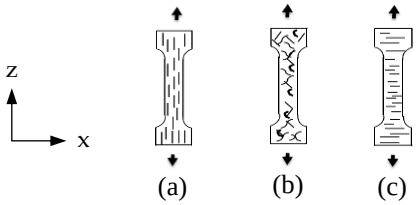

Figure 2.1: Orientation of fibres to the applied force: (a) *z*-orientation; (b) random orientation; and (c) *x*-orientation.

Tensile stress-strain curves of the SBR composites are depicted in Figure 2.2. The non-fibre SBR shows the poorest mechanical properties in comparison with others. It can be seen that the composite reinforced in *z*-orientation has the steepest curve and the composite reinforced in *x*-orientation shows a shallow curve, while the composite reinforced with randomly oriented fibre has an intermediate slope. The composites containing EF have a steeper curve than the composites containing NF for all reinforcement directions.

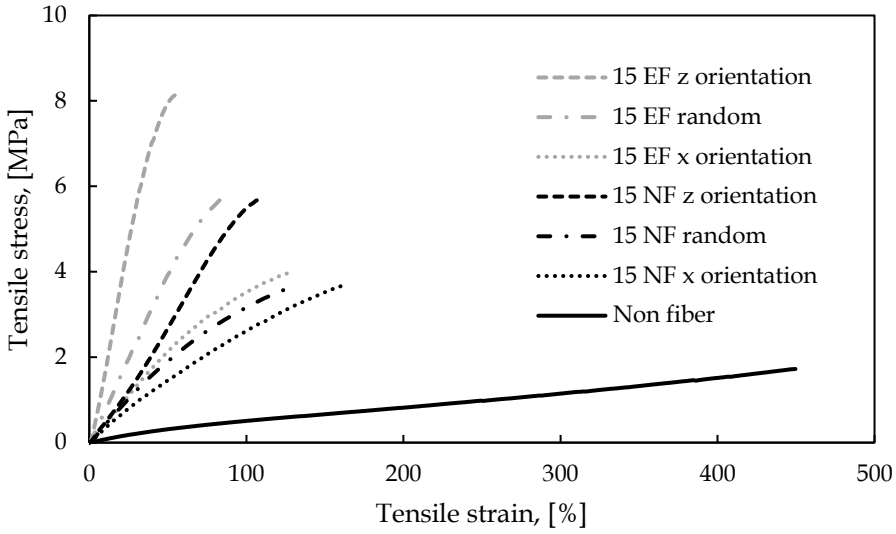

Figure 2.2: Tensile stress-strain curves of the SBR composites: non-fibre SBR and SBR containing 15 NF and 15 EF for several orientations, namely *x*, random and *z*-orientation.

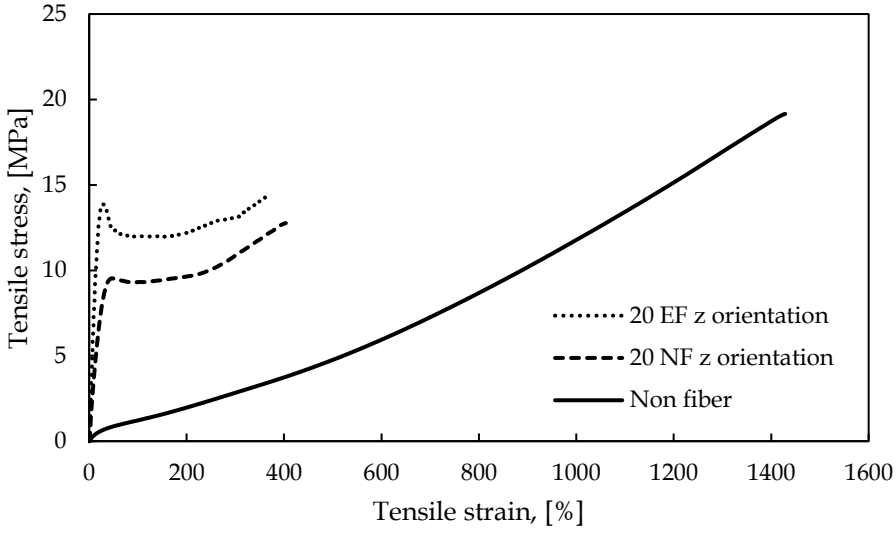

Figure 2.3: Tensile stress-strain curves of the SBR-BR composites: non-fibre SBR-BR and SBR-BR containing 20 NF and 20 EF in *z*-orientation.

Tensile stress-strain curves of the SBR-BR composites are depicted in Figure 2.3. The same trend as the results of SBR composites is observed, in which the

composites containing EF have a steeper curve than those containing NF, while the non-fibre composites show the shallowest curve. Yield stress is observed for the composites containing fibres, both EF and NF, see Figure 2.3.

Three cycles of hysteresis tests at a tensile strain of 250% were performed to prove that the presence of fibre-matrix interaction leads to the improvement of the mechanical properties of the composites. Figure 2.4 shows the tensile and hysteresis tests for the composites containing 20 EF in *z*-orientation. The fibres are oriented in the *z*-direction to minimize the effect of mechanical interlocking of the fibres. Therefore, the effect of adhesion between fibre and elastomer matrix becomes dominant.

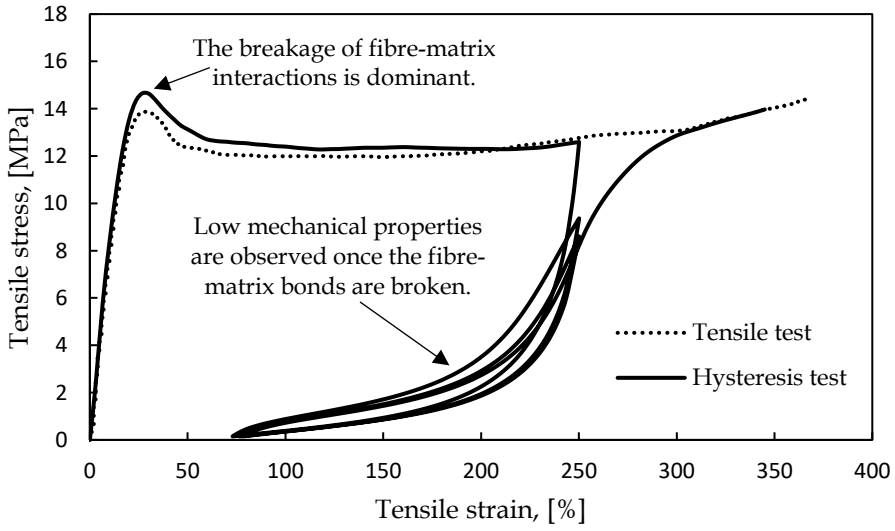

Figure 2.4: Comparison between tensile and hysteresis tests of the SBR-BR containing 20 EF in *z*-orientation.

Yield stress is defined as the stress at which the elastomer starts to deform plastically. For a non-fibre elastomer, no yield stress can be observed because the elastomer deforms plastically at a very small strain, see Figure 2.3, while SBR-BR composites containing 20 EF in *z*-orientation shows that the stress-strain curve is nearly linear up to a strain of approximately 30%. Once the strain exceeds this threshold, yield occurs and the mechanical properties of the composite reduce drastically. Considerable dissipated energy is observed at the first cycle, see Figure 2.4. At the second and third loading stress, poor mechanical properties are observed. A far smaller dissipated energy is observed in the second and third cycles. This phenomenon indicates that the breakage of fibre-matrix interaction is dominant when yield occurs at the first cycle and it greatly influences the mechanical properties of the composite. The dissipated energy which is observed at the second

and third loading can be caused by the breakage of silica interactions, called Mullin's effect. At high tensile strain, the curve of hysteresis test follows the tensile test.

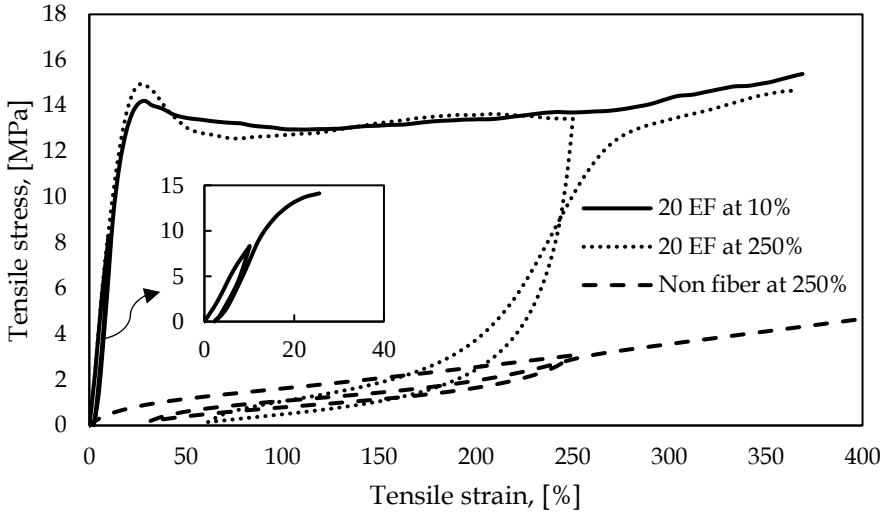

Figure 2.5: Hysteresis curves of the SBR-BR composites: non-fibre SBR-BR at a tensile strain of 250% and SBR-BR containing 20 EF in *z*-orientation at a tensile strain of 10% and 250%.

As mentioned before, the fibre-matrix interactions are broken at a tensile strain of approximately 30%. A hysteresis test was performed at a tensile strain of 10% to prove that the fibre-matrix interaction is still present in this range. The result shows that the dissipated energy is minimum and the steepness of the curve at the second loading is nearly the same as the first loading, see Figure 2.5. It indicates that the fibre-matrix interaction has not broken yet at a tensile strain of 10%.

Hysteresis tests were also performed at a strain of 250% for the SBR-BR composite without fibre and the composite containing 20 EF in *z*-orientation. The results show that the dissipated energy of the 20 EF reinforced elastomer is much larger than that of the non-fibre elastomer. Although this significant dissipated energy comes from the combination of the breakages (such as the breakage of fibre-matrix, silica-silica and silica-matrix interaction), the breakage of the fibre-matrix interaction is dominant, while the dissipated energy of the SBR-BR composite without fibre can be caused by the breakage of silica-matrix and silica-silica interaction. Therefore, a far smaller dissipated energy is observed.

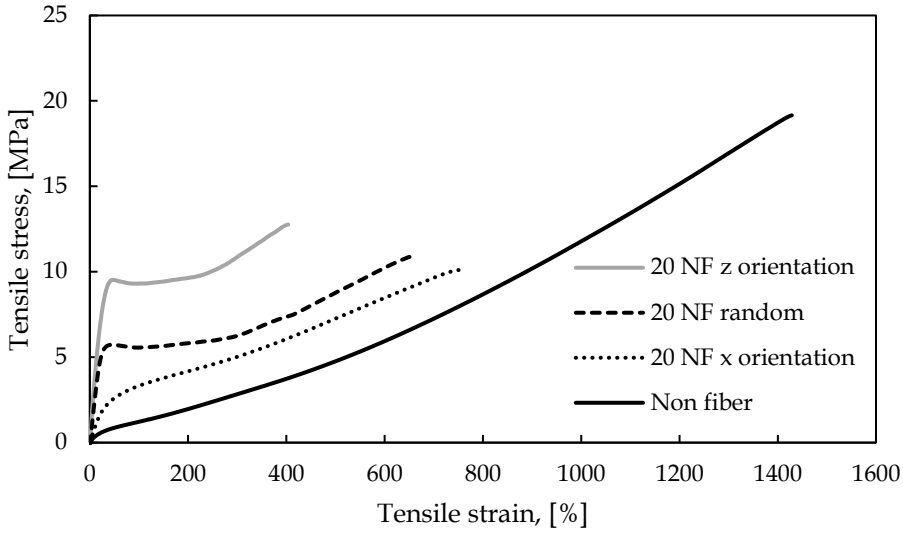

Figure 2.6: Tensile stress-strain curves of SBR-BR composites: non-fibre SBR-BR and SBR-BR containing 20 NF for several orientations, namely *x*, random and *z*-orientation.

The effect of fibre orientation on the stress-strain curve is depicted in Figure 2.6. It can be seen that the non-fibre composite shows a shallower curve than the others. The composite reinforced in the *z*-orientation has the steepest curve and the composite reinforced in the *x*-orientation shows a shallow curve, while the composite in randomly oriented fibre has an intermediate result between those two orientations. After the yield stress is reached, the slopes of the short-cut aramid fibre reinforced SBR-BR curves are nearly the same as the unreinforced ones. It means that the effect of the fibre reinforcement disappears when the fibre-matrix interactions are broken. Once the bonds between the fibres and the elastomer matrix are broken, the effect of fibre diminishes. As a result, the mechanical properties of the composites with and without fibres are nearly the same.

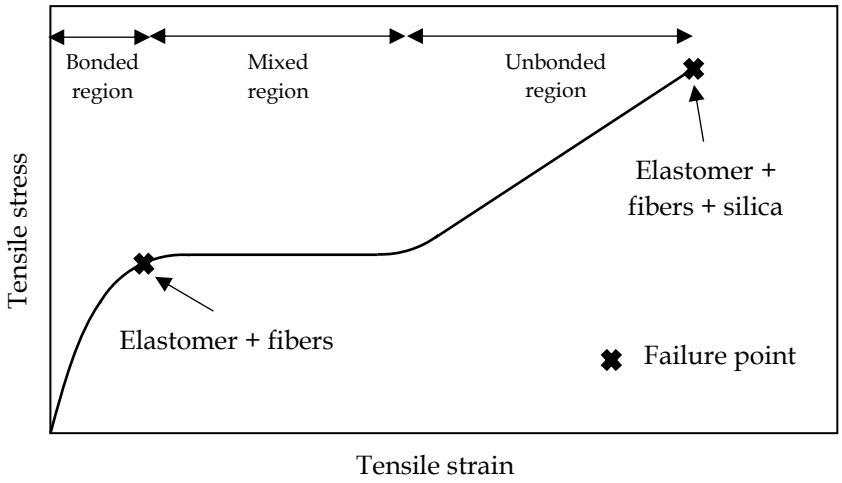

Figure 2.7: Tensile stress-strain of short-cut aramid fibre reinforced elastomer with and without silica, shown schematically.

Figure 2.7 shows a schematic of the stress-strain curve of a short-cut aramid fibre reinforced elastomer. The short-cut aramid fibre reinforced SBR (without silica reinforcement) is observed to be broken at the interface before the yield stress is reached, while the fibres and silica reinforced SBR-BR is broken after the yield stress. This phenomenon can be explained by the fact that the ultimate strain of non-fibre SBR-BR is much larger (1500%) than that of non-fibre SBR (450%), see Figures 2.2 and 2.3. Since the mechanical properties of the non-fibre SBR are poor, the composite will break as soon as the bonds between the fibres and the elastomer matrix are broken.

The tensile storage and loss moduli of SBR and SBR-BR without fibres were measured by a Metravib Viscoanalyser DMA+150 in a temperature sweep mode from -80^{o}C to 80^{o}C, at a frequency of 10 Hz, under dynamic and static strains of 0.1 and 1%, respectively. Figure 2.8 shows that the storage and loss moduli of both materials are high at low temperature and decrease gradually with increasing temperature. At room temperature, the tensile storage and loss moduli do not vary quite as much. Since all of the friction tests were performed at room temperature, the effect of temperature is neglected in this thesis.

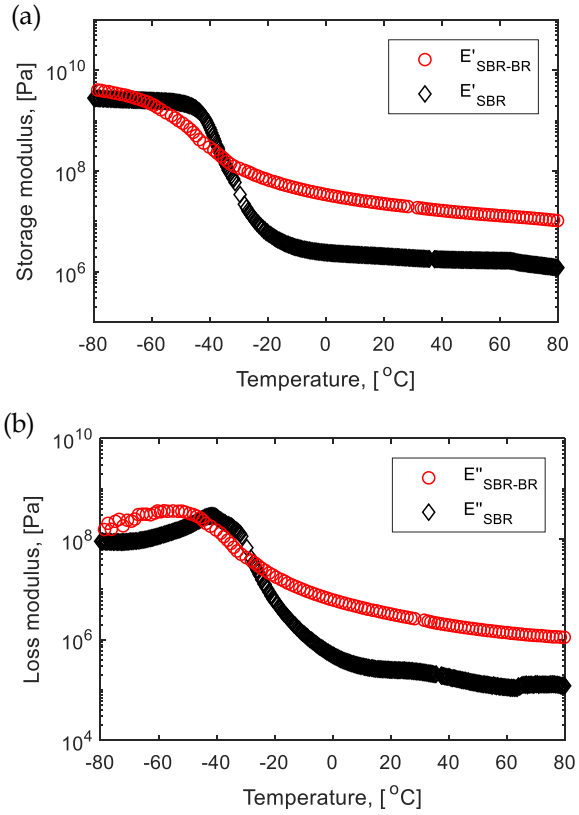

Figure 2.8: a) The storage modulus and b) loss modulus in temperature sweep mode for SBR and SBR-BR, both materials are without fibres.

2.3 Sliding friction mechanism of elastomers

Elastomers are used in several industrial products, such as conveyor belts and wiper blades. Sliding friction often occurs during their usage. Therefore, detailed knowledge of sliding friction between an elastomer and a counter surface is important in improving the performance of the products. Several factors play a role in the sliding friction between an elastomer and a counter surface, such as contact pressure, sliding velocity, temperature and surface roughness. Due to this complexity, the sliding friction phenomenon on elastomers has been discussed actively.

The elastomer friction has two main contributors described as deformation and adhesive friction [23]. The deformation friction depends on the bulk properties

of the elastomer, while the adhesive friction depends on the surface properties of the elastomer. Generally, the coefficient of friction consists of the deformation contribution (F_{def}), the contribution from the frictional shear stress as well as the real contact area (τA), and the normal force contribution (F_N), see Equation 2.1.

$$\mu = \frac{F_{def} + \tau A}{F_N} \tag{2.1}$$

A pin-on-disc tribometer was used to quantify the importance of each contributor. The experiments under dry conditions were conducted to investigate the total friction. The contribution of the deformation friction was investigated by using an additional experiment where the sample surfaces were wetted with a very thin layer of low-viscosity oil (Ondina 927 with a dynamic viscosity of 78 mPas at 20°C) such that the lubricated tribo-system remains in the boundary lubricated regime. The results show that the coefficient of friction of the wet condition decreases drastically in comparison with that of the dry condition for all composites. As an example, the steady-state coefficient of friction of the SBR-BR composite without fibres at a contact pressure of 0.46 MPa and a velocity of 0.2 m/s decreases from 2.2 to 0.08. It shows the limited role of the hysteresis friction in the overall friction. The contribution of frictional shear stress and contact area are dominant in this study.

2.4 Summary

In this chapter, the formulation of the composites used in the present study was explained. Two types of composite formulations were used, namely the optimized formulation of short-cut aramid fibre reinforced SBR and the green tyre formulation of silica and short-cut aramid fibre reinforced SBR-BR. Two types of short-cut aramid fibres were used, namely non-coated fibre (NF) and epoxy coated fibre (EF). The mechanical properties of the composites were reviewed. Hysteresis tests were performed to investigate the interaction between the fibre and elastomer matrix. The composite containing EF is stiffer than those containing NF for both formulations. For the composites containing fibres and silica, the effect of fibres on the mechanical properties of composites diminishes once the tensile strain reached a threshold (~30%). The contribution of deformation friction is limited in the present tribo-system. Therefore, the deformation friction is neglected in this study.

Chapter 3 Tribological Phenomena of Elastomers during Sliding Friction

In this chapter, several tribological phenomena of elastomers in sliding contact with a rigid counter surface are investigated, namely contact area, wavy wear track and formation of a modified surface layer. In applications, the contact between an elastomer and a rigid counter surface occurs not only under static conditions but also under dynamic conditions, such as the tyre-road contact. The contact area between an elastomer and a rigid counter surface as a function of sliding velocity is studied both theoretically and experimentally. A modification of the elastomer surface is another phenomenon during sliding friction. This modification may change the tribological behaviour of the elastomer. The modified surface layer formation as a function of several parameters, namely velocity, contact pressure and roughness of the counter surface, are investigated. Another tribological phenomenon during sliding friction is the stick-slip motion. In applications, this phenomenon must be avoided because it can generate surface irregularities during sliding friction. For a contact between an elastomer and a ball counter surface, the stick-slip phenomenon may form a wavy wear track. An analytical model to predict the occurrence of a wavy wear track at an elastomer surface is developed. Furthermore, experiments are performed to validate the analytical model.

3.1 Contact area as a function of sliding velocity

In chapter 2, it is stated that the contribution of deformation friction in the total friction is limited in this study. Therefore, the coefficient of friction between an elastomer and a counter surface under dry contact is expressed by:

$$\mu = \frac{\tau A}{F_N} \tag{3.1}$$

Where, τ is the frictional shear stress at the contacting surfaces, A is the contact area between the contacting surfaces and F_N is the normal force. A low friction can be achieved when the surface interaction is reduced, which can be done by applying contaminants or a lubrication layer. A modification of the mechanical properties at the elastomer surface is another cause of low friction. Minimizing the contact area between the contacting surfaces also contributes to a decreasing friction.

A contact between an elastomeric material and a rigid counter surface is found in a huge number of applications, such as tyre-pavement, shoes-road and seal-steel contact. It is known that the contact area of elastomeric materials is different under static and sliding conditions. At sliding conditions, the contact area between an elastomeric material and a rigid counter surface is different in both size and shape in comparison with the static condition. Several researchers have studied the contact area between an elastomeric material and a rigid counter surface at different sliding velocities [13, 21, 24-28]. They showed that at a threshold velocity the size of the contact area starts to decrease with increasing velocity. The contact area of the elastomer was found to have an elliptical shape during sliding [21], see Figure 3.1. It shows that the dimension of the contact area in the direction of sliding decreases, while the size of the contact area perpendicular to the direction of sliding is nearly the same.

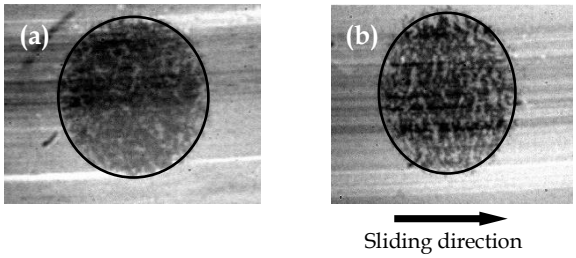

Figure 3.1: The apparent contact area of an elastomer in contact with a flat glass: a) in static contact; b) sliding contact [21].

Several studies suggested that the decreasing contact area under sliding condition correlates with the mechanical properties of the elastomers [21, 23, 24]. Ludema and Tabor [24] proposed that the decreasing contact area under sliding condition is caused by the increasing elastic modulus and is proportional to $E^{-2/3}$. Rodriguez [21] suggested that at high sliding velocity the contact area will reach a limit value which corresponds to the ratio between the modulus at high and at low deformation rate. Next to the dynamic modulus of elastomers, the decreasing contact area of elastomers was also found to be dependent on the time-related properties of elastomers[13, 29]. Busse et al. [13] showed that the contact area of the

elastomer decreases with increasing velocity. The higher the velocity, the lower the contact time, and as a result, a lower contact area will be found.

The contact model for a viscoelastic-anisotropic material has been developed by Rodriguez [19]. It allows calculating the contact area as a function of the anisotropic mechanical properties. The contact area equations for a viscoelastic-anisotropic material are shown in Equations 3.2 and 3.3 [21].

$$a_x(t) = \left(\frac{3RF_N}{4}\right)^{1/3} [I_1 \overline{\phi}(t)]^{1/3} \tag{3.2}$$

$$a_y(t) = \left(\frac{3RF_N}{4}\right)^{1/3} \left(\frac{{I_2}^{1/2}}{{I_1}^{1/6}}\right) [\overline{\phi}(t)]^{1/3} \tag{3.3}$$

Where a_x and a_y are the radii of the contact area in x and y-direction, respectively. R is the radius of the spherical indenter, F_N is the normal force, I_1 and I_2 are two numerical contour integrals that are dependent on the elastic modulus E, shear modulus G, and Poisson's ratio υ in x, y and z-direction (E_x, E_y, E_z, G_{xy}, G_{xz}, G_{yz}, υ_{xy}, υ_{xz}, υ_{yz}) – details are given in Appendix A – and $\bar{\phi}$ is the normalized creep compliance.

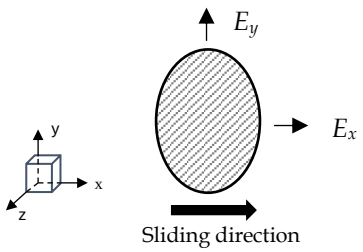

Figure 3.2: The elliptical contact area at sliding condition, shown schematically.

Figure 3.2 shows that during sliding the diameter of the contact area decreases in the x-direction, while the diameter of the contact area in the y-direction is nearly the same as is observed in the experiments, see Figure 3.1. Assuming the properties of the glass disc not to be affected, this apparent stiffening of the contact in sliding direction must be the direct result of stiffening of the elastomer. Since the contact area decreases in the sliding direction, it indicates that the mechanical properties of the elastomer increase only in the direction of sliding (x-direction). Therefore, the contact area of the sliding situation can be predicted by using a contact model for a viscoelastic-anisotropic material in which the "reinforcement" occurs in the x-direction. This means that the mechanical properties of the elastomer in x-direction change as a function of sliding velocity, while the mechanical properties in

perpendicular direction remain the same. Furthermore, the contact time between the elastomer and the glass disc can be estimated by using the diameter of the contact and the velocity. Based on the work of Rodriguez [21] and Busse [13], a flowchart to predict the contact area as a function of sliding velocity is proposed, see Figure 3.3.

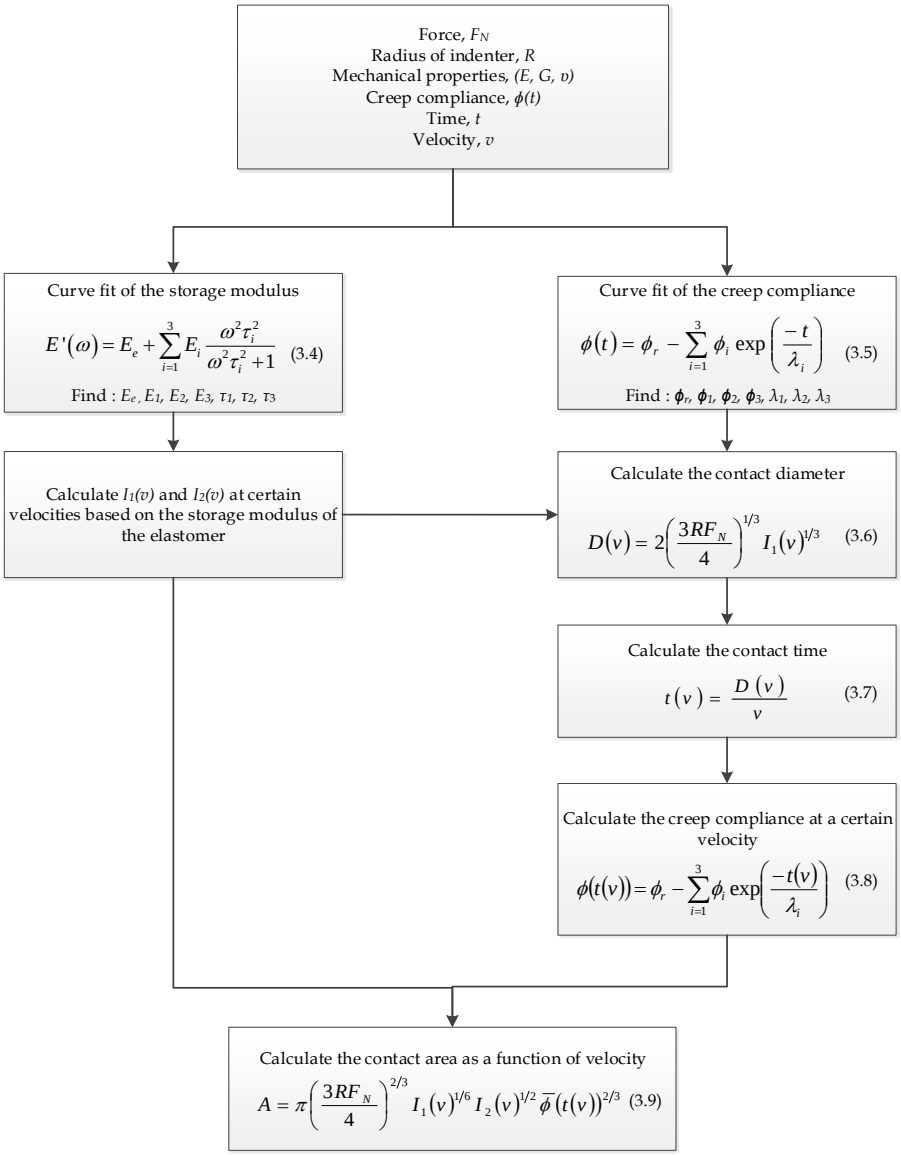

Figure 3.3: Flowchart calculation of the contact area as a function of velocity [30], based on the work of Rodriguez [19] and Busse [13].

Experiments were performed in which a tribological system composed of an elastomeric hemisphere was sliding against a glass plate, see Figure 3.4. The sliding experiments at room temperature were performed at a normal force of 1 N and sliding velocities between 0 m/s (static) and 1 m/s. A camera was fitted normal to the plane of contact to capture the images of the contact area during sliding contact.

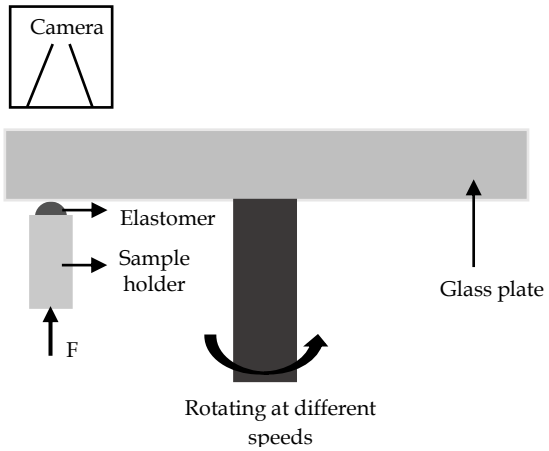

Figure 3.4: The experiment set-up, shown schematically.

The elastomer used is a styrene butadiene rubber (SBR) SE-6233 from Sumitomo. The storage modulus was measured using a Metravib Viscoanalyser DMA+150 at frequency sweep, under dynamic and static strains of 0.1 and 1%, respectively. The creep compliance was determined at a constant stress and at room temperature. The results of the storage modulus and the creep compliance measurements are depicted in Figure 3.5; these experimental data were fitted using Equation 3.4 and Equation 3.5, see Figure 3.3. It can be seen that the experimental data is very well described by the fit equations. The parameter values of the fit equations can be found in Table 3.1.

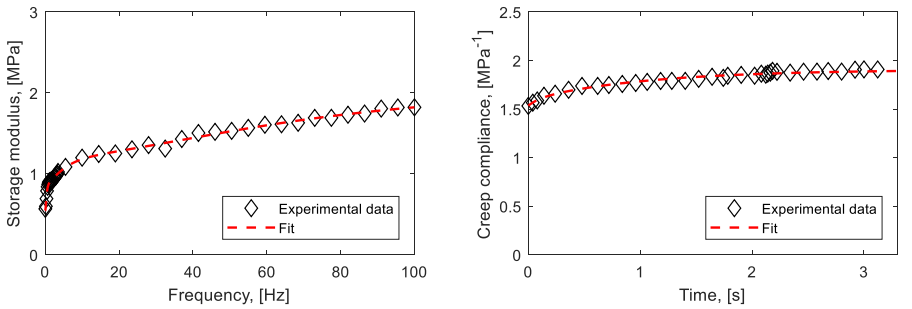

Figure 3.5: (a) Storage modulus and (b) creep compliance of the SBR, experimental data and curve fit.

Table 3.1: Fitting parameters of Equation 3.4 and Equation 3.5.

Dynamic modulus (Equation 3.4)		Creep compliance (Equation 3.5)	
E_e [Pa]	5.46×10^{5}	ϕ_r [Pa^{-1}]	1.91×10^{-6}
E_1 [Pa]	3.70×10^{5}	ϕ_1 [Pa^{-1}]	6.31×10^{-8}
E_2 [Pa]	3.27×10^{5}	ϕ_2 [Pa^{-1}]	3.04×10^{-7}
E_3 [Pa]	8.85×10^{5}	ϕ_3 [Pa^{-1}]	9.83×10^{-9}
τ_1 [s]	2.60	λ_1 [s]	0.10
τ_2 [s]	0.18	λ_2 [s]	1.05
τ_3 [s]	0.014	λ_3 [s]	10.1

The images of the contact area for different sliding velocities can be seen in Figure 3.6. It shows that the shape of the contact area is circular (static situation) until a velocity of 0.004 m/s. An elliptical shape of the contact area is found after a velocity of 0.008 m/s. Three images were taken at each sliding velocity and the average contact areas were calculated. Figure 3.7 shows the contact area at sliding ($A_{dynamic}$) over the static contact area (A_{static}) as a function of sliding velocity. As the plot in the x-axis of Figure 3.7(b) has a logarithmic scale, the static contact is plotted at a sliding velocity of 1×10^{-3} m/s. By using the parameters in Table 3.1 and the tribological condition used in the experiments, the contact area as a function of sliding velocity can be predicted by using Equation 3.4 to Equation 3.9, see Figure 3.3. Figure 3.7 shows that the calculated contact area approaches the experimental results rather well.

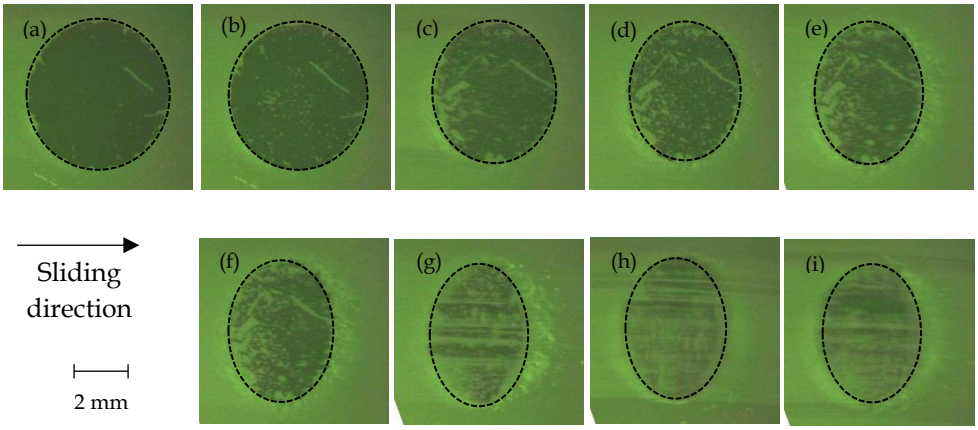

Figure 3.6: The contact area of SBR for several sliding velocities: (a) static; (b) 0.004 m/s; (c) 0.008 m/s; (d) 0.016 m/s; (e) 0.032 m/s; (f) 0.064 m/s; (g) 0.25 m/s; (h) 0.5 m/s; (i) 1 m/s.

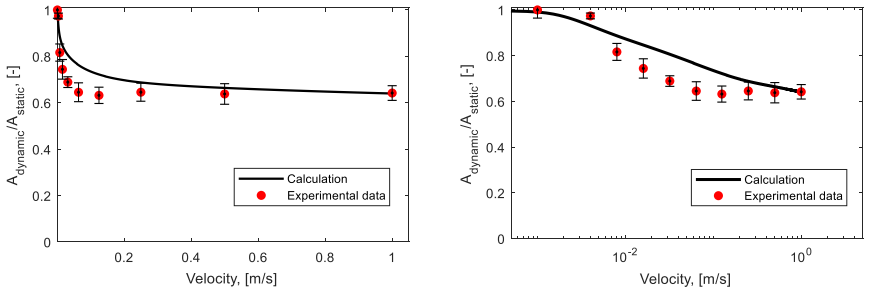

Figure 3.7: The dynamic contact area over the static contact area of SBR for several sliding velocities, comparison between the analytical model and the experimental data: (a) linear scale; (b) logarithmic scale.

An additional experiment was performed to investigate the effect of the glass transition temperature on the dynamic contact area. The SBR SE-6233 from Sumitomo (SBR-1) was compared with an SBR Buna VSL VP PBR 4045 HM from Arlanxeo (SBR-2). The glass transition temperatures of the elastomers were determined using a Metravib Viscoanalyser DMA+150 in temperature sweep mode at a fixed frequency of 10 Hz under dynamic and static strains of 0.1 and 1 %, respectively. Figure 3.8(a) shows that the glass transition temperature of SBR-2 is lower than that of SBR-1.

The contact area of SBR-2 for various sliding velocities was captured under the same tribological condition as the measurement of SBR-1. Figure 3.8(b) shows that the contact area of SBR-2 decreases at a higher velocity (0.125 m/s) than that of

SBR-1 (0.008 m/s). The higher the glass temperature, the lower the sliding velocity at which the contact area starts to decrease. For an elastomer which has a high glass transition temperature, the transition between the elastomeric and glassy regions occurs at a low frequency. As a result, the mechanical properties of the elastomer start to increase at a low frequency, hence the decreasing contact area occurs at a low velocity.

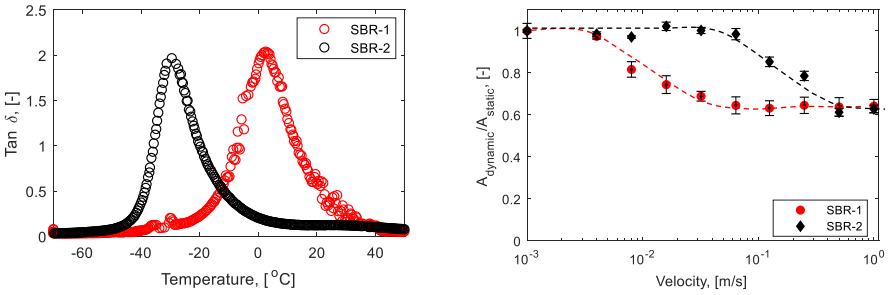

(a) (b)

Figure 3.8: (a) *Tan δ* of SBR-1 and SBR-2 in temperature sweep, (b) the dynamic contact area over the static contact area of SBR-1 and SBR-2 for several velocities.

3.2 Formation of a modified surface layer

Surface conditions such as the existence of a lubricant and wear particles between the contacting bodies may influence the frictional behaviour. A modification that occurs at the surface of elastomers during sliding contact is another phenomenon that influences friction. Several researchers have shown that during sliding contact the mechanical properties of the elastomer surface decrease in comparison with the original (substrate) material [31, 32]. The degradation of the elastomer surface can be caused by mechanical, thermal and chemical processes [32-34]. This modification alters the frictional shear stress during sliding contact and therefore changes friction. In this section, the non-fibre SBR-BR composite was used to investigate the formation of a modified surface layer as a function of tribological conditions, namely normal force, sliding velocity, and roughness of the counter surface.

Figure 3.9 shows the coefficient of friction as a function of sliding distance at a contact pressure of 0.46 MPa and various sliding velocities, namely 0.05, 0.20 and 0.30 m/s. Initially, the coefficient of friction increases, caused possibly by the increased contact area due to wear. Interestingly, although the contact area increases continuously with increasing sliding distance, the coefficient of friction decreases after a certain sliding distance. This phenomenon may be the result of a decreasing frictional shear stress. The composition and the mechanical properties of an

elastomer at the top layer can change due to repeated sliding contact [32]. The decreasing mechanical properties in the top layer of the elastomer will lead to a decreasing frictional shear stress. Therefore, the frictional shear stress at the end of the tests (position 2 in Figure 3.9) is far lower than that at the beginning of the tests (position 1 in Figure 3.9). The decreasing coefficient of friction occurs for all velocities, indicating that modified surface layers are developed for all tests. Finally, for long sliding distances, a lower coefficient of friction is found when a higher sliding velocity is used.

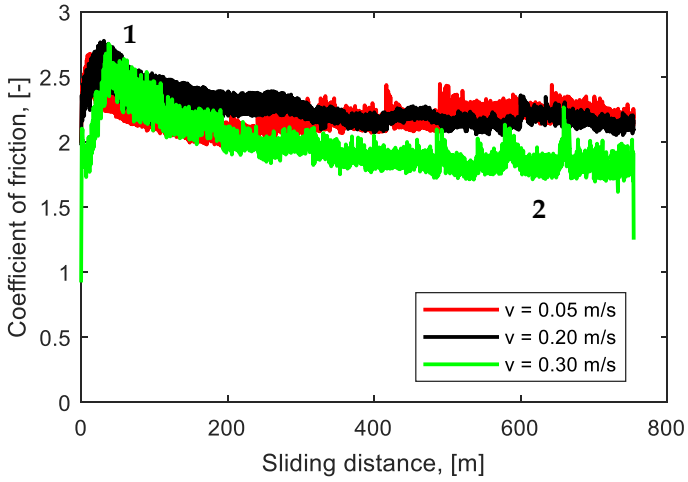

Figure 3.9: Coefficient of friction as a function of sliding distance for different velocities, non-fibre SBR-BR, P = 0.46 MPa.

The average wear volume at velocities of 0.05, 0.20 and 0.30 m/s are 0.47 ± 0.01, 0.99 ± 0.28 and 2.80 ± 0.29 mm^3, respectively. It indicates that the contact area of the material at high velocity is larger than the contact area at low velocity at the end of the test (position 2 in Figure 3.9). Since the coefficient of friction at high velocity shows a lower value than that at a low velocity, the frictional shear stress at high velocity is greatly reduced.

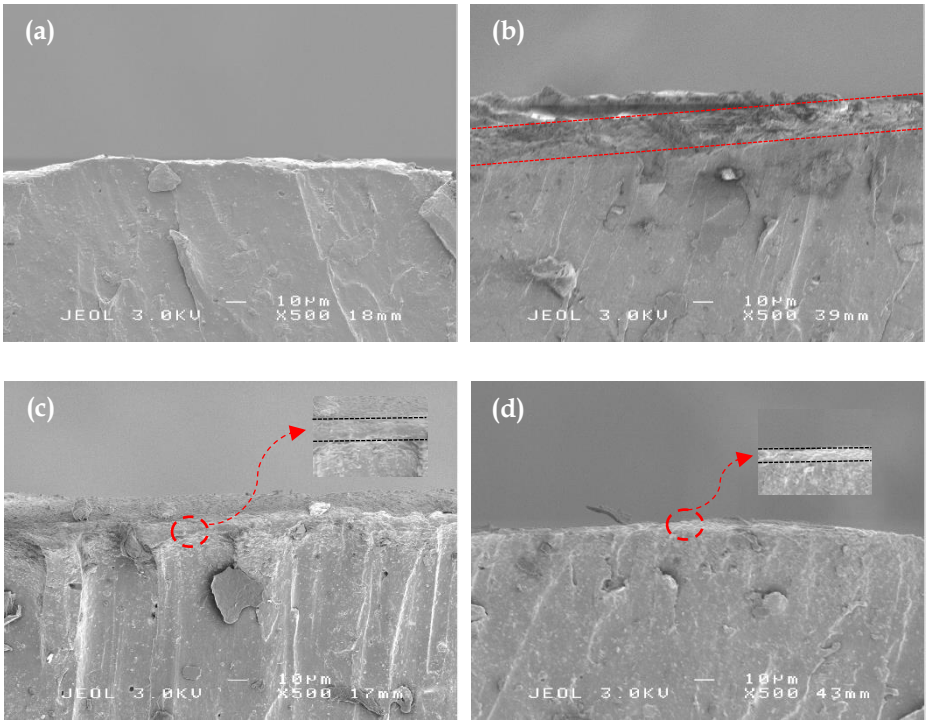

Figure 3.10: SEM cross-section images of the wear track: (a) position 1 (see Figure 3.9) at a velocity of 0.30 m/s; (b) position 2 at a velocity of 0.30 m/s; (c) position 2 at a velocity of 0.20 m/s; and (d) position 2 at a velocity of 0.05 m/s.

To analyse the existence of a modified surface layer, cross-sections of the wear tracks were observed with a Scanning Electron Microscope (SEM). Figure 3.10(a) shows the cross-section at position 1 (see Figure 3.9) of the material with a velocity of 0.30 m/s. The upper part of the image shows the surface of the wear track which was in contact with the counter surface and the bottom part of the image shows the bulk of the material. No difference between the bulk of the material and the material near the wear track is observed. The cross-section at position 2 (see Figure 3.9) of the material with a velocity of 0.30 m/s is given in Figure 3.10(b). It can be seen that a modification of the material has developed at the surface. The thickness of the modified surface layer is approximately 15 μm. A similar procedure was done for the materials with velocities of 0.20 and 0.05 m/s. Figure 3.10(c) and Figure 3.10(d) show that the modified surface layers were developed at the surface of the wear track. The thickness of the modified surface layer for the velocities of 0.20 and 0.05 m/s are approximately 5 μm and 3 μm, respectively.

The degradation in mechanical properties of the modified surface layer was proven using an Atomic Force Microscopy (AFM) [32]. The thickness of the modified

surface layer is the source of the magnitude of the decrease in frictional shear stress. A thicker modified surface layer will lead to a large degradation of the mechanical properties and therefore a larger reduction of the frictional shear stress will be found.

Figure 3.11 shows the coefficient of friction as a function of sliding distance at a sliding velocity of 0.20 m/s for four different contact pressures. Different trends of the coefficient of friction as a function of sliding distance are observed. When a low contact pressure (P = 0.24 MPa) is used, the coefficient of friction increases until the end of the test. A decreasing coefficient of friction is observed when a contact pressure of 0.46 MPa is used. When a contact pressure of 0.66 MPa is used, a relatively constant coefficient of friction is observed once the maximum coefficient of friction is reached. An increasing coefficient of friction until the end of the test is also observed when a high contact pressure (P = 0.78 MPa) is used.

The trend of the coefficient of friction is influenced by the existence of a modified surface layer. When a modified surface layer is present in the wear track, a decreasing coefficient of friction will be observed, see Figure 3.10(c) for a contact pressure of 0.46 MPa. If a decreasing coefficient of friction is not found, the modified surface layer is not developed, see Figure 3.12(a) for a contact pressure of 0.24 MPa.

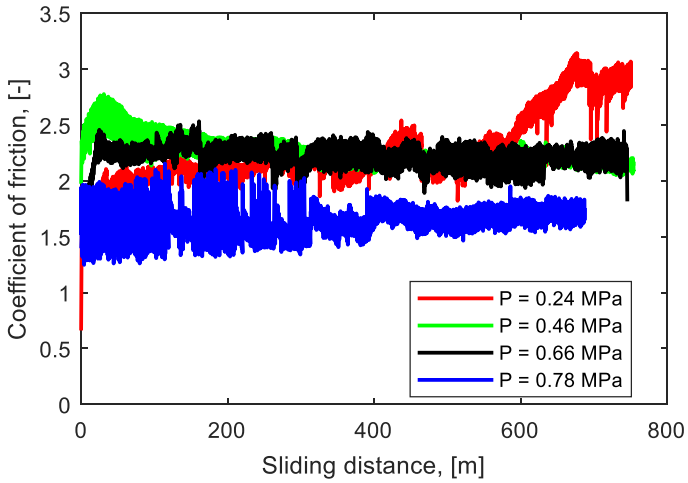

Figure 3.11: Coefficient of friction as a function of sliding distance for different contact pressures, non-fibre SBR-BR, v = 0.20 m/s.

The existence of a modified surface layer is controlled by a competition between the formation rate of the surface layer and the wear rate [35]. Figure 3.12(b) shows the image of the wear and formation processes on the wear surface of the elastomer. When the formation rate is higher than the wear rate, the modified

surface layer will be developed. However, when the formation rate is lower than the wear rate, the modified surface layer will be completely removed by the wear, so no modified surface layer is observed.

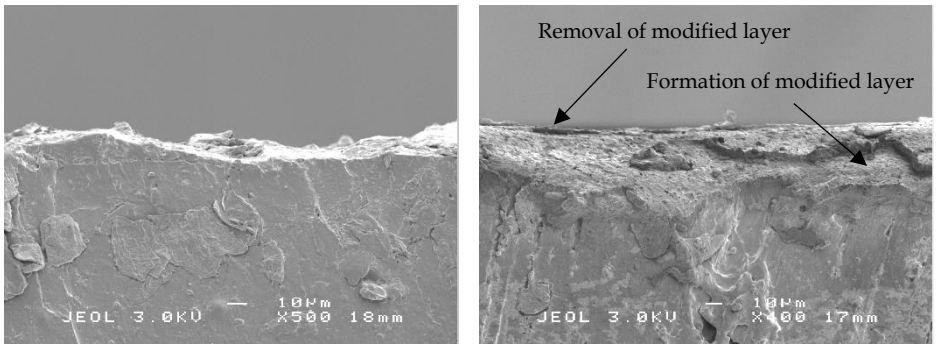

(a) (b)

Figure 3.12: SEM cross-section images of the wear track: (a) at a contact pressure of 0.24 MPa and a velocity of 0.20 m/s; (b) Competition between the formation and removal of the modified surface layer in the wear track.

The effect of the roughness of the counter surface on the coefficient of friction is depicted in Figure 3.13. Three values of the roughness of counter surface were used, namely smooth (roughness = 1.16 ± 0.18 μm), medium (roughness = 2.55 ± 0.16 μm) and rough (roughness = 8.63 ± 0.27 μm). A decreasing coefficient of friction occurs in all cases. As expected, the rough indenter has the lowest coefficient of friction, see Figure 3.13(a). It is caused by the fact that the real contact area between the elastomer and the rough indenter is lower the others, while the coefficient of friction of the smooth indenter is higher than that of the medium roughness of the indenter.

The normalized coefficient of friction (the ratio of the coefficient of friction and the maximum coefficient of friction for each test) of all tests can be seen in Figure 3.13(b). Although the coefficient of friction of each test are different, the decreasing coefficient of friction of those tests show the same behaviour. The differences between the maximum coefficient of friction and the steady-state coefficient of friction is approximately 15% for all tests. This indicates that the modified surface layer is similar under different roughness values of the counter surface.

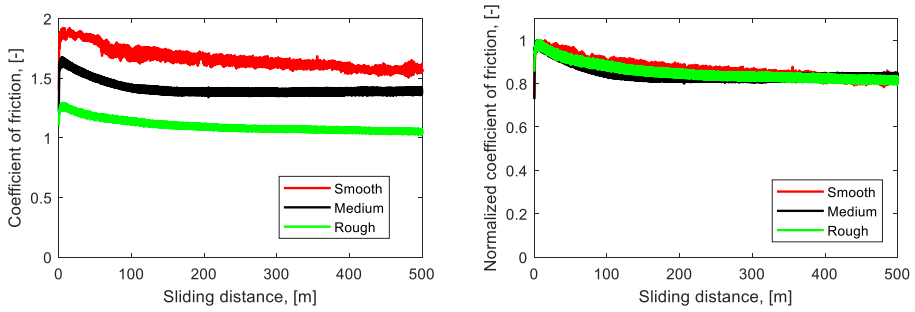

(a) (b)

Figure 3.13: (a) Coefficient of friction and (b) normalized coefficient of friction as a function of sliding distance for different indenter roughness values, non-fibre SBR-BR, v = 0.20 m/s, P = 0.34 MPa.

Based on the experimental results, a mechanism of the competition between the wear depth and formation of the modified layer thickness as a function of sliding distance is proposed, see Figure 3.14. For an unworn surface, the heights of the microscopic asperities are not uniform. When two unworn surfaces are loaded for the first time and move relative to one another, the high spots of the asperities are reduced due to the wear process. Therefore, the wear increases quite quickly at the beginning of the test and slows down gradually because the wear surface becomes smoother [36]. Elastomers are not an exception in this concept [37, 38].

On the other hand, the modified layer also grows with increasing sliding distance. There are several possible sources of the degradation of the mechanical properties at the top layer. Part of the frictional energy exerted in the elastomer is absorbed by heat generation. The generated heat may change the mechanical properties of the elastomer through increasing temperature [39]. The evolution of the elastomer network is another possible source of the degradation of the mechanical properties. The breakage of filler-matrix interaction due to repeated stress and strain exerted on the elastomer (Mullins and Payne effects) can be a determining factor in the mechanical degradation of elastomers [40]. The degradation of mechanical properties does not only happen in tensile loading but also under compression and shear loading [41, 42]. The repeated stress during sliding contact in combination with heat generation in the elastomer may break the filler-matrix interaction, so the degradation of the mechanical properties will be found at the top layer of the elastomer. The formation of the modified layer increases marginally at an earlier stage of the contact than the wear, which increases quickly at the early stage.

There are three possible results due to the competition between the wear and the formation. Figure 3.14(a) shows schematically that the wear is larger than

the layer formation, so no modified surface layer will be observed. As a result, the decreasing coefficient of friction phenomenon is not found. This phenomenon occurs when the energy input is too low or too high.

Figure 3.14(b) shows the coefficient of friction is constant once a maximum coefficient of friction is reached. At the beginning of the test, the wear depth is larger than the thickness formation of the modified surface layer. As a result, no modified surface layer will be found. The coefficient of friction increases since the contact area between the elastomer and the counter surface grows due to the wear process. After a certain sliding distance, the wear rate reduces because the wear surface becomes smooth and only a small amount of wear occurs. The wear and the formation rate will be approximately the same, so the coefficient of friction will reach a steady-state value. This phenomenon occurs in the test at a contact pressure of 0.66 MPa, see Figure 3.11.

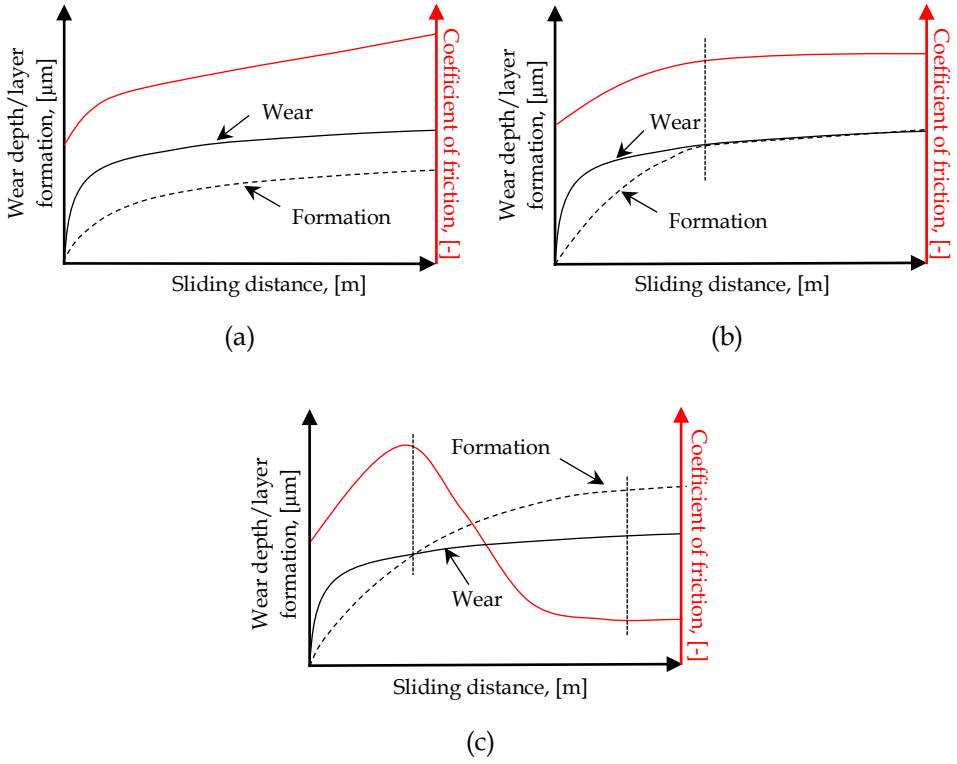

Figure 3.14: The schematic wear depth, layer formation and coefficient of friction as a function of sliding distance: (a) formation < wear; (b) formation ≈ wear; (c) formation > wear.

The third possibility can be seen in Figure 3.14(c). At the beginning of the test, the wear depth is greater than the thickness of layer formation, so the coefficient of friction increases. At a certain sliding distance, the formation rate will be greater than the wear rate because the wear surface is smooth. As a result, the modified surface layer will be developed and the coefficient of friction decreases until the minimum value is reached. The steady-state coefficient of friction will be found when the wear and the formation rate are nearly the same.

P [MPa] / v [m/s]	0.24	0.46	0.66	0.78
0.05		△		
0.20	○	◊	◁	▷
0.30		□		

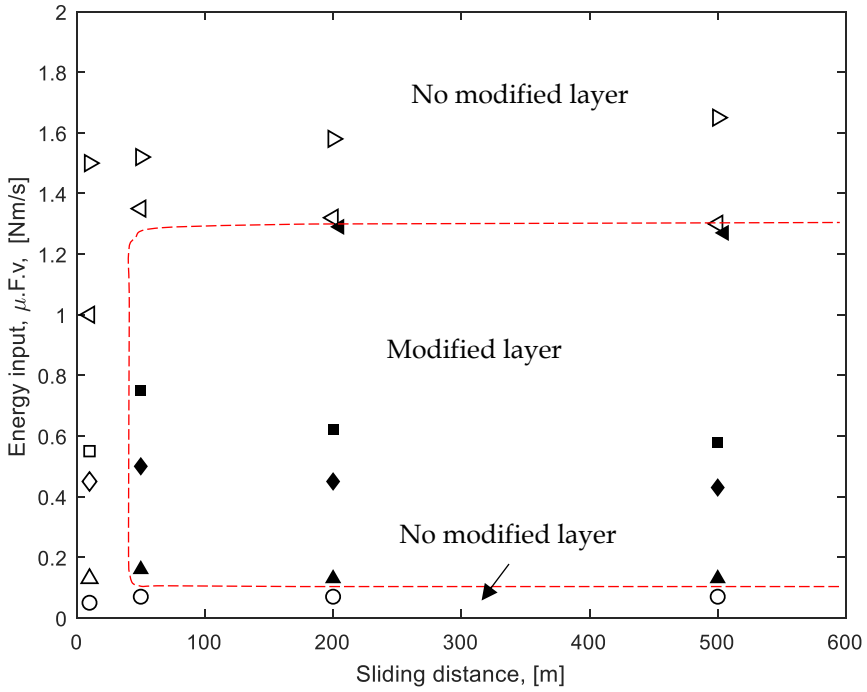

Figure 3.15: Schematic map of a modified surface layer formation, the existence of a modified surface layer is indicated with bold markings.

It has been observed that the formation of a modified surface layer depends on the velocity, contact pressure and sliding distance. Based on the experimental results, a map of the modified surface layer formation is proposed, see Figure 3.15.

The formation of a modified surface layer depends on the energy input and the sliding distance. At a short sliding distance, no modified layer will be formed because the wear rate is much greater than the surface layer formation rate. The highest wear rate occurs during the running-in phase. By increasing the sliding distance, the modified surface layer may be formed when the energy input is high enough. However, when the energy input is too low, the modified surface layer will not be developed even when a long sliding distance is performed. The modified surface layer is also not observed when the energy input is too high because the wear is too high.

The effect of material properties of the elastomer is not taken into account in the present study. However, it may influence the lines in the map. Better mechanical properties of an elastomer, for instance, will result in a low wear rate. However, at the same time, the formation of a modified surface layer is more difficult.

3.3 Wavy wear track

Elastomeric materials that are in contact with a rigid counter surface often produce a periodic feature. Such a periodic pattern often generates surface instabilities at the elastomer surface. The resulting dynamics and fluctuations significantly reduce the performance of the rolling/sliding system, especially with respect to the positional accuracy, stability [43], vibration and noise [44]. Due to these disadvantages, the development of periodic wear patterns should be prevented in practical applications. The development of periodic features and wear patterns have been investigated previously using needle [45-48] and blade [37, 49-53] indenters as a counter surface.

For a sliding friction situation between an elastomer and a rigid sphere, a macro wear pattern known as wavy wear track may be created on the elastomer surface. This wavy wear track generates severe vibration in the system and furthermore influences both the frictional and wear behaviour. Several experimental studies have been reported considering the stick-slip motion for the sliding contact between a rigid ball and an elastomer flat surface [54-56]. However, the key parameters that influence the occurrence of a wavy wear track are not fully understood and, as a result, there is no method available to describe or predict the formation and the properties of the wavy wear track.

During sliding contact, oscillations may occur both in the normal and tangential (sliding) direction. For a high sliding velocity, the normal direction oscillation of the elastomer surface dominates the total dynamic response, meaning that the vibrations in tangential direction can be neglected. This study focuses on the

macro scale irregularity of the wear track due to the normal oscillation of the system. The normal oscillation frequency of the system is defined as [57]:

$$f_n = \frac{1}{2\pi}\sqrt{\frac{k_n\left(1-{\xi_f}^2\right)}{m_w+m_f}} \tag{3.10}$$

where f_n is the frequency of the indenter system in normal direction, k_n is the normal stiffness of the elastomer, ξ_f is the damping factor of the indenter frame, m_w is the dead weight mass and m_f is the inertia mass of the indenter frame. Since the materials used in the present study behave in an isotropic-viscoelastic manner, the indentation depth can be estimated as [19]:

$$\delta = \left(\frac{9{F_N}^2}{16{E^*}^2 R}\bar{\phi}(t)\right)^{1/3} \tag{3.11}$$

where δ is the indentation depth, F_N is the normal force, E^* is the effective elastic modulus, R is the radius of the spherical counter surface, and $\bar{\phi}(t)$ is the normalized creep compliance. The stiffness in normal direction of the material is defined as the ratio of the normal force and the indentation depth:

$$k_n = \frac{F_N}{\delta} \tag{3.12}$$

The wave length (Δx_n) of the wavy wear pattern is the ratio of the given velocity (v) and the normal frequency of the system, which is defined as:

$$\Delta x_n = 2\pi v\sqrt{\frac{m_w+m_f}{k_n\left(1-{\xi_f}^2\right)}} \tag{3.13}$$

Figure 3.16(a) shows the different locations of the waves between the different cycles. The aforementioned term 'cycle' means one revolution of the disc. When the locations of the waves are different in each cycle, the wear track becomes relatively smooth after a large number of cycles, and the wavy wear track will not be visible, see Figure 3.16(b). However, when the locations of waves are at the same position in every cycle, the wavy wear track will be visible at the surface after the test. This means that a wavy wear track will be visible when the ratio between the circumferential distance of the wear track and the wave length is an integer. The number of wavy wear patterns in the circumferential of wear track can be expressed as:

$$n = \frac{2\pi r}{\Delta x_n} \tag{3.14}$$

where, n is the number of the wavy wear patterns and r is the radius of the wear track.

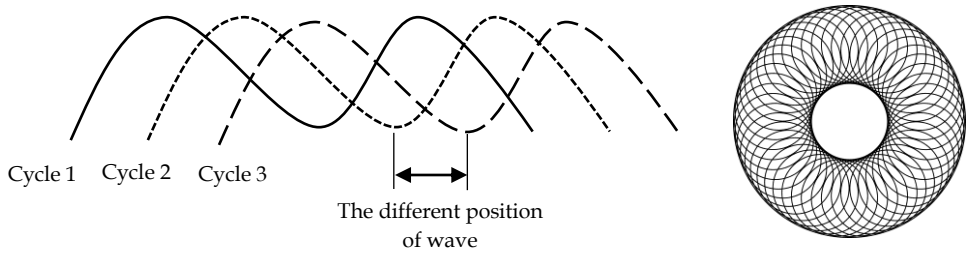

(a) (b)

Figure 3.16: (a) The waves at three different locations, (b) the final wear track for a large number of cycles when the locations of waves are different in each cycle, shown schematically.

A pin-on-disc tribometer was equipped with a ball with a radius of 12.5 mm, sliding against an elastomer flat disc. The tests were performed under dry conditions and at room temperature. Table 3.2 lists the operating conditions that were used in the present study. For the SBR-BR material, a different radius of the wear track was used, see test #1 to test #3 in Table 3.2. The normal force and sliding velocity were varied for the SBR material. Due to the lack of a damper in the pin-on-disc tribometer set-up, the damping factor of the counter surface frame is neglected (ξ_{nd} = 0). The inertia mass of the frame in the present study is approximately 0.26 Kg.m^2. Since the type and the dimension of the rigid ball are the same for all tests, the inertia mass of the counter surface frame (m_f) is the same for all tests.

Figure 3.17 shows the wear tracks for all tests at the end of the tests. It can be seen that the wavy wear tracks are visible in tests #1, test #5 and test #6, while relatively smooth wear tracks are observed in test #2 to test #4. The comparison between the analytical model and the experimental results for all tests are summarized in Table 3.2. It can be seen that the number of the wavy wear pattern in the circumferential direction for test #2 to test #4 are not integers. As a result, no wavy wear pattern is observed, while the number of wavy wear patterns for test #1, test #5 and test #6 are in agreement with the experimental results. In this thesis, the operating conditions to analyse the tribological behaviour of short-cut aramid fibre reinforced elastomers were chosen to avoid the wavy wear track.

Table 3.2: The comparison between analytical model results and experimental results.

Tests ID	Disc material	Operating conditions			Δx_n [mm]		$\frac{2\pi r_{track}}{\Delta x_n\ (model)}$
		Force [N]	Velocity [m/s]	Radius of track [mm]	model	experiment	
#1	SBR-BR	2	0.2	6	7.56	7.54	4.99 ≈ 5
#2	SBR-BR	2	0.2	12.5	7.56	-	10.39
#3	SBR-BR	2	0.2	19	7.56	-	15.80
#4	SBR	3	0.2	12	7.81	-	9.65
#5	SBR	5	0.2	12	8.37	8.38	9.01 ≈ 9
#6	SBR	5	0.3	12	12.55	12.56	6.01 ≈ 6

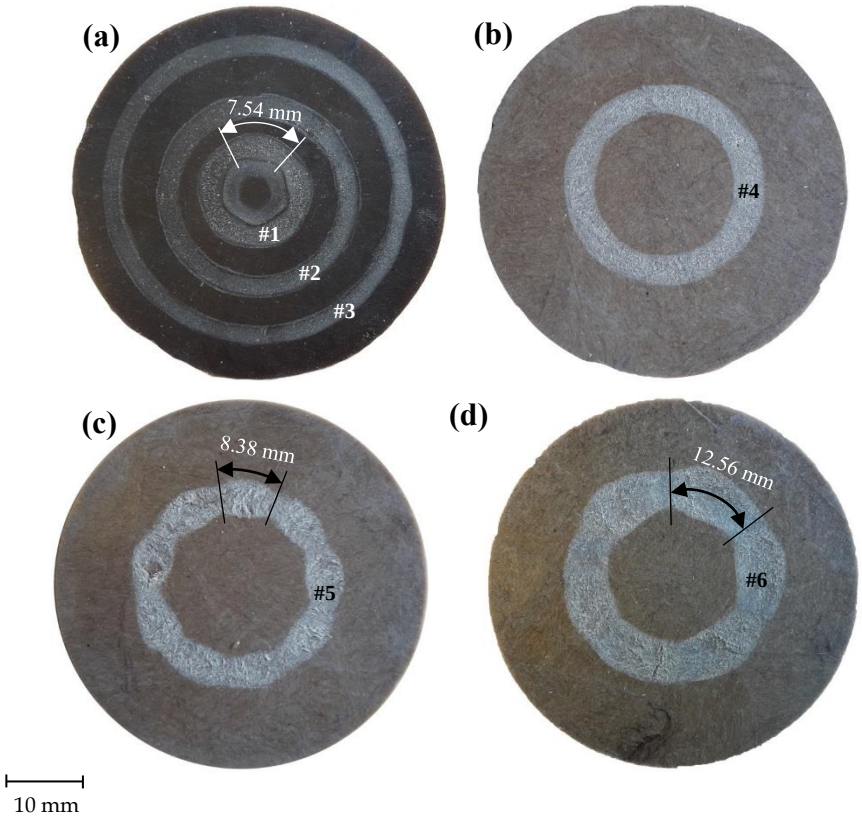

Figure 3.17: The wear tracks in the elastomer surfaces for all tests, (a) test #1 to #3, (b) test #4, (c) test #5 and (d) test #6.

3.4 Summary

The tribological phenomena of elastomers during sliding friction were investigated in this chapter. The effect of velocity on the contact area of elastomers was studied both theoretically and experimentally. The contact area of elastomers decreases with increasing velocity. It is influenced by the mechanical properties of the elastomers. The existence of a modified surface layer during sliding friction was studied considering the effect of normal force, velocity and surface roughness of the counter surface. The existence of a modified surface layer depends on the competition between the formation rate of the layer and the wear rate. A map of a modified surface layer formation is proposed based on the experimental results. Another phenomenon which is investigated in this chapter is the occurrence of a wavy wear track. The wavy wear track will be visible when the ratio between the circumferential distance of the wear track and the wave length is an integer. An analytical model was developed to predict the occurrence of a wavy wear track, and it shows good agreement with the experimental results.

Chapter 4 Friction, Wear and Noise of Fibre Reinforced Elastomers

Friction, wear and noise generation are important phenomena during sliding contact of elastomeric materials. Wear reduction of elastomers can be achieved by minimizing the propagation of cracks during sliding contact. Adding fillers like silica and fibres is a way of stopping the propagation of cracks, and adding fillers into the elastomers may also influence the noise generation due to friction. During sliding contact, wear phenomenon alters the contacting surfaces and therefore changes frictional behaviour. Understanding the wear processes of short-cut aramid fibre reinforced elastomers and their relation to friction and noise generation may contribute to making an optimum design and prolong the lifetime of elastomer based products. In this chapter, the friction, wear and friction-induced noise of short-cut aramid fibre reinforced elastomers with and without silica reinforcement are investigated.

4.1 Short-cut aramid fibre reinforced elastomers

In this section, friction and wear mechanism of elastomers reinforced with solely short-cut aramid fibres is investigated. The elastomers are reinforced only with the short-cut aramid fibres without other reinforcing fillers, so as to obtain a better understanding of the tribological behaviour of short-cut aramid fibre reinforced elastomers. Moreover, the effect of reinforcement direction of fibres, the effect of the amount of fibre, and the validity of Amontons' law are studied.

4.1.1 Friction and wear mechanism

Wear of elastomer plays an essential role in the frictional behaviour. During sliding contact, the surface roughness changes due to wear of the elastomer surface. The alteration of surface roughness changes the real contact area between the elastomer and the rigid counter surface, and furthermore friction changes. A detailed

examination of the wear process on the friction behaviour may enable an understanding of the relation between wear and friction of short-cut aramid fibre reinforced elastomers. The wear processes and their relation to friction of the SBR composite containing 15 NF with randomly oriented fibres are studied in this sub-section.

Figure 4.1 shows the coefficient of friction as a function of sliding distance for the SBR composite containing 15 NF with randomly oriented fibres. In general, the behaviour of the coefficient of friction has four distinct stages: (1) the coefficient of friction increases, (2) the coefficient of friction reaches a maximum, (3) the coefficient of friction decreases drastically and (4) the coefficient of friction reaches a steady-state value. The wear process of short-cut aramid fibre reinforced elastomers at every stage is studied by using a Keyence VHX-5000 Microscope.

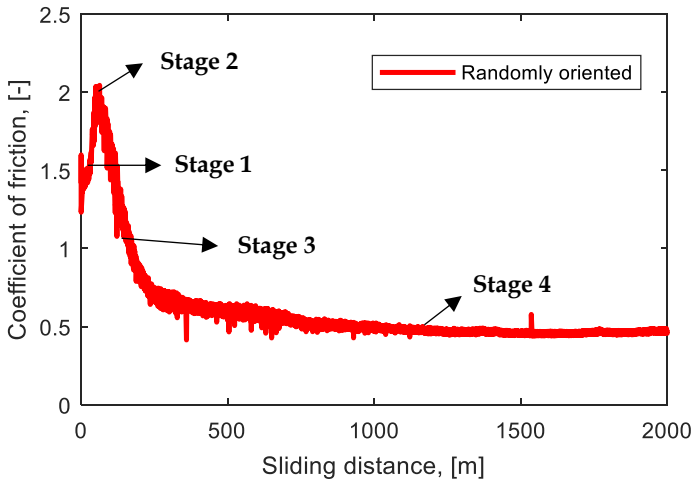

Figure 4.1: Coefficient of friction as a function of sliding distance of the SBR composite containing 15 NF with randomly oriented fibres, P = 0.2 MPa, v = 0.2 m/s.

Figure 4.2 shows the wear images at every stage indicated in Figure 4.1. At the first stage of the coefficient of friction curve, initiation of cracks occurs in the elastomer matrix because of its poor mechanical properties, see Figure 4.2(a). Because of wear, the contact area between the composite and the counter surface increases. Therefore, the coefficient of friction increases in this stage, see Figure 4.1. In the second stage of the coefficient of friction curve, the coefficient of friction reaches a maximum value. The wear mechanism in this stage is depicted in Figure 4.2(b). It shows that some elastomer matrix pull-out from the composite takes place.

When many elastomer particles are pulled out from the matrix, some of the fibres stick out of the composite, see Figure 4.2(c). They are present on the wear surface and align in the direction of sliding. The existence of fibres on the wear surface will result in an increasing surface roughness, which leads to the reduction of the real contact area between the elastomer and the counter surface. Hence, the coefficient of friction decreases to approximately four times lower than that of the maximum value, see the third stage in Figure 4.1.

Due to the repeated sliding contact, the processes of initiation and propagation of cracks occur continuously. After a certain sliding distance, many fibres cover the wear surface, see Figure 4.2(d). They orient in the direction of sliding and prevent the composite from the initiation and the propagation of cracks. As a result, wear of the composite is reduced. Since the counter surface is in contact mainly with the fibres, the coefficient of friction is controlled by the fibres and reaches a steady state value.

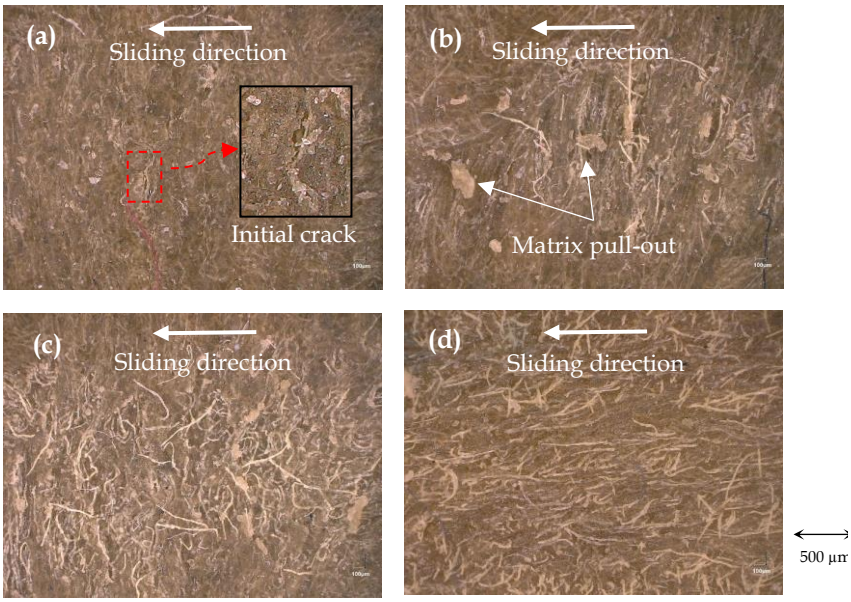

Figure 4.2: Wear processes of short-cut aramid fibre reinforced elastomers: (a) the first stage; (b) the second stage; (c) the third stage; and (d) the fourth stage of the coefficient of friction curve (see Figure 4.1).

Basically, the wear of an elastomer can be minimized if the crack mean free path is reduced [58]. Figure 4.3(a) shows the crack propagated in the non-fibre SBR from the cross-section view of the wear track. The wear of the composite can be minimized if this crack is avoided or stopped. Adding fibres is a way to stop this

crack. Instead of penetrating further into the composite, the crack will be stopped by the fibres and it bends to the composite's surface when the crack reaches these fibres, see Figure 4.3(b).

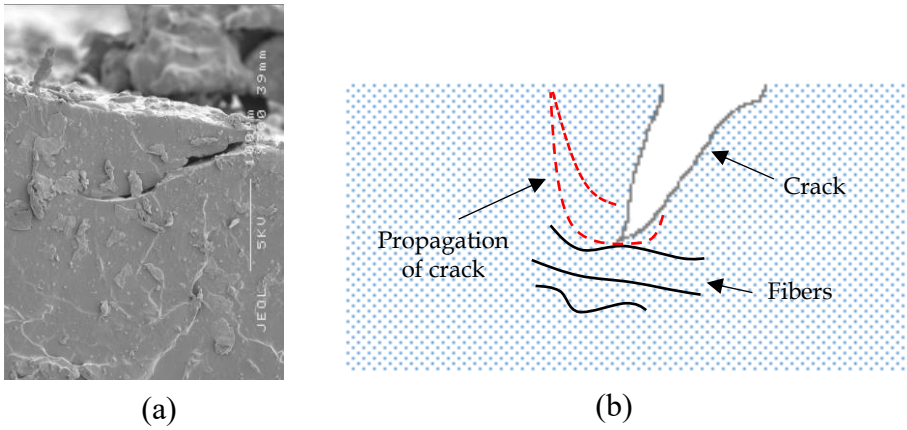

Figure 4.3: (a) Crack propagation of the non-fibre SBR composite, cross-section view; (b) Crack is stopped by fibres and it bends to the elastomer surface, shown schematically.

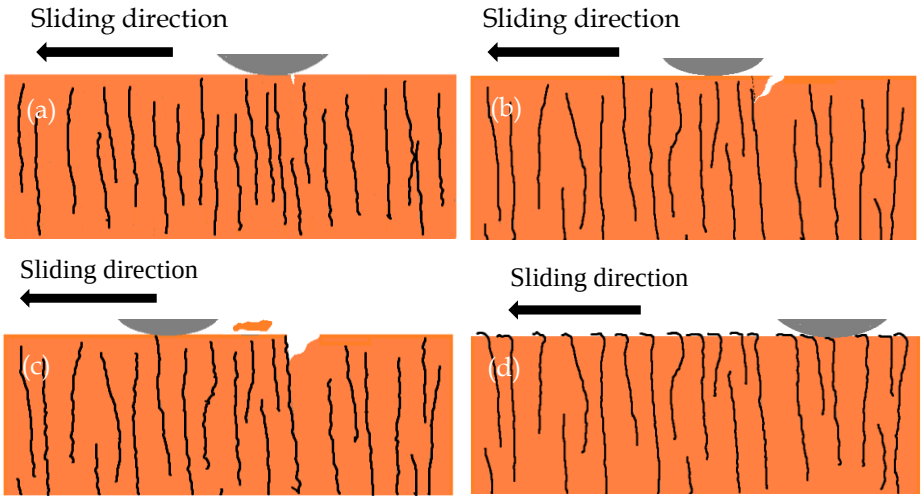

Figure 4.4: Wear process of short-cut aramid fibre reinforced elastomers, shown schematically: (a) initiation of the crack in the elastomer matrix; (b) propagation of the crack; (c) the elastomer matrix is pulled out because the crack bends to the elastomer surface; and (d) the part of the fibres that protrude above the surface bend and align in the direction of sliding.

Based on the experimental results, the wear processes of short-cut aramid fibre reinforced elastomers can be explained by Figure 4.4. In the initial part of the sliding distance, cracks are formed in the elastomer matrix because it has poorer mechanical properties than the fibre. The cracks are initiated in the trailing edge of the contact because the strain is concentrated at that area [46], see Figure 4.4(a). The propagation of cracks occurs in the direction of sliding. When the crack reaches the fibre it stops, and it bends to the elastomer surface instead of penetrating further into the composite, see Figure 4.4(b). Due to the repeated sliding contact, parts of the elastomer matrix will be pulled out from the composite, see Figure 4.4(c). Depending on the orientation of fibres and the fibres-matrix bonds, some fibres can be pulled out completely, cut off, or only a part of the fibres which stick out from the composite will be present on the wear surface and align in the sliding direction, see Figure 4.4(d).

4.1.2 The effect of reinforcement direction

The effect of fibre orientation in short-cut aramid fibre reinforced elastomers was investigated using three types of reinforcement directions, namely longitudinal, transverse and normal orientation. Longitudinal orientation means that the fibres are oriented in the sliding direction. Transverse orientation means that the fibres are oriented perpendicularly to the sliding direction. Normal orientation means that the fibres are oriented perpendicular to the composite's surface, see Figure 4.5. The operating conditions of the pin-on-disc tribometer experiments for these composites were a velocity of 0.2 m/s, a contact pressure of 0.2 MPa and at ambient temperature. The tests were repeated three times for each composite. The normal load was adapted depending on the reinforcement direction based on the anisotropic-viscoelastic contact model [19].

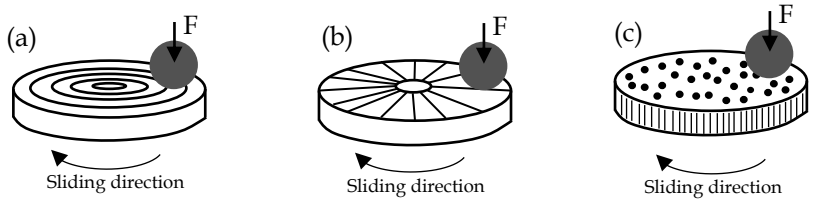

Figure 4.5: Fibre orientation of the composites for tribometer tests, shown schematically: (a) longitudinal orientation; (b) transverse orientation; and (c) normal orientation.

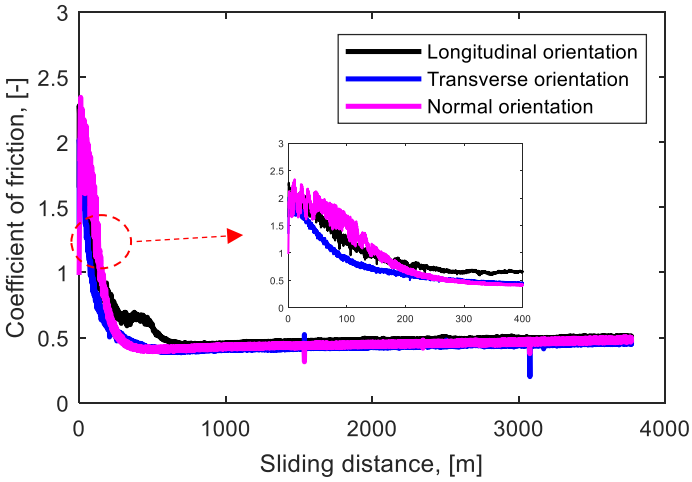

Figure 4.6: Coefficient of friction as a function of sliding distance for the SBR containing 15 NF for several reinforcement directions.

The results of the tribometer tests for all reinforcement directions are depicted in Figure 4.6. The coefficient of friction for all reinforcement directions shows different values in the running-in process (the sliding distance from 0 to ~ 700 m). However, after a sliding distance of approximately 700 m, the coefficients of friction show the same steady-state values for all reinforcement directions. The tribometer tests were stopped at a sliding distance of 3770 m. Although these composites have different mechanical properties, causing the contact areas to be different [59], the coefficient of friction are the same for all composites at the steady-state situation. It suggests that the surface properties control the coefficient of friction. In this case, the coefficient of friction is controlled by the existence of fibres on the wear surface. Figure 4.7 shows the wear surfaces of all composites at the end of the tests. It can be seen that the fibres are present on the wear surface for all composites and they align in the sliding direction.

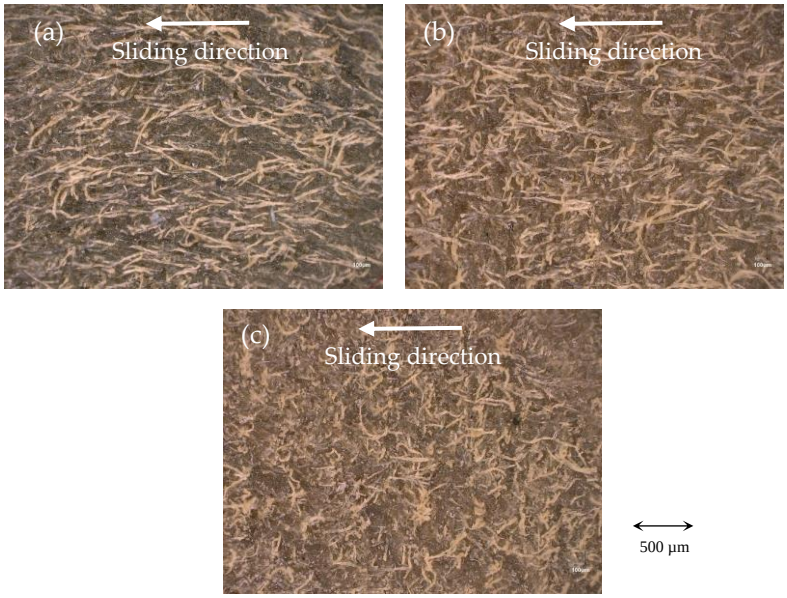

Figure 4.7: The wear surfaces at the end of the tribometer tests for all composites: (a) longitudinal orientation; (b) transverse orientation; and (c) normal orientation.

The specific wear rates for all reinforcement directions can be seen in Figure 4.8. It shows that the composite containing fibres in normal direction gives the lowest specific wear rate, while no significant difference in specific wear rate is observed between the composite containing fibres in longitudinal and transverse orientation. When the fibres are aligned parallel to the surface composite, i.e. longitudinal and transverse orientation, the fibre pull-out occurs easier than that in normal orientation. Therefore, the specific wear rates of the composites reinforced in longitudinal and transverse orientation are higher than that for the normal orientation. The difference between transverse and longitudinal orientation is less clear. Several studies concluded that the wear of the composites containing transversely oriented fibres is greater than those containing longitudinally oriented fibres [60, 61]. However, other studies show the opposite results [62-64].

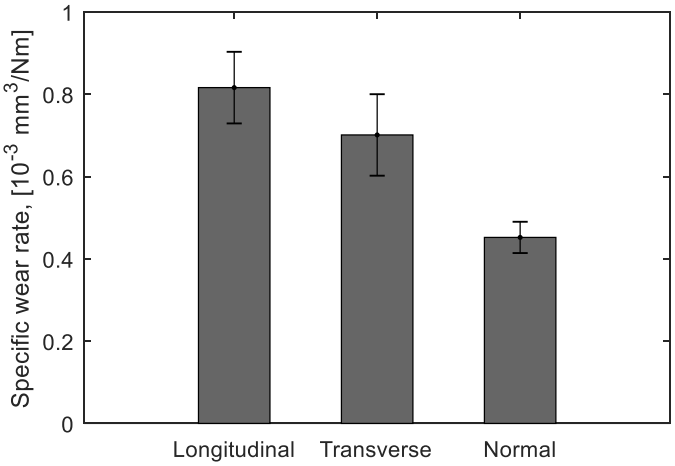

Figure 4.8: The specific wear rates of the SBR composites containing 15 NF for three types of reinforcement directions, P = 0.2 MPa, v = 0.2 m/s.

When the fibres are aligned in the normal direction, the fracture of fibres will require a tensile loading due to a mechanical pulling action at the interface. However, the pull-out mechanism occurs with difficulty since the composite containing fibres in normal orientation are deeply embedded in the matrix and offer the greatest resistance to detachment. Moreover, the lateral deformation will be constrained by the presence of neighbouring fibres, and fibres which stick out from the matrix will orient to the direction of sliding. Figure 4.7(c) shows that the composite containing fibres in normal orientation has shorter fibres on the wear surface than those in longitudinal and transverse orientation. As a result, the composite containing fibres in normal orientation shows the lowest specific wear rate.

4.1.3 The effect of fibre amount

The effect of fibre amount in the composite was investigated using three types of SBR composites, namely non-fibre SBR, SBR containing 3 NF and SBR containing 15 NF. The reinforcement direction of fibres for these composites is randomly oriented. The operating conditions for the non-fibre SBR and SBR containing 3 NF were a contact pressure of 0.075 MPa, a velocity of 0.1 m/s and ambient temperature. Due to the load limitation of the pin-on-disc tribometer, a contact pressure of 0.15 MPa was used for the SBR containing 15 NF. The tribometer tests were stopped at a sliding distance of 500 m.

The results show that the specific wear rates of the non-fibre SBR, SBR containing 3 NF and SBR containing 15 NF are 0.255 ± 0.008 mm^3/Nm, 0.133 ± 0.002 mm^3/Nm, and 0.008 ± 0.001 mm^3/Nm, respectively. The wear rate of the SBR containing 3 NF is lower than that of the non-fibre SBR. A far lower specific wear rate is observed for the SBR containing 15 NF than for the other SBR composites.

Figure 4.9 shows the wear characteristics of all SBR composites after tribometer tests. Figure 4.9(a) shows that the non-fibre SBR has a large crack at the wear surface. It is caused by the lack of inhomogeneous particles in the composite which can stop the propagation of cracks. The previous study showed that the larger the cracks, the lower the wear resistance [58]. This result confirms that the unreinforced composite has the worst wear resistance.

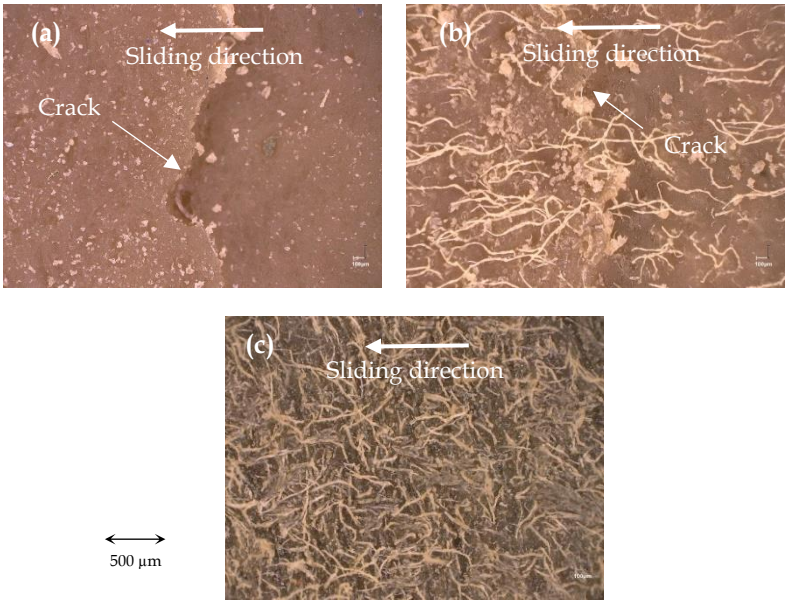

Figure 4.9: Wear surfaces after tribometer tests: (a) non-fibre SBR; (b) SBR containing 3 NF; (c) SBR containing 15 NF.

For the SBR containing 3 NF, cracks are also found at the wear surface, see Figure 4.9(b). Since only a small amount of fibres is added to the elastomer, the distance between those fibres in the elastomer is relatively large. Therefore, the cracks can penetrate further into the composite easily, so the wear resistance cannot be increased effectively. For SBR containing 15 NF, no cracks are found at the wear surface. Many fibres are present on the wear surface and align in the direction of

sliding at the end of the tests, see Figure 4.9(c). As a result, SBR containing 15 NF has better wear resistance than any of the other SBR composites. Although the fibres are also present on the wear surface of the SBR containing 3 NF, those fibres cannot protect the composite from the propagation of cracks under cyclic loading. Hence, the specific wear rate of SBR containing 15 NF is far lower than that containing 3 NF.

4.1.4 The validity of Amontons' law

Amontons' law states that the friction force is proportional to the normal force and is independent of the apparent contact area. In other words, the coefficient of friction does not depend on the normal force and the apparent contact area. In this subsection, the validity of Amontons' law is investigated using the SBR reinforced with 15 NF and 15 EF.

Figure 4.10 shows the results of the tribometer tests for the SBR composites containing 15 EF and 15 NF for several reinforcement directions. The operating conditions used in these tests were a contact pressure of 0.2 MPa, a velocity of 0.2 m/s and ambient temperature. Since the type and the reinforcement direction of fibres are different, the composites have different mechanical properties, see Figure 2.2. It causes the apparent contact area to be different [59]. Interestingly, the tribometer results show that the steady-state coefficient of friction of all composites are the same. It suggests that the coefficient of friction is independent of the apparent contact area.

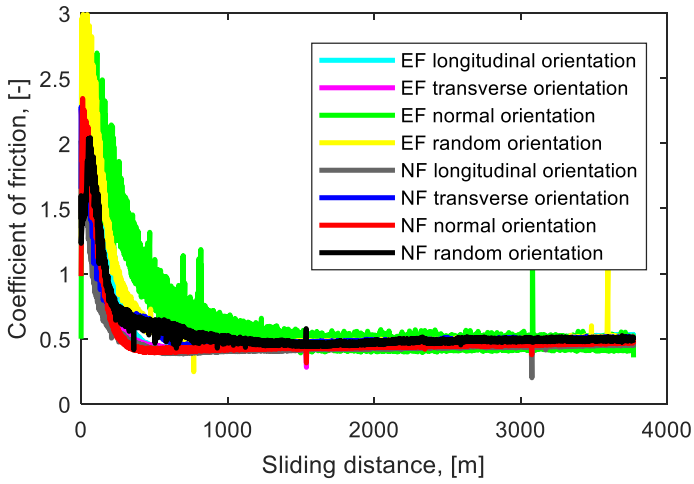

Figure 4.10: Coefficient of friction as a function of sliding distance for the SBR containing 15 EF and 15 NF for several reinforcement directions, P = 0.2 MPa, v = 0.2 m/s.

The validity of Amontons' law was investigated by varying the contact pressure in the tribometer tests. Figure 4.11 shows the coefficient of friction as a function of sliding distance of the SBR containing 15 EF at four different contact pressures. It can be seen that the steady-state coefficients of friction are uniform for contact pressures of 0.2 MPa, 0.25 MPa or 0.29 MPa, while the steady-state coefficient of friction changes when a contact pressure of 0.4 MPa is applied. Therefore, short-cut aramid fibre reinforced elastomers follow Amontons' law as long as the contact pressure does not exceed a threshold value. Once the contact pressure exceeds that threshold, Amontons' law is not valid anymore.

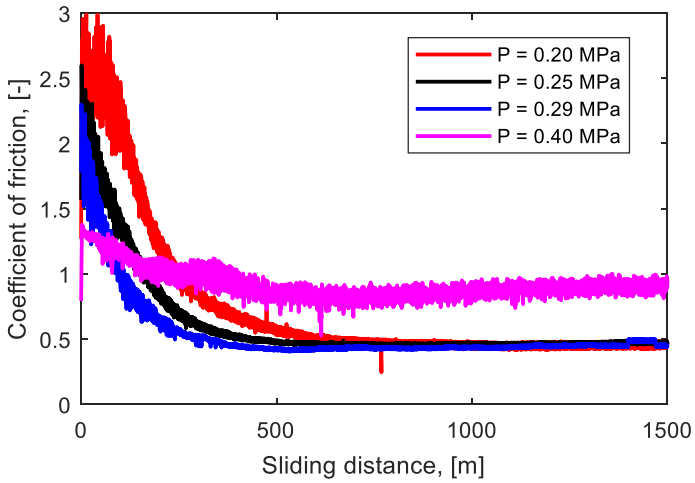

Figure 4.11: Coefficient of friction as a function of sliding distance for the SBR containing 15 EF at different contact pressures, v = 0.2 m/s.

Similarly, pin-on-disc tribometer tests at various contact pressures were also conducted with SBR containing 15 NF. Figure 4.12 shows the coefficients of friction at the steady-state phase for SBR containing 15 NF and 15 EF. It can be seen that both composites have a threshold contact pressure, at which Amontons' law is not valid when the contact pressure exceeds that threshold. For the SBR containing 15 NF, Amontons' law is not valid when a contact pressure of 0.24 MPa is applied, whereas Amontons' law is not valid when a contact pressure of 0.40 MPa is applied to the SBR containing 15 EF.

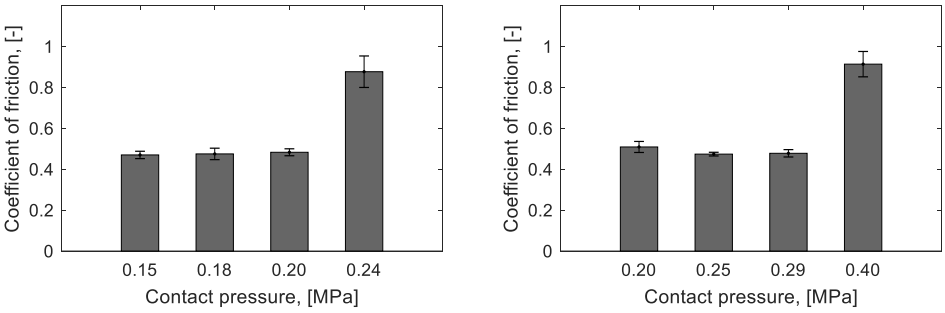

Figure 4.12: Steady-state coefficient of friction at various contact pressures: (a) SBR composite containing 15 NF; (b) SBR composite containing 15 EF.

The wear surfaces of the composites after the tribometer tests in which Amontons' law is valid and not valid are depicted in Figure 4.13. When many fibres are present on the wear surface and align in the sliding direction, the coefficient of friction follows Amontons' law, see Figure 4.13(a). Once the contact pressure exceeds the threshold, many fibres are pulled out from the composite, and severe wear is found. Hence, fewer fibres are present on the wear surface, see Figure 4.13(b). It was observed that the threshold contact pressure of the SBR containing 15 EF is greater than the SBR containing 15 NF. This can be explained by the different interfacial interaction between the fibres and elastomer matrix of those composites. The EF result in a better interfacial interaction with an elastomer matrix than the NF, as shown in the mechanical properties of those composites, see Figure 2.2. Therefore, a higher contact pressure is required to pull out many fibres from the composite as shown in Figure 4.13(b).

It was known that Amontons' law is not valid for rubber-like materials [46]. However, Amontons' law was found to be valid for short-cut aramid fibre reinforced elastomer below a threshold contact pressure. The proportionality between the real contact area and the normal force may be the source of this phenomenon. For plastic materials, plastic flow in the asperity contact region explains the proportionality between the real contact area and the normal force. However, for elastomers, the local pressure in the asperity contact regions reaches the rupture stress [27]. For short-cut aramid fibre reinforced elastomers, the proportionality between the real contact area and the normal force may be the result of the small ratio between the real and the apparent contact area. Persson suggested that the normal force is proportional to the real contact area when the ratio between the real and the apparent contact area is less than 10% [65]. The presence of fibres on the wear surface causes the counter surface to be in contact mainly with the fibres, so the real contact area is rather small. In this situation, Amontons' law will be valid. When the applied

contact pressure exceeds the threshold, many fibres are pulled out from the composite and the fibres will also be strongly pushed by the counter surface into the composite. As a result, the counter surface is in contact not only with the fibres but also with the elastomer matrix. In this situation, Amontons' law will be not valid.

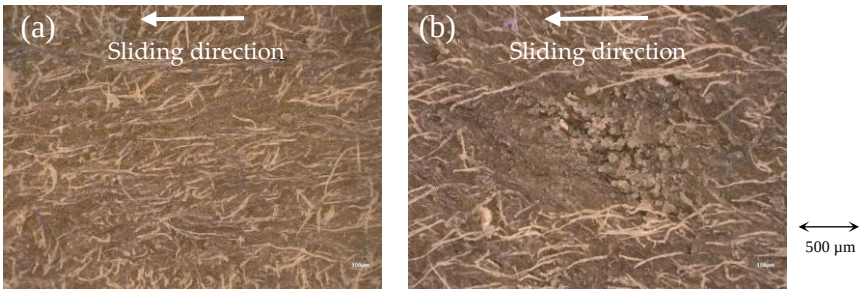

Figure 4.13: Wear surfaces after tribometer tests: (a) when Amontons' law is valid; (b) when Amontons' law is not valid.

4.2 Silica and short-cut aramid fibre reinforced elastomers

In the previous section, the composites are reinforced only with short-cut aramid fibres. Although the wear resistance increased, a high amount of wear still occurs in the composites. The lack of a small filler in the elastomer matrix leads to worse mechanical properties of the elastomer matrix. Therefore, the opening and propagation of cracks occur in the elastomer matrix easily. In this section, the tribological behaviour of elastomers which are reinforced with silica and short-cut aramid fibres is examined to investigate the effect of fibres in the composite for more realistic applications.

4.2.1 Friction and wear mechanism

Adding silica to the composite increases the mechanical properties of the composite drastically, see Figure 2.3. It may also change the tribological behaviour of the composite. Friction and wear mechanisms were investigated using SBR-BR reinforced by 20 NF randomly oriented. Two levels of energy input were used, namely high energy input (a contact pressure of 2.4 MPa and a velocity of 0.3 m/s) and low energy input (a contact pressure of 0.8 MPa and a velocity of 0.2 m/s). Figure 4.14 shows that at low energy input, the coefficient of friction increases at the beginning of the test. After a certain sliding distance, the coefficient of friction shows a constant value once reached the maximum coefficient of friction. Regarding the

stage of the coefficient of friction curve in Figure 4.1, the result of low energy input indicated that only the second stage is reached. A decreasing coefficient of friction is not found in this case. For high energy input, the coefficient of friction increases at a short sliding distance (first stage). Then it reaches a maximum coefficient of friction (second stage). After a sliding distance of ~ 1250 m, the coefficient of friction decreases until the end of the test (third stage). For a very long test duration, the coefficient of friction may reach the fourth stage once the rigid counter surface is in contact mainly with the short-cut aramid fibres.

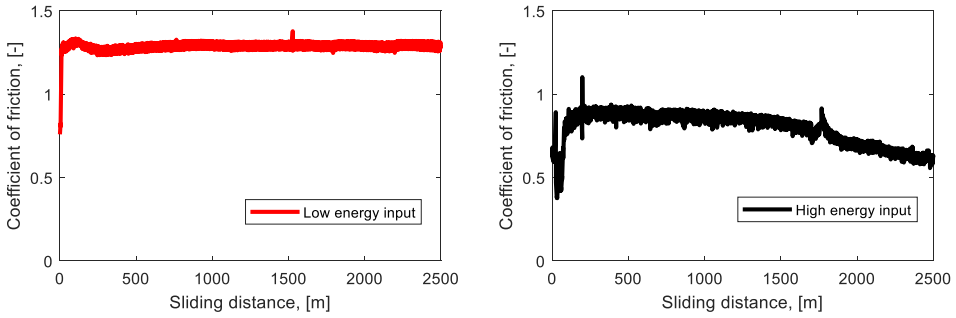

Figure 4.14: Coefficient of friction as a function of sliding distance of the SBR-BR containing 20 NF with randomly oriented fibres: (a) low energy input, Pv = 0.16 MPa.m/s; (b) high energy input, Pv = 0.72 MPa.m/s.

The wear surfaces of both composites after the tribometer tests is shown in Figure 4.15. For the composite at low energy input, a relatively smooth wear track is found at the wear surface, see Figure 4.15(a). The fibres which align parallel to the sliding surface are easy to be pulled out. Some grooves in the wear surface are found due to fibre pull-out. While the fibres which are deeply embedded in the matrix show greater resistance to detachment, only a small part of the fibres which stick out from the matrix are present on the wear surface. Figure 4.15(a) corresponds with the wear process of Figure 4.2(b), at which the coefficient of friction reaches a maximum coefficient of friction (second stage). The wear volume of the composite at low energy input is 7.13 ± 0.77 mm^3 (the specific wear rate is 0.24 × 10^{-3} ± 0.03 × 10^{-3} mm^3/Nm).

When high energy input is used, a higher wear loss is found for the composite than that at low energy input. The wear volume of the composite at high energy input is 17.38 ± 4.42 mm^3 (the specific wear rate is 0.60 × 10^{-3} ± 0.15 × 10^{-3} mm^3/Nm). As the contact pressure increases, each asperity of the counter surface penetrates deeper into the surface and increases wear. Moreover, a high velocity may increase the temperature, resulting in poorer mechanical properties of the

composite. Figure 4.15(b) shows the wear surface at high energy input after the test. It can be seen that many fibres exist on the wear surface. Since some elastomer matrix are pulled out, fibres which stick out from the elastomer matrix align to the direction of sliding. A rough surface is found at the high energy input test. Figure 4.15(b) corresponds to the wear process in Figure 4.2(c). This wear process causes the coefficient of friction to decrease.

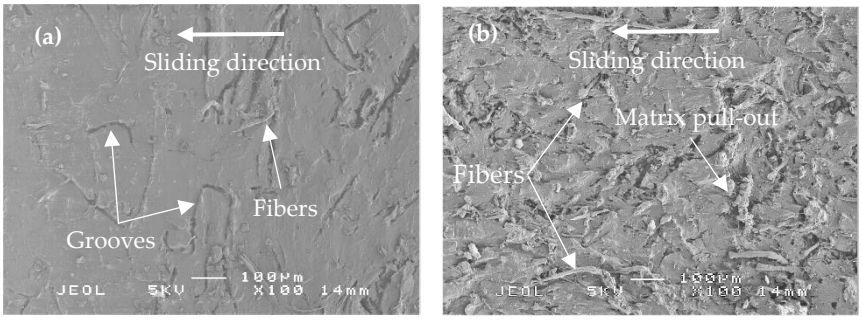

Figure 4.15: Wear surfaces of the SBR-BR containing 20 NF with randomly oriented fibres: (a) low energy input; (b) high energy input.

Wear of elastomers which are reinforced by silica and short-cut aramid fibre is lower than that of elastomers which are reinforced by solely short-cut aramid fibres. Since the size of the silica filler is very small (in the order of nanometres) and dispersed in the whole composite, they will stop the cracks at short length. For short-cut aramid fibre reinforced elastomers, the propagation of cracks will stop after rather long cracks, see Figure 4.16(a). As a result, wear of short-cut aramid fibre reinforced elastomers is higher than that of silica and short-cut aramid fibre reinforced elastomers. When the elastomers are reinforced with silica and short-cut aramid fibres, there are two possible wear processes:

1. When a low energy input is used, the crack will reach the inhomogeneous particle (silica) at a short propagation length, see Figure 4.16(b). Therefore, the wear particles of the elastomer matrix are rather small, and the wear track is relatively smooth, see Figure 4.15(a). Since only a few fibres exist on the wear surface, a decreasing coefficient of friction does not occur for this situation.
2. When a high energy input is used, the silica-matrix bonds will break, then the propagation of cracks extends to reach the fibre, see Figure 4.16(c). Since several fibres stick out from the elastomer matrix and exist on the wear surface, the coefficient of friction reduces, as found in the third stage of the friction curve in Figure 4.1. The decreasing coefficient of friction is caused by the reduction of the real contact area between the composite and the counter surface.

A high concentration of silica and fibres leads to reduction of the distance between these fillers in the composite. It will increase the wear resistance because the crack mean free path is reduced. However, a too high concentration of silica and/or fibres will lead to the agglomeration of filler networks and reduces the bond between the filler and elastomer matrix. As a result, the filler-matrix bond may be easily broken by propagation of cracks, hence the wear increases. A strong bond between the matrix and fillers is necessary to avoid pull-out in order to increase the wear resistance of the composite.

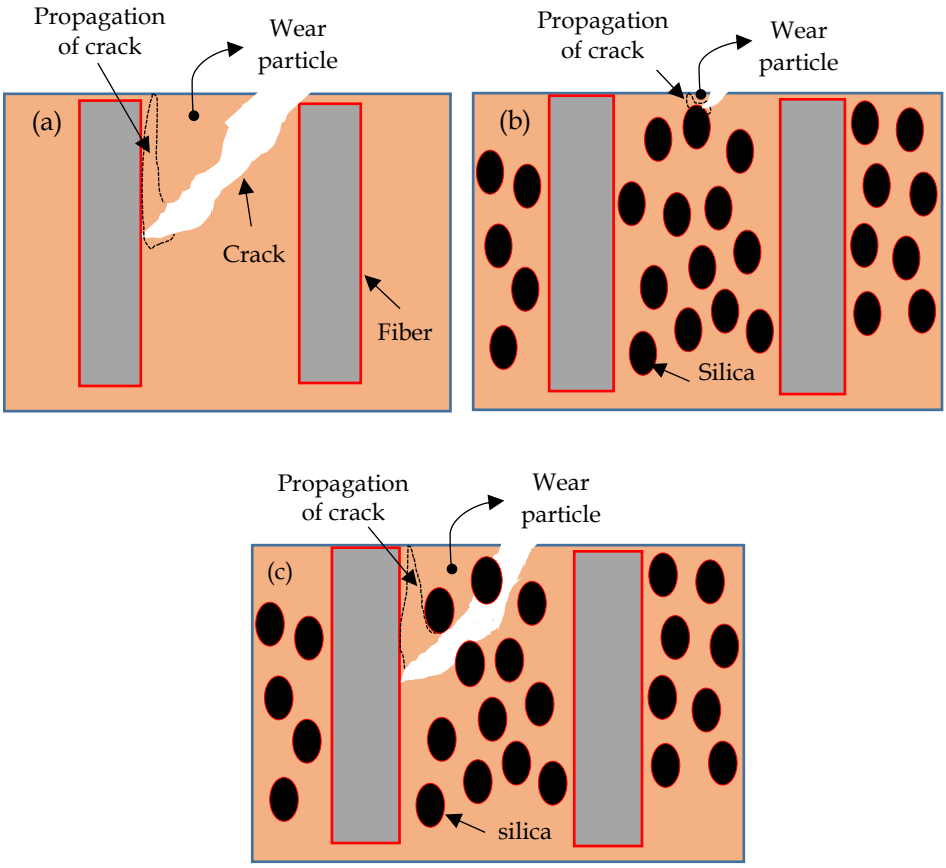

Figure 4.16: The process of crack propagation: (a) elastomer is reinforced with fibres; (b) elastomer is reinforced with fibres and silica at low energy input; and (c) high energy input, shown schematically.

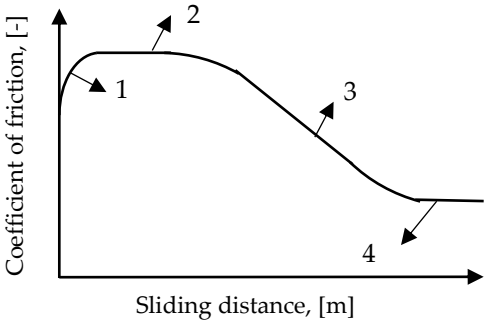

Figure 4.17: Friction behaviour of short-cut aramid fibre reinforced elastomers, shown schematically.

Based on the experimental results, a general friction behaviour of short-cut aramid fibre reinforced elastomers is proposed, see Figure 4.17. The coefficient of friction develops in four stages:

1. At the initial part of sliding distance, the contact area increases due to wear. As a result, the coefficient of friction increases.
2. The coefficient of friction reaches a maximum value. When the wear loss is low, and only a few fibres protrude on the wear surface, the coefficient of friction will be constant.
3. Once many elastomer matrix pull out from the composite, and the fibres exist on the wear surface, the coefficient of friction decreases drastically. It is caused by the reduction of the real contact area between the contacting surfaces.
4. The coefficient of friction reaches a steady-state value when many fibres cover the wear surface, and the counter surface is mainly in contact with the fibres.

4.2.2 The effect of epoxy coated fibre

Adding silica and EF into the elastomers increases the mechanical properties of elastomeric composites in comparison with those with silica and NF, see Figure 2.3. In this sub-section, the effect of epoxy coated fibre on the tribological behaviour of silica and short-cut aramid fibre reinforced elastomers is discussed. The SBR-BR containing 20 NF and 20 EF with randomly oriented fibres were studied. Two types of contact pressures were used in the tests, namely 0.68 MPa and 0.80 MPa and a sliding velocity of 0.20 m/s at ambient temperature. The tribometer tests were stopped after the steady state phase is reached (200 m).

Figure 4.18 shows the coefficient of friction as a function of sliding distance for all tests. The coefficient of friction reaches a steady state value after a short sliding

distance. No decreasing coefficient of friction is observed in the tests as is seen in the elastomers reinforced by solely short-cut aramid fibres. The steady state coefficient of friction for the SBR-BR containing EF is lower than those containing NF. It can be caused by the contact area of the SBR-BR containing EF being smaller than the one containing NF, as the mechanical properties of the SBR-BR containing EF are higher than those containing NF.

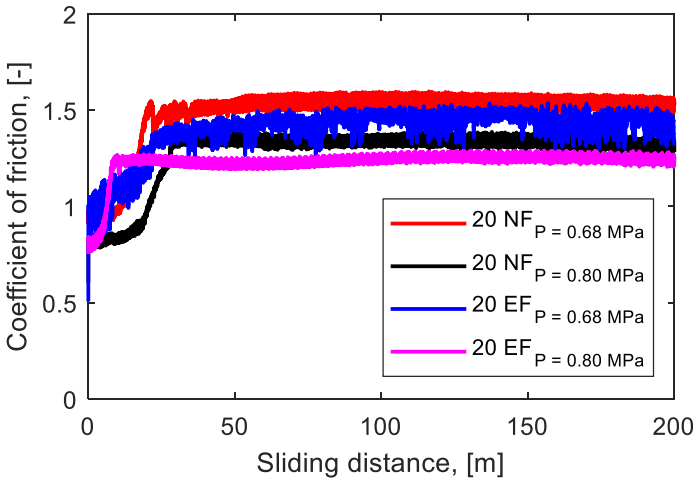

Figure 4.18: Coefficient of friction as a function of the sliding distance of SBR-BR containing 20 NF and 20 EF for two contact pressures, 0.68 MPa and 0.80 MPa, v = 0.20 m/s.

For the elastomers reinforced by solely short-cut aramid fibres, the steady state coefficients of friction are the same under different contact pressures below the threshold contact pressure, while the coefficient of friction of silica and short-cut aramid fibres reinforced elastomer are different under different contact pressures. The higher the contact pressure, the lower the coefficient of friction. The Hertz theory states that the relation between the coefficient of friction and the normal force is $\mu \sim F^{-1/3}$. While the Amontons' theory states that the coefficient of friction is independent of the force. The elastomers which are reinforced with silica and short-cut aramid fibres in contact with a counter surface is located somewhere in between the Hertz theory and the Amontons' theory. For example, the SBR-BR containing 20 NF has a steady state coefficient of friction of 1.53 ± 0.04 at a contact pressure of 0.68 MPa (F = 5 N). When a contact pressure of 0.8 MPa (F = 8.2 N) is used, the steady state coefficient of friction decreases to 1.35 ± 0.05.

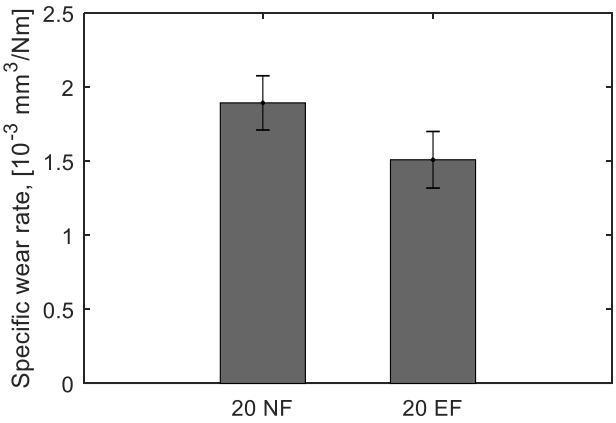

Figure 4.19: Specific wear rate of the SBR-BR containing 20 EF and 20 NF, randomly oriented.

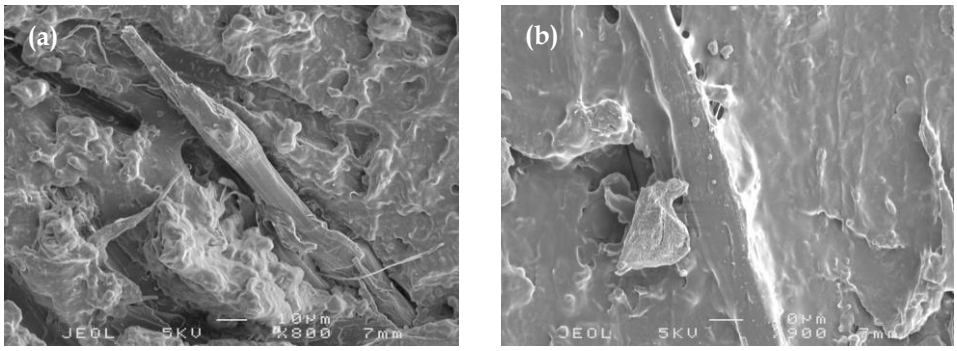

Figure 4.20: SEM photographs of wear surface of the SBR-BR containing (a) NF and (b) EF.

Figure 4.19 shows the average specific wear rates of the composites after the tribometer tests. It can be seen that the specific wear rate of the SBR-BR containing EF is lower than those containing NF. It is caused by the better mechanical properties of the SBR-BR containing EF than containing NF. This is due to a better fibre-matrix interaction in the SBR-BR containing EF. A better interaction between EF and the matrix at the wear surface after a tribometer test can be seen in Figure 4.20. It is clearly seen that there is an interaction between EF and elastomer matrix, while the interaction between NF and the elastomer matrix is not visible.

4.3 Friction-induced noise of short-cut aramid fibre reinforced elastomers

In the present section, the friction-induced noise of short-cut aramid fibre reinforced elastomer is investigated. The noise generation is studied in relation to the friction and wear mechanism that was discussed in sections 4.1 and 4.2.

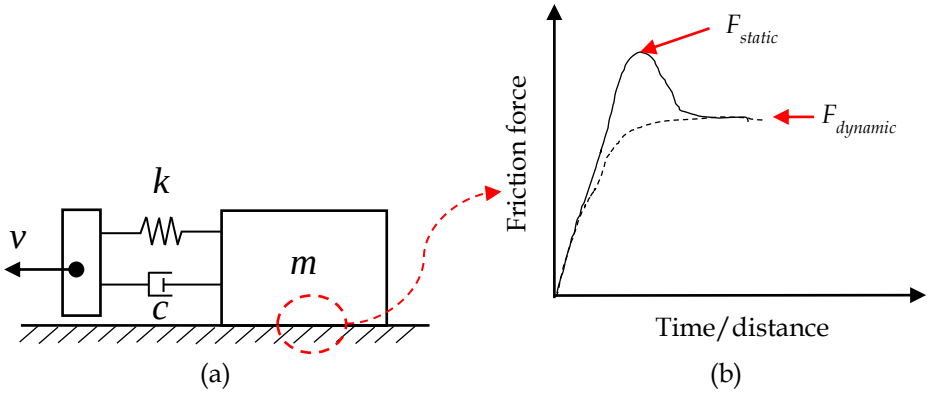

Figure 4.21: (a) Mass-spring system model; (b) stick-slip phenomenon, shown schematically.

Figure 4.21(a) shows the mass-spring system model of a material in contact with a rigid flat. Before motion of mass m starts, the contacting surfaces are in static friction. Once a drive system starts to move mass m, the friction force suddenly decreases. This phenomenon is called stick-slip; it occurs when the static friction force is greater than the dynamic force, see Figure 4.21(b). When the static friction is the same as the dynamic friction, no stick-slip will be observed. The stick-slip may generate vibrations in the system; furthermore, it induces noise either at the contacting surfaces or via the structural system.

The experiments of friction-induced noise were conducted using a pin-on-disc tribometer. The frictional noise was measured using a real-time sound pressure analyser. A microphone was placed as near as possible to the contact between the composite and the counter surface. An acceleration sensor was mounted on the pin holder to measure the vibrations due to sliding contact, see Figure 4.22. The vibration was measured in tangential (sliding) direction. The pin-on-disc tribometer was placed in a chamber to minimize the effect of noise from the other sources. The microphone was calibrated with a sound calibrator at the beginning of the test. A-weighting was used to emphasize the noise generation in which the human ear is most sensitive (2 – 5 kHz). The acquisition rates of the acceleration sensor and the

real-time sound pressure analyser are 20 kHz, whereas the acquisition rate of the pin-on-disc tribometer is 100 Hz. The sound pressure is converted to sound pressure level using the following equation:

$$SPL = 20log\frac{p_1}{p_0} \tag{4.1}$$

where SPL is the sound pressure level (dB), p_1 is the measured sound pressure (Pa), and p_0 is the reference sound pressure (20 µPa). When the measured sound pressure doubles, the SPL increases 3 dB.

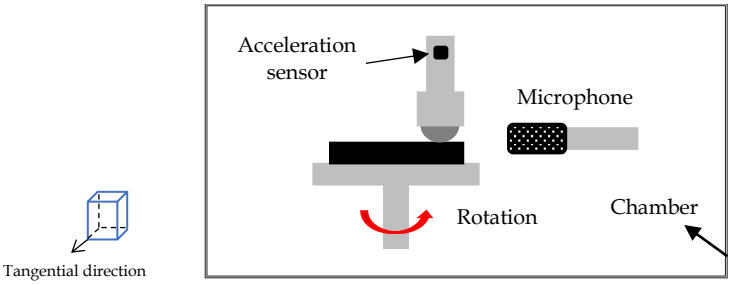

Figure 4.22: Experimental set-up, shown schematically.

The SPL at unloading condition was recorded to investigate the effect of noise generation due to the test rig. The equivalent friction-induced noise was determined by deducting these values from the SPL values measured under loading condition [66]. The SPL due to friction was calculated using the following equation:

$$SPL_{fric} = 20log\left(10^{SPL_l/20} - 10^{SPL_u/20}\right) \tag{4.2}$$

Where SPL_{fric} is the sound pressure level due to friction, SPL_l and SPL_u are the sound pressure level under loading and unloading condition respectively. The natural frequency of the system was measured at the position where the counter surface is in contact with the composite surface. The results show that the natural frequencies of the tangential vibration occur at 50 Hz and 700 Hz.

Table 4.1: Operating conditions of friction-induced noise tests.

	Composites	Contact pressure [MPa]	Velocity [m/s]
The effect of fibre reinforcement	Non-fibre SBR Vs. SBR-3 EF	0.075	0.10
The effect of contact pressure	SBR-15 EF	0.20 0.25 0.29	0.10
The effect of velocity	SBR-15 EF	0.20	0.05 0.10 0.20
The effect of epoxy coated fibre	SBR-15NF Vs. SBR-15 EF	0.20	0.10
The effect of the friction stage	SBR-15 EF	0.20	0.20

Table 4.1 lists the materials and operating conditions that were used in the friction-induced noise tests. The fibre direction of the composites used in the tests is randomly oriented. The effect of fibre reinforcement on the friction-induced noise was investigated using non-fibre SBR and SBR containing 3 EF. The contact pressure and velocity were varied for SBR containing 15 EF to investigate the effect of velocity and contact pressure on the friction-induced noise. The effect of epoxy coated fibres on the friction-induced noise was investigated using SBR containing 15 NF and 15 EF. In sub-section 4.1.1, it was discussed that a fibre reinforced elastomer has four friction stages that are influenced by wear processes during sliding friction. In this section, the effect of the friction stage on the noise generation were investigated using SBR containing 15 EF. The effect of the friction stage was investigated at stage 1, 3 and 4 (see Figure 4.17) since stage 2 only occurs at a very short time for short-cut aramid fibre reinforced elastomers (without silica reinforcement).

The equivalent sound pressure level due to friction (SPL_{fric}) of each test was evaluated for 10 seconds. The tests were repeated three times for each test. Figure 4.23 shows that by adding 3 EF, the SPL_{fric} is reduced in comparison with the non-fibre SBR. Furthermore, a higher contact pressure will result in a higher SPL_{fric}, see Figure 4.23. The friction-induced noise of SBR containing 15 EF is lower than that of SBR containing 15 NF.

Applying an epoxy coating on the fibre surface was found to increase the mechanical properties of the composites in comparison with that of the non-coated fibre composites, see Figure 2.2. The effect of epoxy coated fibres on the friction-induced noise is shown in Figure 4.23. It shows that the SPL_{fric} of SBR containing 15

EF is lower than that of SBR containing 15 NF. Figure 4.24 shows that the SPL_{fric} increases with increasing velocity.

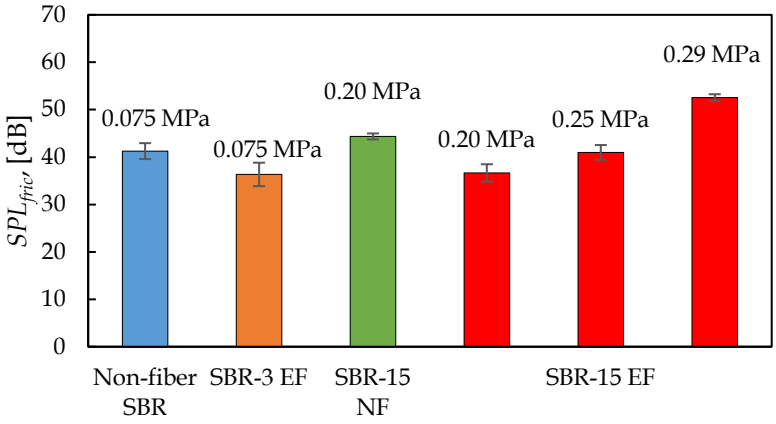

Figure 4.23: Equivalent SPL_{fric} of non-fibre SBR, SBR containing 3 EF, SBR containing 15 NF and SBR containing 15 EF for several contact pressures, v = 0.10 m/s.

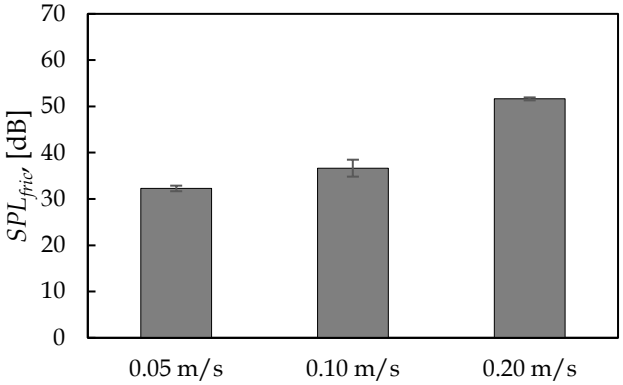

Figure 4.24: Equivalent SPL_{fric} of SBR containing 15 EF for several velocities; P = 0.20 MPa.

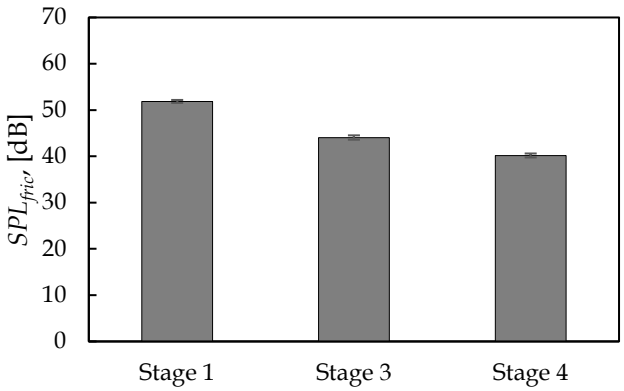

Figure 4.25: Equivalent SPL_{fric} of SBR containing 15 EF at stage 1, stage 3 and stage 4, P = 0.20 MPa, v = 0.20 m/s.

The wear processes of short-cut aramid fibre reinforced elastomers greatly influences the friction-induced noise of the composites. Figure 4.25 shows that the friction-induced noise is different under various friction stages. The highest SPL_{fric} was found at stage 1, while the SPL_{fric} at stage 3 shows an intermediate value between the stages 1 and 4. It means that the presence of fibres on the wear surface reduces the SPL_{fric}. It is known that a soft material leads to adhesive bonding between the contacting materials causing stick-slip and may generate vibrations in the system. At stage 4, the counter surface is mainly in contact with the fibres which has stiffer properties than the elastomer matrix. This condition leads to the reduction of the vibrations as can be seen in Figure 4.26e. It is also confirmed by the amplitude of the friction force at stage 4 which is far lower than that of stage 1, see Figure 4.29(e).

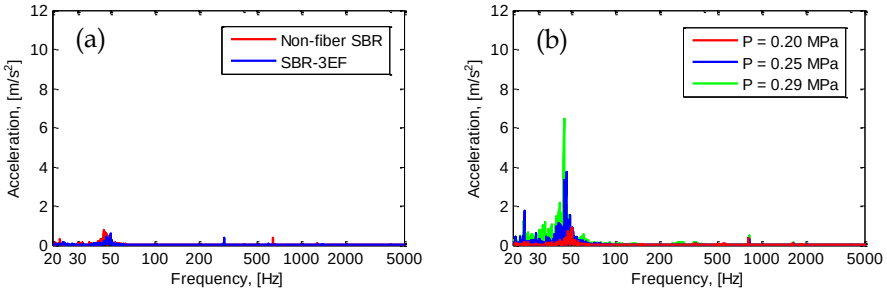

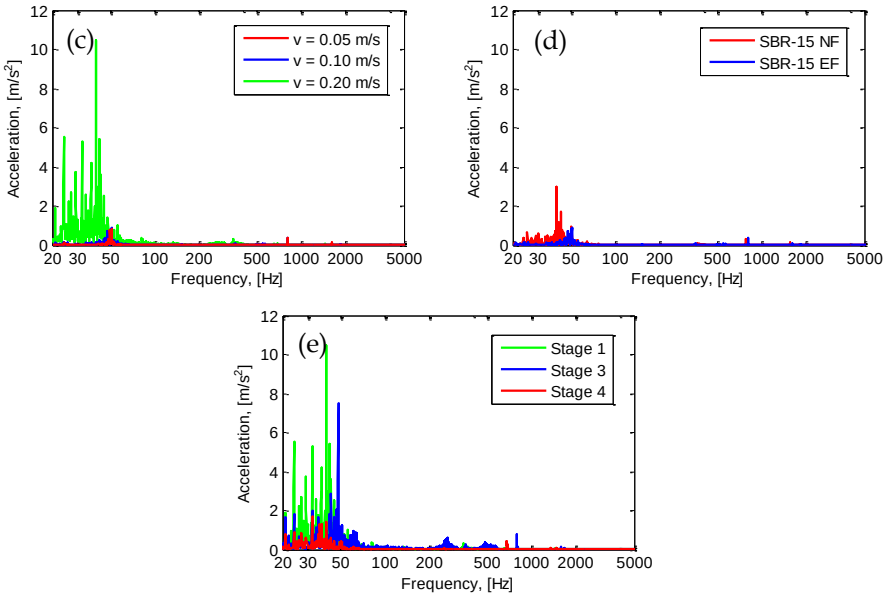

Figure 4.26: Frequency spectrum of tangential vibrations: (a) the effect of fibre reinforcement, P = 0.075 MPa, v = 0.10 m/s; (b) the effect of contact pressure, v = 0.10 m/s; (c) the effect of velocity, P = 0.20 MPa; (d) the effect of epoxy coated fibres, P = 0.20 MPa, v = 0.10 m/s; (e) the effect of friction stage, P = 0.20 MPa, v = 0.20 m/s.

Figure 4.26 shows the vibration of the pin holder in tangential direction for all tests. It can be seen that when velocities of 0.05 and 0.10 m/s are applied, the pin holder vibrates at a frequency of approximately 50 Hz, which is the natural frequency of the test rig in tangential direction. While a random frequency at 20-50 Hz was found when a velocity of 0.20 m/s is applied. It is worth noting that a high vibration signal is found when the SPL_{fric} is high. For example, the vibration signal of SBR containing 15 EF at a contact pressure of 0.29 MPa is higher than that at a contact pressure of 0.20 MPa, see Figure 4.23 and Figure 4.26(b).

Figure 4.27(a) shows the frequency spectrum of sound pressure under unloading and static conditions (environment noise). It can be seen that the dominant frequency of noise due to the environment occurs at 25, 45 and 100 Hz. Once a velocity is applied, the sound pressures increase at a frequency of approximately 500 Hz, while the dominant frequencies of environment noise remain constant, see Figure 4.27(b). This indicates that the noise due to the motor occurs at a frequency of approximately 500 Hz. It is worth noting that the higher the velocity, the higher the amplitude of sound pressure at a frequency of approximately 500 Hz. The equivalent SPL under unloading conditions for velocities of 0.05, 0.10 and 0.20

m/s are 40.93, 45.41 and 51.63 dB, respectively. Although the amplitude of the sound pressure due to the motor (500 Hz) is not high, it greatly influences the equivalent *SPL* since it occurs at a higher frequency than the environment noise. Figure 4.27(c) shows that the sound pressures of non-fibre SBR and SBR containing 3 EF at a frequency of ~ 50 Hz are similar. It also shows that a higher noise is found at a frequency of ~ 500 Hz than in the unloaded condition, meaning that the motor noise under loading conditions is greater than that for the unloaded condition. The increasing motor noise under loading conditions in comparison with the unloading condition is found for all tests, see Figure 4.27(c-g). A strong correlation between the vibration and noise generation is found for all tests. The noise at a frequency of 50 Hz increases when the vibration at that frequency increases, see Figure 4.26 and Figure 4.27. This indicates that the sliding friction generates vibration in the pin holder and that noise is generated due to the structure of the test rig.

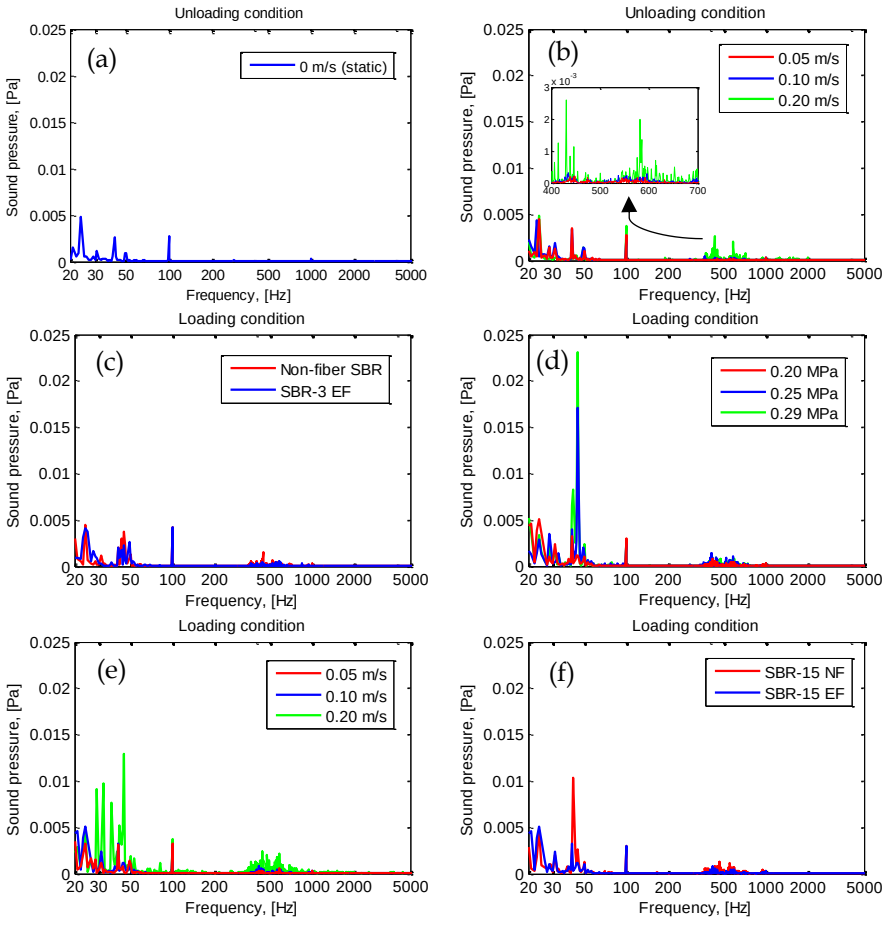

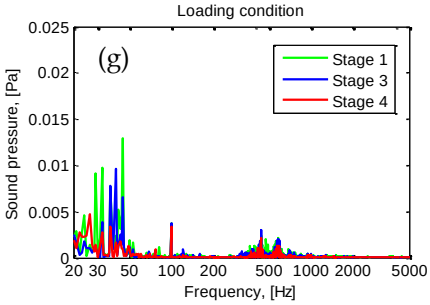

Figure 4.27: Frequency spectrum of noise: (a) unloading and static conditions; (b) unloading condition for velocities of 0.05, 0.10 and 0.20 m/s; (c) the effect of fibre reinforcement, P = 0.075 MPa, v = 0.10 m/s; (d) the effect of contact pressure, v = 0.10 m/s; (e) the effect of velocity, P = 0.20 MPa; (f) the effect of epoxy coated fibres, P = 0.20 MPa, v = 0.10 m/s; (g) the effect of the friction stage, P = 0.20 MPa, v = 0.20 m/s.

It was mentioned that noise due to the motor increases under loading conditions. In all cases, the noise due to the motor (~ 500 Hz) was found to increase when the friction force is high, while the noise due to pin holder vibration (~ 50 Hz) increases when the amplitude of the friction force signal is high, for example see Figure 4.28. It shows that a high amplitude of the friction force signal will result in a high level of noise due to pin holder vibration (~ 50 Hz), see Figure 4.28(b). Moreover, the motor noise increases at a high friction force because the motor needs more power to maintain the desired velocity. As a result, a higher noise is generated by the motor, see Figure 4.28(c). Therefore, the friction-induced noise can be reduced in two ways: (1) by reducing the amplitude of the friction force to reduce noise due to the pin holder vibration and (2) by reducing the level of friction force to reduce noise due to the motor.

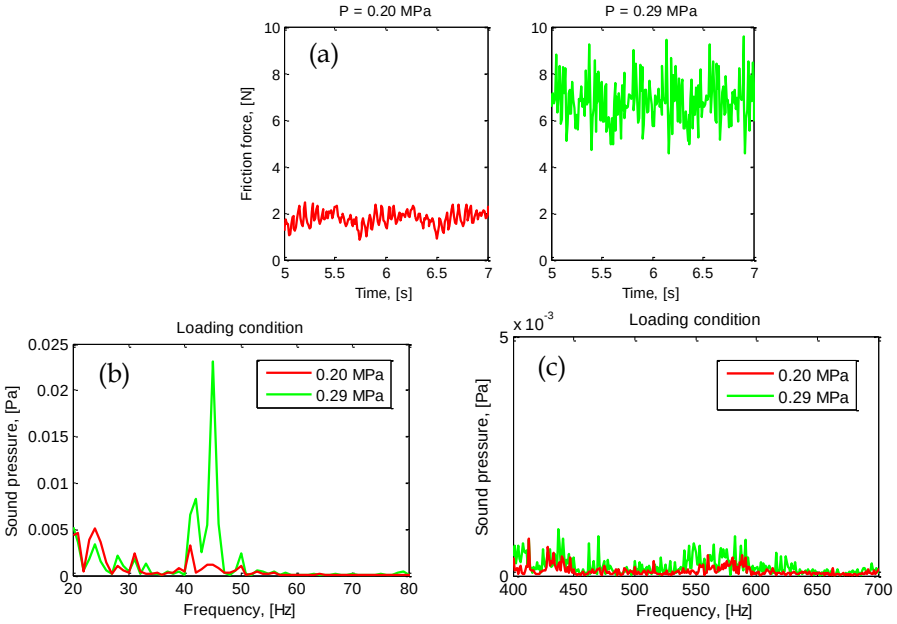

Figure 4.28: (a) Friction force of SBR containing 15 EF for different contact pressure; (b) Noise generation due to pin holder vibration; (c) noise generation due to test rig, v = 0.10 m/s.

Figure 4.29(a) shows that the amplitude of the friction force of both non-fibre SBR and SBR containing 3 EF is low. As a result, the vibration and noise due to pin holder (~ 50 Hz) is low, see Figure 4.26(a) and Figure 4.27(c). The increasing SPL_{fric} of non-fibre SBR is caused by the motor noise since the friction force of non-fibre SBR is higher than that of SBR containing 3 EF. Figure 4.29(b) shows that the higher the contact pressure, the higher the level and amplitude of the friction force. Therefore, the increasing SPL_{fric} is caused by both noise due to pin holder vibration and motor noise. This is also found for the investigation with respect to the fibre type (NF and EF) and friction stage, see Figure 4.29(d) and Figure 4.29(e). Figure 4.29(c) shows that the level and the amplitude of friction force are low at a velocity of 0.05 m/s, resulting in low SPL_{fric}, see Figure 4.24. At a velocity of 0.10 m/s, both the level and amplitude of friction force increases. A high amplitude of friction force is found when a velocity of 0.20 m/s is applied, whereas the level of friction force is similar as the friction force at a velocity of 0.10 m/s. As a result, the SPL_{fric} at velocities of 0.10 and 0.20 m/s are higher than that at 0.05 m/s.

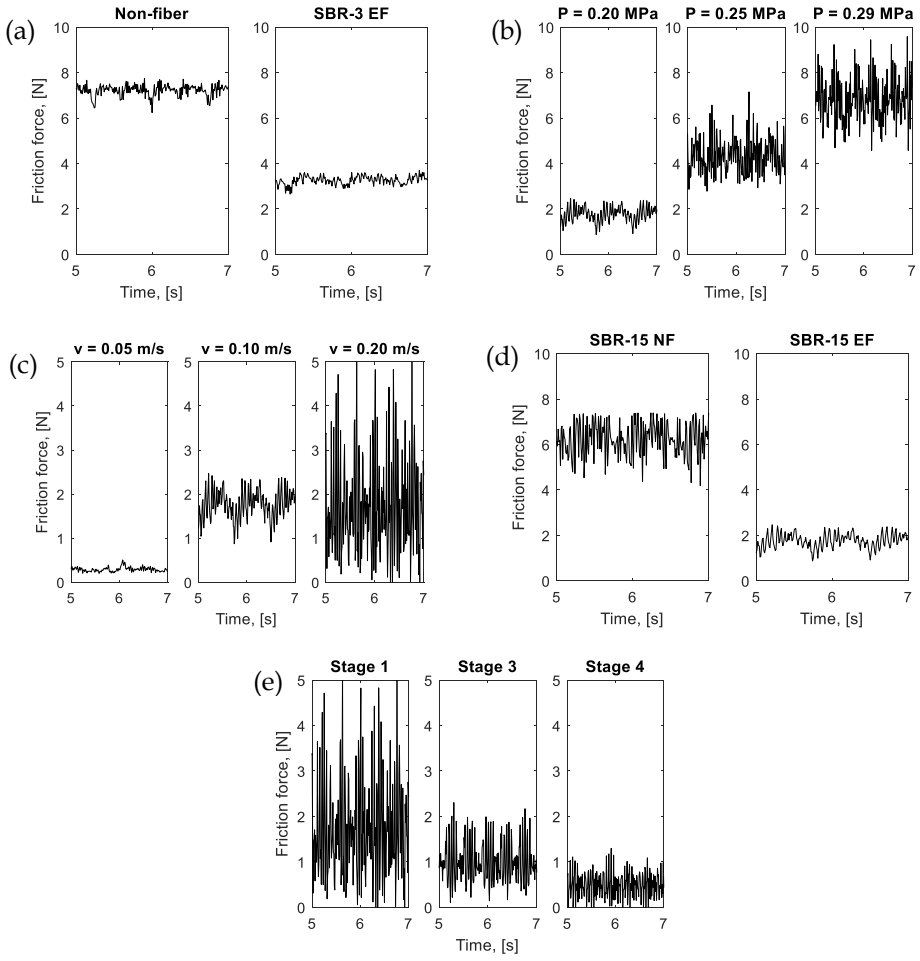

Figure 4.29: Friction force-time characteristics: (a) the effect of fibre reinforcement, P = 0.075 MPa, v = 0.10 m/s; (b) the effect of contact pressure, v = 0.10 m/s; (c) the effect of velocity, P = 0.20 MPa; (d) the effect of fibre type, P = 0.20 MPa, v = 0.10 m/s; (e) the effect of the friction stage, P = 0.20 MPa, v = 0.20 m/s.

The loss and storage moduli were measured to investigate the effect of mechanical properties on the friction-induced noise. Figure 4.30 shows that the storage and loss moduli of the SBR containing 15 EF at room temperature are higher than those containing 15 NF. A stiffer material leads to the reduction of stick-slip and thus less vibration of the system. In the other hand, a higher loss modulus gives a higher capability of the material to absorb energy and noise. As a result, the friction-induced noise of the SBR containing 15 EF is lower than that containing 15

NF. Furthermore, the presence of fibres on the wear surface was found to reduce vibrations and noise since it reduces the stick-slip, see Figure 4.31.

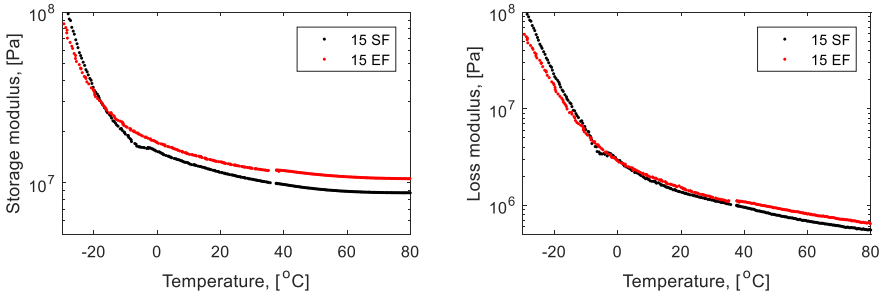

Figure 4.30: Storage and loss moduli of the composites containing 15 NF and 15 EF at temperature sweep.

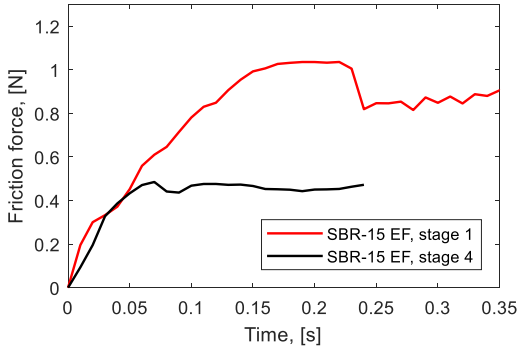

Figure 4.31: Stick-slip phenomenon of SBR containing 15-EF at stage 1 and stage 4, P = 0.20 MPa, v = 0.001 m/s.

4.4 Summary

Friction and wear mechanisms of short-cut aramid fibre reinforced elastomers were discussed in this chapter. To gain a better understanding of the fundamental phenomena of friction and wear in short-cut aramid fibre reinforced elastomers, no other fillers (such as carbon black and silica) were added into the composites. The propagation of the cracks greatly influences the wear of the composites during sliding friction. The wear alters the wear surface and therefore influences the frictional behaviour of the composites. The steady-state coefficient of friction of short-cut aramid fibre reinforced elastomers with various fibre orientations show

the same values due to the presence of fibres on the wear surface. The composite containing fibres in normal orientation shows the lowest wear. The higher the amount of fibres the lower the wear because the propagation of cracks will be stopped effectively. Moreover, the presence of fibres on the wear surface will prevent the initiation and propagation of the cracks. Since many fibres are present on the wear surface, the rigid counter surface is in contact mainly with the fibres. Therefore, the real contact area is far lower than the apparent contact area. In this situation, Amontons' law is valid. Amontons' law is not valid anymore when many fibres are pulled out from the composite so that the contact occurs between the rigid counter surface and the combination of fibres and matrix. For the composite containing EF, a higher contact pressure is required to break Amontons' law. It is caused by the interaction of matrix-EF is stronger than that of matrix-NF. Therefore a higher contact pressure is needed to pull out many EF.

Friction and wear mechanism of silica and short-cut aramid fibre reinforced elastomers was conducted to investigate the effect of fibres in the composites for a more realistic application. Basically, the mechanism of short-cut aramid fibre reinforced elastomers with or without silica reinforcement are the same. However, for silica and short-cut aramid fibre reinforced elastomers, a higher energy input is needed to obtain the friction and wear mechanism as found in the short-cut aramid fibre reinforced elastomers. The presence of silica in the elastomer matrix reduces the initiation and propagation of cracks effectively.

Friction-induced noise of short-cut aramid fibre reinforced elastomer was investigated at several operating conditions. Adding fibres into the composites reduces the friction induced noise. The SPL_{fric} increases with increasing contact pressure and velocity. The SPL_{fric} of SBR containing 15 EF is lower than those containing 15 NF. The presence of fibres on the wear surface decreases friction-induced noise.

Chapter 5 Conclusions and Recommendations

In this thesis, friction, wear and noise of short-cut aramid fibre reinforced elastomers are studied. Several phenomena of elastomers during sliding friction are investigated both experimentally and theoretically. In this chapter, the main results of this study and the recommendations for future research are summarized.

5.1 Conclusions

Chapter 2: Materials and Mechanism of Sliding Friction

- The mechanical properties of the elastomer composites containing EF-fibres are higher than those containing NF-fibres. The effect of fibres on the mechanical properties of the composites containing silica and fibres diminishes once the tensile strain passed a threshold.
- The contribution of deformation friction on the total friction is limited in the present study. Therefore, the deformation friction is neglected.

Chapter 3: Tribological Phenomena of Elastomers during Sliding Friction

- The contact area of an elastomeric material in contact with a rigid counter surface is different both in shape and size, during static and sliding conditions. Basically, the size and the shape of the contact area depend on the sliding velocity and the dynamic mechanical properties of the elastomer, such as storage modulus and creep compliance.
- The existence of a modified surface layer depends on the competition between the formation rate and the wear rate. Therefore, it depends on the contact pressure and velocity. A map of the formation of a modified surface layer was developed based on the experimental results.
- The occurrence of a wavy wear track depends on the frequency of the normal oscillation and the circumferential length of the wear track. The frequency of

the oscillation depends on the mechanical properties of the elastomer, the diameter of the ball counter surface, the operational conditions (velocity and force) and the inertia mass of the indenter frame. When the wavelength of the wear pattern is an integer part of the wear track, the wavy pattern becomes visible.

Chapter 4: Friction, Wear and Noise of Fibre Reinforced Elastomers

- The coefficient of friction of a short-cut aramid fibre reinforced elastomer can be distinguished by four stages. In every stage, the coefficient of friction is influenced by the wear process of the composite. To reinforce elastomers next to short-cut aramid fibres with silica is effective for reducing wear because the silica filler can reduce the crack mean free path effectively.
- The Amontons' law is valid for contact pressures below a certain threshold. Once the contact pressures are higher than the threshold, the Amontons' law is not valid anymore. A high threshold is found for the EF-fibres reinforced elastomers. This is caused by a better surface interaction between the EF-fibres and the elastomer matrix than for the NF-fibres and the elastomer matrix. Therefore, a higher contact pressure is needed to pull out fibres from the composite.
- The friction-induced noise of the composites containing EF-fibres is lower than those containing NF-fibres due to their high storage modulus. At steady state friction, the presence of fibres on the wear surface reduces friction-induced noise.

5.2 Discussion and recommendations for future research

In this section, two findings related to this thesis will be addressed, namely (1) the modified surface layer of elastomeric materials during sliding friction and (2) friction-induced noise of short-cut aramid fibre reinforced elastomers.

The formation of a modified surface layer at the surface of the elastomers was found to be influenced by energy input. The modified surface layer is found for short-cut fibre reinforced elastomers as well, see Figure 5.1. A diagram was constructed based on the experimental results. It is expected that the formation of these layers depends not only on the energy input but also on the material properties of elastomeric materials. Further investigation into the effect of these properties in relation to the modified surface layer should be conducted.

Figure 5.1: The modified surface layer of short-cut aramid fibre reinforced elastomers, shown as a cross-section image.

In the present study, the investigation of friction-induced noise was conducted using only composites containing 3 and 15 phr fibres. Further research is needed to find an optimum amount of fibre to reduce friction-induced noise. Furthermore, the contribution of the noise generation at the contacting surfaces on the total noise was unclear in the present study. Microphone arrays should be applied to detect the contribution of each noise source to the total noise [67].

Appendix A

Swanson [68] uses the procedure of Willis [69] to determine the contact area of an orthotropic material. The contact model is similar to the contact model developed by Hertz in [70]. However, the elastic material properties are represented by the numerical solutions of two contour integrals I_1 and I_2, see Equation A.1 and Equation A.2, where $\tilde{w}$ is the Fourier transform of the normal displacement due to a point load and depends on the nine independent constants.

$$I_1 = \int_0^{2\pi} \tilde{w}(\varepsilon\eta_1, \eta_2){\eta_1}^2 d\theta \tag{A.1}$$

$$I_2 = \int_0^{2\pi} \tilde{w}(\varepsilon\eta_1, \eta_2){\eta_2}^2 d\theta \tag{A.2}$$

The problem is defined by the stress equilibrium equation (where σ indicates the stresses, repeated subscript denotes summation and comma denotes differentiation), the stress-strain equation and the boundary conditions can be written as follows:

$$\sigma_{ij,j} = 0 \text{ and } \sigma_{ij} = C_{ijkl}u_{k,l} \qquad \text{for } z \geq 0 \tag{A.3}$$

$$\sigma_{zz} = -\delta(x)\delta(y)F_N \qquad \text{for } z = 0 \tag{A.4}$$

Combining the two equations and introducing the convention that Latin suffixes take values of *x, y, z* and Greek suffixes take values of *x, y* gives

$$C_{i\alpha k\beta}u_{k,\alpha\beta} + (C_{i\alpha kz} + C_{izk\alpha})u_{k,\alpha z} + C_{izkz}u_{k,zz} = 0 \tag{A.5}$$

Taking the Fourier transform in the x and y-directions, using $\xi = (\xi_1, \xi_2)$ as the Fourier transform parameters and $x = (x, y)$, the displacement in the Fourier domain is

$$\tilde{u}_k(\xi, z) = \sum_{A=1}^{6} a_{k^A}(\xi) exp[im_A(\xi)z] \tag{A.6}$$

where

$$\left[C_{izkz}m_A^2 + (C_{i\alpha kz} + C_{izk\alpha})\xi_\alpha m_A + C_{i\alpha k\beta}\xi_\alpha\xi_\beta\right]a_{k^A} = 0 \tag{A.7}$$

m_A is one of the six roots, obtained by setting the determinant of the matrix in Equation A.7 to zero. Since the displacement must be finite far from the load, only the roots with positive imaginary parts are retained. By substituting these roots back

in Equation A.7, the first two rows of the ratios a_{1A}/a_{3A} and a_{2A}/a_{3A} are obtained. By applying the Fourier transform to the boundary conditions and substituting Equation A.6, the remaining constant are obtained.

$$\sum_{A=1}^{3}\left[m_A\left(a_{1A}/a_{3A}\right)+\xi_1\right]a_{3A}=0 \tag{A.8}$$

$$\sum_{A=1}^{3}\left[m_A\left(a_{2A}/a_{3A}\right)+\xi_2\right]a_{3A}=0 \tag{A.9}$$

$$\sum_{A=1}^{3}\left[C_{xxzz}\xi_1\left(a_{1A}/a_{3A}\right)+C_{yyzz}\xi_2\left(a_{2A}/a_{3A}\right)-C_{zzzz}m_A\right]a_{3A}=\frac{-i}{\pi} \tag{A.10}$$

The procedures to calculate I_1 and I_2 are as follows:

Step 1. Select a starting value for ε.

Step 2. Compute the integrals I_1 and I_2 of Equation A.1 and Equation A.2.
Integrals are computed by incrementing θ, using $\eta_1 = cos\theta$ and $\eta_2 = sin\theta$. Then set $\xi_1 = \varepsilon cos\theta$ and $\xi_2 = sin\theta$. Compute the roots and solve for the coefficients a_{3A} from Equation A.8 to Equation A.10. This gives

$$\widetilde{w}(\varepsilon\eta_1,\eta_2)=\sum_{A=1}^{3}a_{3A} \tag{A.11}$$

The integrals are then determined by numerically integrating these functions to get I_1 and I_2.

Step 3. A new value of ε is determined by using $\varepsilon = (I_2/I_1)^{1/2}$. This value then be used in step 1, and steps 1 to 3 are repeated until the solution for ε converges.

More details of this procedure can be found in Swanson [68].

References

1. Varghese, S., B. Kuriakose, S. Thomas, and K. Joseph, *Effect of adhesion on the equilibrium swelling of short sisal fiber reinforced natural rubber composites.* Rubber Chemistry and Technology, 1995. **68**(1): pp. 37-49.
2. Coran, A.Y., K. Boustany, and P. Hamed, *Short-fiber – rubber composites: the properties of oriented cellulose-fiber – elastomer composites.* Rubber Chemistry and Technology, 1974. **47**(2): pp. 396-410.
3. Setua, D.K. and S.K. De, *Short silk fibre reinforced nitrile rubber composites.* Journal of Materials Science, 1984. **19**(3): pp. 983-999.
4. Rajesh, C., G. Unnikrishnan, E. Purushothaman, and S. Thomas, *Cure characteristics and mechanical properties of short nylon fiber-reinforced nitrile rubber composites.* Journal of Applied Polymer Science, 2004. **92**(2): pp. 1023-1030.
5. Stamhuis, J.E., *Mechanical properties and morphology of polypropylene composites. III. Short glass fiber reinforced elastomer modified polypropylene.* Polymer Composites, 1988. **9**(4): pp. 280-284.
6. Kashani, M.R., *Aramid-short-fiber reinforced rubber as a tire tread composite.* Journal of Applied Polymer Science, 2009. **113**(2): pp. 1355-1363.
7. Goettler, L.A. and W.F. Cole, *Short fiber-filled rubber composites.* Handbook of Elastomers, 2001.
8. De, S.K. and J.R. White, *Short fibre-polymer composites*. 1996: Elsevier.
9. Vleugels, N., *Short fibre-reinforced elastomeric composites, fundamental routes towards improvement of the interfacial interaction of short-cut aramid fibres in a SBR compound, to improve friction and wear properties*, PhD Thesis. Enschede, The Netherlands: University of Twente. 2017.
10. Moore, D.F., *The friction and lubrication of elastomers*. Vol. 9. 1972: Pergamon.
11. Persson, B.N.J., *On the theory of rubber friction.* Surface Science, 1998. **401**(3): pp. 445-454.
12. Grosch, K.A., *Visco-elastic properties and the friction of solids: Relation between the friction and visco-elastic properties of rubber.* Nature, 1963. **197**: pp. 858-859.
13. Busse, L., I. Boubakri, and M. Klüppel, *Friction master curves for rubber on dry and wet granite: experiments and simulations.* KGK. Kautschuk, Gummi, Kunststoffe, 2011. **64**(5): pp. 35-39.
14. Persson, B.N.J. and A.I. Volokitin, *Rubber friction on smooth surfaces.* The European Physical Journal E, 2006. **21**(1): pp. 69-80.
15. Rorrer, R.A.L. and V. Juneja, *Friction-induced vibration and noise generation of instrument panel material pairs.* Tribology International, 2002. **35**(8): pp. 523-531.

16. Mo, J.L., Z.G. Wang, G.X. Chen, T.M. Shao, M.H. Zhu, and Z.R. Zhou, *The effect of groove-textured surface on friction and wear and friction-induced vibration and noise.* Wear, 2013. **301**(1): pp. 671-681.
17. Min, D., S. Jeong, H.H. Yoo, H. Kang, and J. Park, *Experimental investigation of vehicle wiper blade's squeal noise generation due to windscreen waviness.* Tribology International, 2014. **80**: pp. 191-197.
18. Van Beek, A., *Advanced engineering design: Lifetime performance and reliability. 2012.* Delft University of Technology.
19. Rodriguez, N.V., M.A. Masen, and D.J. Schipper, *A contact model for orthotropic-viscoelastic materials.* International Journal of Mechanical Sciences, 2013. **74**: pp. 91-98.
20. Datta, R.N., *Reduced hysteresis in truck tread compounds by using aramid short fibers.* Rubber Chemistry and Technology, 2006. **79**(1): pp. 26-38.
21. Rodriguez, N.V., *Contact and friction in systems with fibre reinforced elastomers*, PhD Thesis. Enschede, The Netherlands: University of Twente. 2012.
22. Rauline, R., *(to Compagnie Generale des Establissements Michelin) EU 0501227.* 1992.
23. Lorenz, B., B. Persson, S. Dieluweit, and T. Tada, *Rubber friction: comparison of theory with experiment.* The European Physical Journal E, 2011. **34**(12): pp. 129.
24. Ludema, K.C. and D. Tabor, *The friction and visco-elastic properties of polymeric solids.* Wear, 1966. **9**(5): pp. 329-348.
25. Arvanitaki, A., B. Briscoe, M. Adams, and S. Johnson, *The friction and lubrication of elastomers.* Tribology Series, 1995. **30**: pp. 503-511.
26. Vorvolakos, K. and M.K. Chaudhury, *The effects of molecular weight and temperature on the kinetic friction of silicone rubbers.* Langmuir, 2003. **19**(17): pp. 6778-6787.
27. Persson, B.N.J., I.M. Sivebæk, V.N. Samoilov, K. Zhao, A.I. Volokitin, and Z. Zhang, *On the origin of Amonton's friction law.* Journal of Physics: Condensed Matter, 2008. **20**(39): pp. 395006.
28. Momozono, S., H. Takeuchi, Y. Iguchi, K. Nakamura, and K. Kyogoku, *Dissipation characteristics of adhesive kinetic friction on amorphous polymer surfaces.* Tribology International, 2012. **48**: pp. 122-127.
29. Busse, L., A. Le Gal, and M. Klüppel, *Modelling of dry and wet friction of silica filled elastomers on self-affine road surfaces*, in *Elastomere Friction*. 2010, Springer. pp. 1-26.
30. Khafidh, M., N.V. Rodriguez, M.A. Masen, and D.J. Schipper, *The effect of velocity on the nominal contact area of elastomeric materials: Comparison between theory and experiment*, in *Proceedings of the 6th World Tribology Congress*. 2017: Beijing.

31. Degrange, J.-M., M. Thomine, P. Kapsa, J.-M. Pelletier, L. Chazeau, G. Vigier, G. Dudragne, and L. Guerbe, *Influence of viscoelasticity on the tribological behaviour of carbon black filled nitrile rubber (NBR) for lip seal application.* Wear, 2005. **259**(1): pp. 684-692.
32. Mokhtari, M. and D.J. Schipper, *Existence of a tribo-modified surface layer of BR/S-SBR elastomers reinforced with silica or carbon black.* Tribology International, 2016. **96**: pp. 382-388.
33. Martínez, L., R. Nevshupa, D. Felhös, J.L. de Segovia, and E. Roman, *Influence of friction on the surface characteristics of EPDM elastomers with different carbon black contents.* Tribology International, 2011. **44**(9): pp. 996-1003.
34. Karger-Kocsis, J., A. Mousa, Z. Major, and N. Békési, *Dry friction and sliding wear of EPDM rubbers against steel as a function of carbon black content.* Wear, 2008. **264**(3): pp. 359-367.
35. Mokhtari, M., D.J. Schipper, N. Vleugels, and J.W. Noordermeer, *Existence of a tribo-modified surface layer on SBR elastomers: balance between formation and wear of the modified layer.* Tribology Letters, 2015. **58**(2): pp. 22.
36. Zhang, S.-W., *Tribology of elastomers*. Vol. 47. 2004: Elsevier.
37. Fukahori, Y. and H. Yamazaki, *Mechanism of rubber abrasion. Part I: Abrasion pattern formation in natural rubber vulcanizate.* Wear, 1994. **171**(1-2): pp. 195-202.
38. Liang, H., Y. Fukahori, A.G. Thomas, and J.J.C. Busfield, *Rubber abrasion at steady state.* Wear, 2009. **266**(1): pp. 288-296.
39. Persson, B.N.J., *Rubber friction: role of the flash temperature.* Journal of Physics: Condensed Matter, 2006. **18**(32): pp. 7789.
40. Nakazono, T. and A. Matsumoto, *Mechanical aging behavior of styrene-butadiene rubbers evaluated by abrasion test.* Journal of Applied Polymer Science, 2011. **120**(1): pp. 379-389.
41. Rickaby, S.R. and N.H. Scott, *Cyclic stress-softening model for the Mullins effect in compression.* International Journal of Non-Linear Mechanics, 2013. **49**: pp. 152-158.
42. Rickaby, S.R. and N.H. Scott, *Orthotropic cyclic stress-softening model for pure shear during repeated loading and unloading.* The IMA Journal of Applied Mathematics, 2014. **79**(5): pp. 869-888.
43. Maegawa, S., F. Itoigawa, and T. Nakamura, *Dynamics in sliding friction of soft adhesive elastomer: Schallamach waves as a stress-relaxation mechanism.* Tribology International, 2016. **96**: pp. 23-30.
44. Nakano, K. and S. Maegawa, *Safety-design criteria of sliding systems for preventing friction-induced vibration.* Journal of Sound and Vibration, 2009. **324**(3–5): pp. 539-555.

45. Schallamach, A., *Abrasion of rubber by a needle.* Journal of Polymer Science, 1952. **9**(5): pp. 385-404.
46. Schallamach, A., *Friction and abrasion of rubber.* Wear, 1958. **1**(5): pp. 384-417.
47. Thomas, A.G. *Factors influencing the strength of rubbers*. in *Journal of Polymer Science: Polymer Symposia*. 1974. Wiley Online Library.
48. Champ, D.H., E. Southern, and A.G. Thomas, *Fracture mechanics applied to rubber abrasion*, in *Advances in Polymer Friction and Wear*. 1974, Springer. pp. 133-144.
49. Liang, H., Y. Fukahori, A.G. Thomas, and J.J.C. Busfield, *Rubber abrasion at steady state.* Wear, 2009. **266**(1–2): pp. 288-296.
50. Coveney, V. and C. Menger, *Initiation and development of wear of an elastomeric surface by a blade abrader.* Wear, 1999. **233–235**: pp. 702-711.
51. Fukahori, Y., H. Liang, and J.J.C. Busfield, *Criteria for crack initiation during rubber abrasion.* Wear, 2008. **265**(3–4): pp. 387-395.
52. Fukahori, Y. and H. Yamazaki, *Mechanism of rubber abrasion.* Wear, 1994. **178**(1): pp. 109-116.
53. Fukahori, Y. and H. Yamazaki, *Mechanism of rubber abrasion. Part 3: How is friction linked to fracture in rubber abrasion?* Wear, 1995. **188**(1–2): pp. 19-26.
54. Schallamach, A., *How does rubber slide?* Wear, 1971. **17**(4): pp. 301-312.
55. Koudine, A.A. and M. Barquins, *Formation of micro-ridges on the surface of Schallamach waves propagating in the contact area between a moving rubber sample and a glass lens.* Journal of Adhesion Science and Technology, 1996. **10**(10): pp. 951-961.
56. Maegawa, S. and K. Nakano, *Mechanism of stick-slip associated with Schallamach waves.* Wear, 2010. **268**(7–8): pp. 924-930.
57. Setiyana, B., R. Ismail, J. Jamari, and D.J. Schipper, *An analytical study of the wear pattern of an abraded rubber surface: the interaction model.* Tribology - Materials, Surfaces & Interfaces, 2018: pp. 1-7.
58. Persson, B.N.J., *Theory of powdery rubber wear.* Journal of Physics: Condensed Matter, 2009. **21**(48): pp. 485001.
59. Khafidh, M., D.J. Schipper, M.A. Masen, N. Vleugels, and J.W.M. Noordermeer, *Friction of short-cut aramid fiber reinforced elastomer*, in *Proceedings of the 6th World Tribology Congress*. 2017: Beijing.
60. Wada, N. and Y. Uchiyama, *Friction and wear of short-fibre-reinforced rubber composites under various sliding speeds and loads.* Wear, 1993. **162**: pp. 930-938.
61. Nak-Ho, S. and N.P. Suh, *Effect of fiber orientation on friction and wear of fiber reinforced polymeric composites.* Wear, 1979. **53**(1): pp. 129-141.
62. Chand, N. and U.K. Dwivedi, *Influence of fiber orientation on high stress wear behavior of sisal fiber-reinforced epoxy composites.* Polymer Composites, 2007. **28**(4): pp. 437-441.

63. Lancaster, J.K., *The effect of carbon fibre reinforcement on the friction and wear of polymers.* Journal of Physics D: Applied Physics, 1968. **1**(5): pp. 549.
64. Shim, H.H., O.K. Kwon, and J.R. Youn, *Effects of fiber orientation and humidity on friction and wear properties of graphite fiber composites.* Wear, 1992. **157**(1): pp. 141-149.
65. Persson, B.N.J., *Contact mechanics for randomly rough surfaces.* Surface Science Reports, 2006. **61**(4): pp. 201-227.
66. Atinkaynak, A., Z. Parlar, and V. Temiz. *The effect of sliding speed on the friction induced noise in polyamide-steel contact*. in *INTER-NOISE and NOISE-CON Congress and Conference Proceedings*. 2007. Institute of Noise Control Engineering.
67. Botteldooren, D., T. Van Renterghem, F. Van Der Eerden, P. Wessels, T. Basten, and B. De Coensel. *Industrial sound source localization using microphone arrays under difficult meteorological conditions*. in *INTER-NOISE and NOISE-CON Congress and Conference Proceedings*. 2017. Institute of Noise Control Engineering.
68. Swanson, S.R., *Hertzian contact of orthotropic materials.* International Journal of Solids and Structures, 2004. **41**(7): pp. 1945-1959.
69. Willis, J.R., *Hertzian contact of anisotropic bodies.* Journal of the Mechanics and Physics of Solids, 1966. **14**(3): pp. 163-176.
70. Johnson, K.L., *Contact mechanics*. 1987: Cambridge University Press.

PART II

PAPER A

The Formation of a Modified Surface Layer on Elastomeric Materials

M. Khafidh[1,2*], D.J. Schipper[1], M.A. Masen[3]

[1] Faculty of Engineering Technology, University of Twente, P.O. Box 217, 7500AE, Enschede, The Netherlands.
[2] Dutch Polymer Institute DPI, P.O. Box 902, 5600AX Eindhoven, The Netherlands.
[3] Department of Mechanical Engineering, Imperial College London, Exhibition Road, London, SW7 2AZ, United Kingdom.
*email: m.khafidh@utwente.nl

Abstract
Surface modification of an elastomer may be formed during sliding contact with a rigid counter surface. This alteration leads to a change of mechanical properties at the surface and as a result a change in frictional behaviour. Therefore, investigations related to the formation of a modified surface layer on elastomers and its effect on friction are of importance. In the present study, the formation of a modified surface layer on elastomer reinforced by silica is studied. Sliding friction is performed using a pin-on-disc tribometer. Several parameters are varied, namely contact pressure, velocity and roughness of the counter surface. The existence of a modified surface layer is investigated by using a Scanning Electron Microscope (SEM). The results show that the existence of a modified surface layer depends on the competition between the formation rate of the layer and the wear rate. The formation of the layer depends on the contact pressure, velocity and sliding distance. A map of the formation of a modified surface layer is developed.

Keywords: elastomer, modified surface layer, sliding friction, wear.

1. Introduction

Elastomers are used in several industrial products, such as conveyor belts, tyres and wiper blades. Sliding friction often occurs during their usage. Detailed knowledge of sliding friction between an elastomer and a counter surface is an important factor in improving the performance of those products. Several factors play a role in the sliding friction between an elastomer and a counter surface, such as contact pressure, sliding velocity, temperature and surface roughness.

The elastomer friction has two main contributors: hysteresis and adhesion [1]. The hysteresis contribution originates from the internal damping in the bulk of elastomer due to the oscillating forces exerted from the counter surface onto the

elastomer surface. It will be more pronounced with a rough counter surface and/or a high contact pressure because the elastomeric material will deform as a result of harder asperities ploughing through it [2]. Mechanical properties of the bulk elastomer determine the hysteresis contribution [3], while the adhesion contribution comes from the attractive forces between the contacting bodies [4]. When the sliding velocity is low and the surface materials are smooth, the adhesion contribution will be dominant [5, 6]. Generally, the total coefficient of friction depends on the hysteresis friction (F_{def}), the adhesive friction (F_{adh}) and the normal force (F_N), see Eq. 1, while the adhesive friction for dry contact is defined as $F_{adh} = A.\tau$ [2], where A is the contact area and τ is the shear stress.

$$\mu_{total} = \frac{F_{def}+F_{adh}}{F_N} \quad (1)$$

Since the mechanical properties of elastomeric materials are not constant but have a time-related dependency, contact models take into account the viscoelastic behaviour of elastomeric materials [7-9]. Furthermore, the contact area for an elastomeric material is different under static and dynamic conditions [10-12]: the contact area typically decreases with increasing sliding velocity. This is caused by the fact that the mechanical properties of elastomeric materials change under static and dynamic conditions. A contact model for a viscoelastic material under sliding conditions has been developed previously [13].

Next to the contact area, the frictional shear stress between the contacting bodies is of importance for determining the friction. Surface conditions, such as the presence of a lubricant or wear particles in the contact between the contacting bodies, will influence the magnitude of frictional shear stress. Modification that occurs at the surface of elastomers during sliding contact is another complication in specifying the contribution to the frictional shear stress. It is known that a surface modification is developed during sliding contact for other materials such as metals [14] and ceramics [15]. Elastomers are not an exception in this context. Rodriguez [16] used Scanning Electron Microscopy (SEM) and Energy-Dispersive X-ray Spectroscopy (EDS) to show a modified surface layer on the tread of a car tyre. The surface modification of elastomers during sliding contact was also reported by other studies [17-19]. The mechanical properties of the modified surface layer were shown to be worse than the original (substrate) material [19-21]. The degradation of the elastomer surface can be caused by mechanical, thermal or chemical processes [19, 22]. This modification alters the interfacial shear stress during sliding contact and therefore influences the friction [16]. Recently, Mokhtari [23] suggested that the development of a modified surface layer of elastomers depends on the competition between the formation and removal of a surface layer during sliding contact.

Although there are a substantial number of studies describing the modified surface layer of elastomers, the underlying mechanism and how the tribological condition affect the modified surface layer are still not fully understood. The present study aims to investigate the occurrence of a modified surface layer by varying several tribological conditions, namely contact pressure, sliding velocity and roughness of the counter surface. By employing a sliding contact between a Styrene-Butadiene Rubber (SBR)−Butadiene Rubber (BR) material and a rigid counter surface, the occurrence of a modified surface layer and its relation to friction are investigated.

2. Materials and Methods

2.1 Material

An elastomer based on styrene-butadiene rubber (SBR) and butadiene rubber (BR) reinforced with 80 phr (parts per hundred rubber) of highly dispersible silica was used in the present study. The formulation of the elastomer is based on a silica-reinforced passenger car tyre tread, called 'Green Tyre' [24]. Details of the formulation in phr are given in Table 1. The materials were mixed in an internal mixer. Vulcanized elastomers with a thickness of 2 mm were prepared for the tensile and the Dynamic Mechanical Analyzer (DMA) tests, while vulcanized elastomers with a thickness of 5 mm were prepared for tribometer tests.

Table 1. Material formulation of the elastomers.

Ingredients	Supplier	Amount, in phr
SBR, Buna VSL 5025-2 HM	Buna VSL 5025-2 HM Lanxess, Leverkusen, Germany	97.3*
BR, KBR 01	Kumho KBR Seoul, S-Korea	30.0
Silica Ultrasil VN3	Rhodia Silices Lyon, France	80.0
Zinc oxide (ZnO)	Sigma Aldrich, St. Louis, MO, United States	2.5
Stearic acid (SA)	Sigma Aldrich, St. Louis, MO, United States	2.5
TDAE oil	Hansen & Rosenthal, Hamburg, Germany	6.7
bis-(tri-ethoxy-silyl propyl) tetrasulfide (TESPT)	Evonik GmbH, Essen, Germany	7.0
6PPD stabilizer	Flexsys Brussels, Belgium	2.0
TMQ stabilizer	Flexsys Brussels, Belgium	2.0
Sulfur	Sigma Aldrich, St. Louis, MO, United States	1.4

N-Cyclohexyl Benzothiazole Sulfenamide (CBS)	Flexsys Brussels, Belgium	1.7
Di-Phenyl Guanidine (DPG)	Flexsys Brussels, Belgium	2.0

* Containing 37.5 wt% oil

2.2 Mechanical characterization

The dynamic properties of the elastomer were determined using a Metravib Viscoanalyser DMA+150. The loss tangent (*tan δ*) of the elastomer was measured in temperature sweep mode between -80°C and 80°C, at a fixed frequency of 10 Hz, under dynamic and static strains of 0.1 and 1 %, respectively. Tensile measurements were performed using an Instron tensile tester 3343 series, according to ISO 37 at a crosshead speed of 500 mm/min.

2.3 Experimental method

A pin-on-disc tribometer was used for evaluating the frictional behaviour of the elastomers. Three types of investigations were performed to observe the formation of a modified surface layer on the elastomer, namely (1) the effect of velocity, (2) the effect of contact pressure and (3) the effect of indenter roughness.

A relatively smooth steel pin with an arithmetic average surface roughness of 0.52 ± 0.09 μm was used for evaluating the effect of velocity and contact pressure. Details of the operating conditions of the tribometer tests are given in Table 2. Three types of indenter roughness values were used to investigate the effect of surface roughness on the formation of the modified surface layer. The arithmetic average roughness of the spherical indenters with a cut-off length of 800 μm are 1.16 ± 0.18 μm, 2.55 ± 0.16 μm and 8.63 ± 0.27 μm.

Table 2. Operating conditions of the tribometer tests.

	Contact pressure (MPa)	Velocity (m/s)	Roughness of counter surface (μm)
The effect of velocity	0.46	0.05 0.20 0.30	0.52
The effect of contact pressure	0.24 0.46 0.66 0.78	0.20	0.52
The effect of indenter roughness	0.34	0.20	1.16 2.55 8.63

The volumetric wear after tribological testing for each elastomer disc was measured using a Keyence Confocal Microscope VK 9700. The measurement of the wear volume was repeated in four different spots of the wear track for each elastomer. A Jeol JSM 6400 Scanning Electron Microscope (SEM) was used to scan the wear surface of the elastomers.

The tribometer tests in wet condition were performed to investigate the contribution of hysteresis component in the total friction. The elastomer surface was wetted by a very thin layer of oil (Ondina 927 with a dynamic viscosity of 78 mPas at 20°C) such that the lubricated tribo-system given the tests conditions remains in the boundary lubrication regime. By doing this, the adhesion friction is minimized and the hysteresis friction will be dominant. The results show that the coefficient of friction under wet condition decreases drastically in comparison with the dry condition. As an example, the steady-state coefficient of friction for the elastomer with a contact pressure of 0.46 MPa and a velocity of 0.20 m/s decreases from 2.20 to 0.08. In the system studied, it shows the limited role of hysteresis friction on the overall friction. Therefore, the contribution of hysteresis on friction is neglected in the present study.

3. Results

3.1 Mechanical properties

Figure 1 shows that the elastomer behaves nonlinearly. To define the mechanical properties of the elastomer is not straightforward. Therefore, in the present study, the elastic modulus of the elastomer was defined at a strain of 2%. A strain that is expected in the tests at which the material behaves linearly [25]. The elastic modulus of the elastomer used in the present study is 4.69 ± 0.20 MPa.

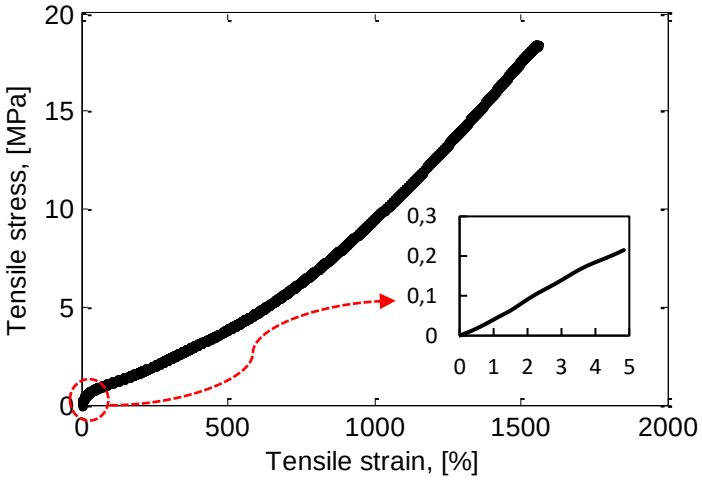

Figure 1. Tensile stress-strain relation of the elastomer.

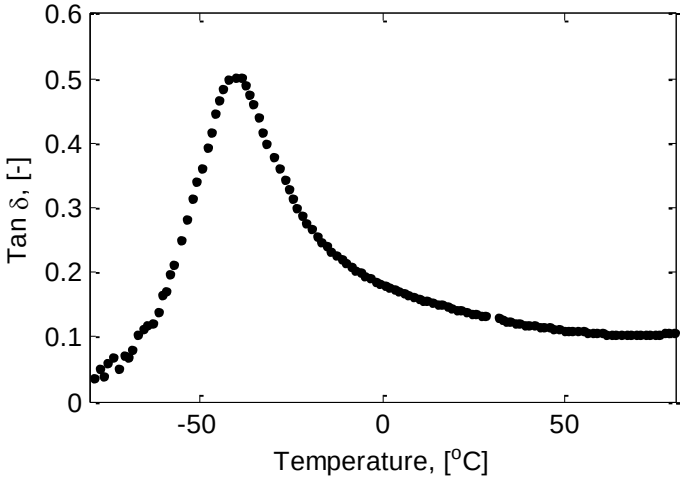

Figure 2. Loss tangent (*tan δ*) as a function of temperature (-80°C to 80°C).

The measured loss tangent (*tan δ*), which is the ratio between the loss modulus (*E″*) and the storage modulus (*E′*) as a function of temperature, can be seen in Figure 2. The glass temperature of the elastomer is characterized by the maximum value of the loss tangent (*tan δ*). For the elastomer used in the present study, the glass temperature occurs at approximately -40°C, meaning it will be in the elastomeric region at room temperature.

3.2 The effect of sliding velocity

The frictional behaviour of elastomeric materials is known to be dependent on the sliding velocity [26]. This is because the mechanical properties of the elastomeric materials depend on the velocity. Figure 3 shows that a higher velocity leads to a lower coefficient of friction. At the beginning of the test, the contact area increases due to wear and the coefficient of friction increases as a result. Interestingly, although the contact area grows continuously with increasing sliding distance, the coefficient of friction decreases after a certain sliding distance. This phenomenon is the result of a decreasing frictional shear stress. The composition and the mechanical properties of elastomer in the top layer changes due to repeated sliding [19]. The decreasing mechanical properties in the top layer of the elastomer will lead to a decreasing frictional shear stress. Therefore, the frictional shear stress at the end of the tests (position 2) is far lower than that at the beginning of the tests (position 1), see Figure 3. The decreasing coefficient of friction occurs for all velocities, it indicates that modified surface layers are developed for all tests. The maximum coefficient of friction is nearly the same for all tests. However, for long sliding distances, a lower coefficient of friction is found when a higher sliding velocity is applied.

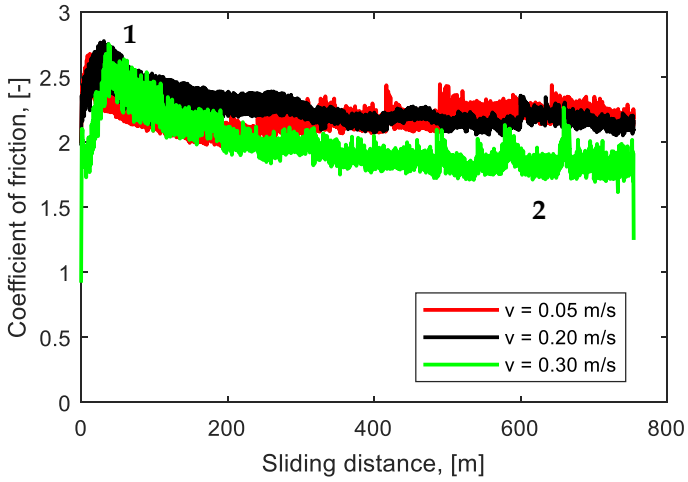

Figure 3. Coefficient of friction as a function of sliding distance at different sliding velocities, P = 0.46 MPa.

Images of the wear surface and wear profile at different sliding velocities are depicted in Figure 4. It can be seen that the wear increases with increasing sliding velocity. The effect of contact temperature due to heat generation is more pronounced at a high sliding velocity. It may degrade the mechanical properties of the elastomer [27], thus a higher wear will be observed. The average wear volume at a velocity of 0.30 m/s is 6 times higher than that at a velocity of 0.05 m/s, while the average wear volume at a velocity of 0.20 m/s is 2 times higher than that at a velocity of 0.05 m/s, see Figure 5. It indicates that the contact area of the elastomer at high velocity is larger than the one at low velocity at the end of the test (position 2 in Figure 3). However, the coefficient of friction of the elastomer at high velocity shows a lower value than that of the elastomer at low velocity. Therefore, the decrease in frictional shear stress of the elastomer at high velocity is far higher than that of the elastomer at low velocity.

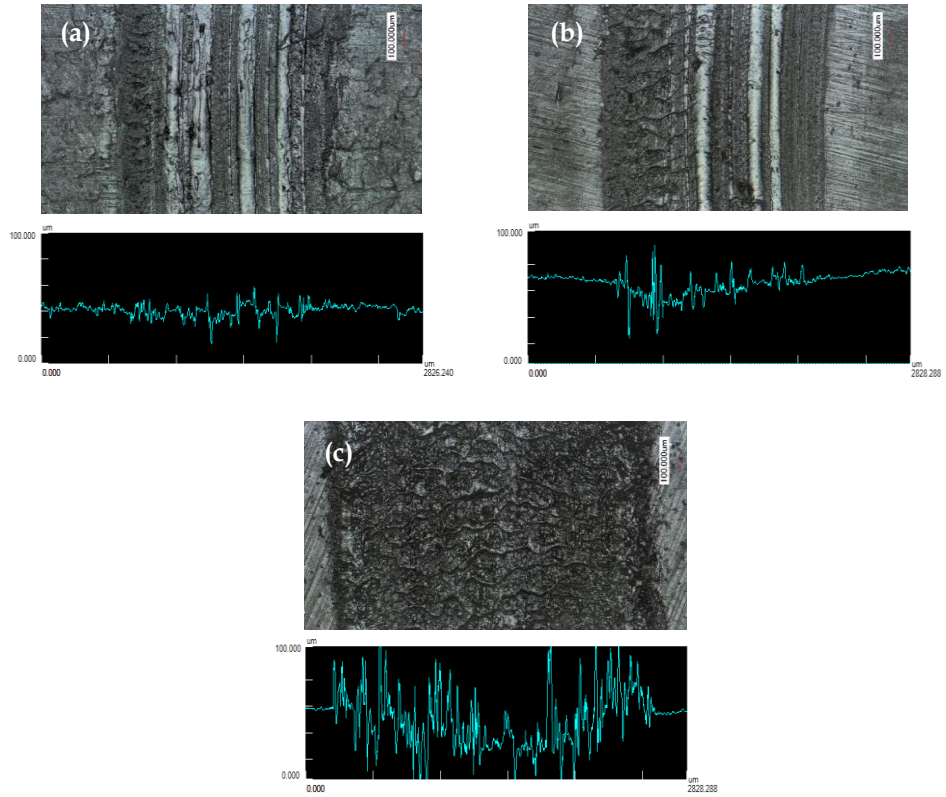

Figure 4. Wear surfaces and wear profiles of the elastomers at velocities of: (a) 0.05 m/s; (b) 0.20 m/s; and (c) 0.30 m/s.

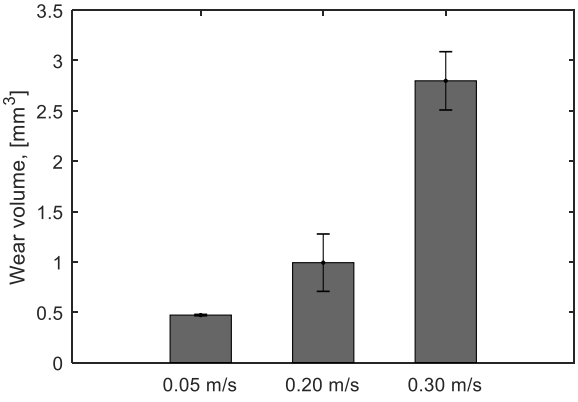

Figure 5. Wear volumes of the elastomers for different velocities.

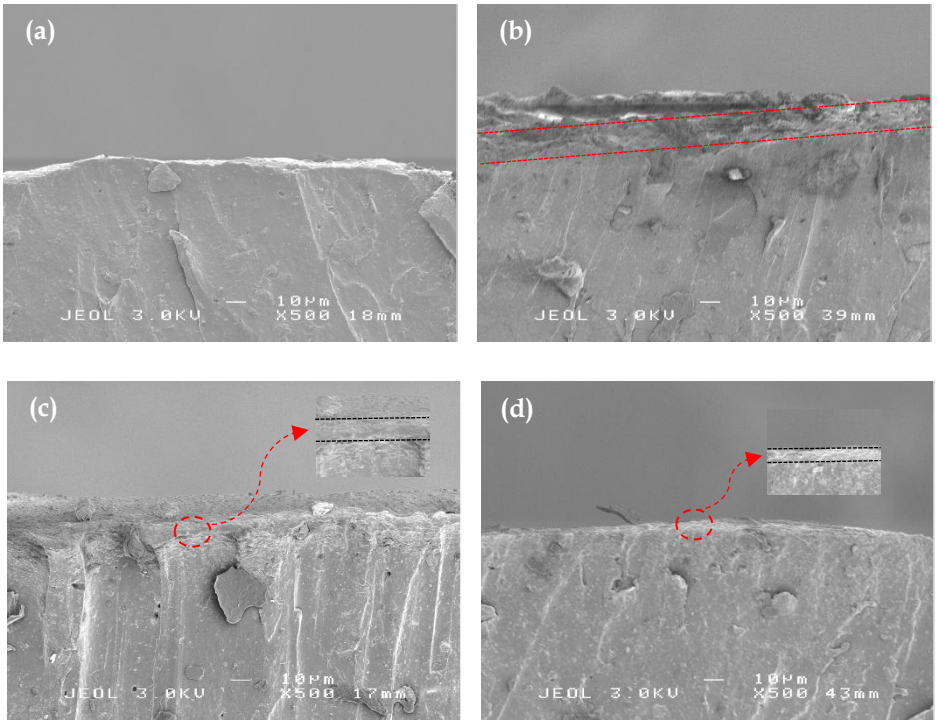

Figure 6. SEM cross-section images of the wear track: (a) position 1 (see Figure 3) at a velocity of 0.30 m/s; (b) position 2 at a velocity of 0.30 m/s; (c) position 2 at a velocity of 0.20 m/s; (d) position 2 at a velocity of 0.05 m/s, P = 0.46 MPa.

To analyse the existence of a modified surface layer, cross-sections of the wear tracks were studied using a Scanning Electron Microscope (SEM). Figure 6(a) shows the cross-section at position 1 (see Figure 3) of the elastomer with a velocity of 0.30 m/s. The upper part of the image shows the surface of the wear track which is in contact with the counter surface and the bottom part of the image shows the bulk of the elastomer. No difference between the bulk of the elastomer and the material near the wear track is observed. While the cross-section view at position 2 (see Figure 3) of the elastomer with a velocity of 0.30 m/s is given in Figure 6(b). It can be seen that a modification of the elastomer at the surface has developed, in which the surface material has a different appearance compared to the bulk material. The thickness of the modified surface layer is approximately 15 μm. A similar procedure was carried out for the elastomers with velocities of 0.20 m/s and 0.05 m/s. Figures 6(c) and 6(d) show that modified surface layers have developed at the surface of the wear track. The thickness of the modified surface layer for the velocities of 0.20 m/s and 0.05 m/s are approximately 5 μm and 3 μm, respectively.

The degradation in mechanical properties of the modified surface layer was proven using an Atomic Force Microscopy (AFM) [19]. The thickness of the modified surface layer is the source of the magnitude of the decrease in frictional shear stress. A thicker modified surface layer will lead to a large reduction of the mechanical properties and therefore a larger reduction of the frictional shear stress will be found.

3.3 The effect of contact pressure

Figure 7 shows the coefficient of friction as a function of sliding distance at a sliding velocity of 0.20 m/s for four different contact pressures. Different trends of the coefficient of friction as a function of sliding distance are observed. When a low contact pressure (0.24 MPa) is applied, the coefficient of friction increases until the end of the test. A decreasing coefficient of friction is observed when a contact pressure of 0.46 MPa is applied. When a contact pressure of 0.66 MPa is applied, the coefficient of friction increases until a maximum value is reached. Subsequently, a relatively constant coefficient of friction is observed after the maximum coefficient of friction is reached. An increasing coefficient of friction is also observed when a high contact pressure (0.78 MPa) is applied. The trend of the coefficient of friction is influenced by the existence of a modified surface layer. When a modified surface layer is present in the wear track, a decreasing coefficient of friction will be observed, see Figure 6(c) for a contact pressure of 0.46 MPa. A decreasing coefficient of friction will not be found when the modified surface layer is not developed, see Figure 8(a) for a contact pressure of 0.24 MPa.

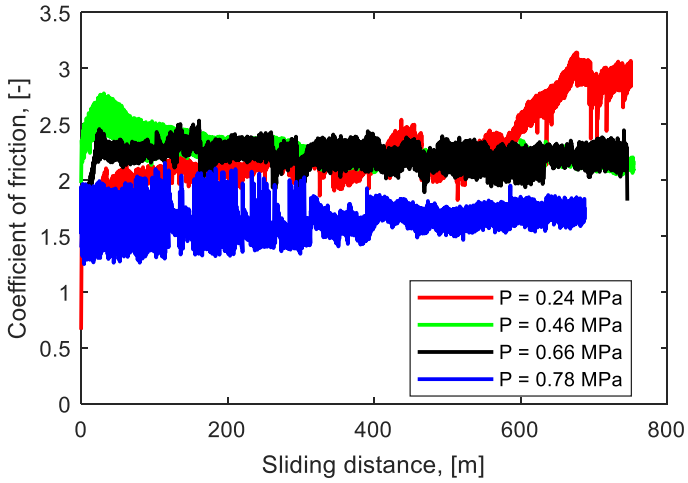

Figure 7. Coefficient of friction as a function of sliding distance for different contact pressures, v = 0.20 m/s.

The existence of a modified surface layer is controlled by a competition between the formation rate of the surface layer and the wear rate [23]. Figure 8(b) shows the image of the wear process and formation process on the wear surface of the elastomer. When the formation rate is higher than the wear rate, the modified surface layer will be developed. However, when the formation rate is lower than the wear rate, the modified surface layer will be completely removed by the wear, so no modified surface layer is observed. The competition between the wear rate and the formation rate depends on several factors, such as mechanical properties of the elastomer, contact pressure, velocity and sliding distance.

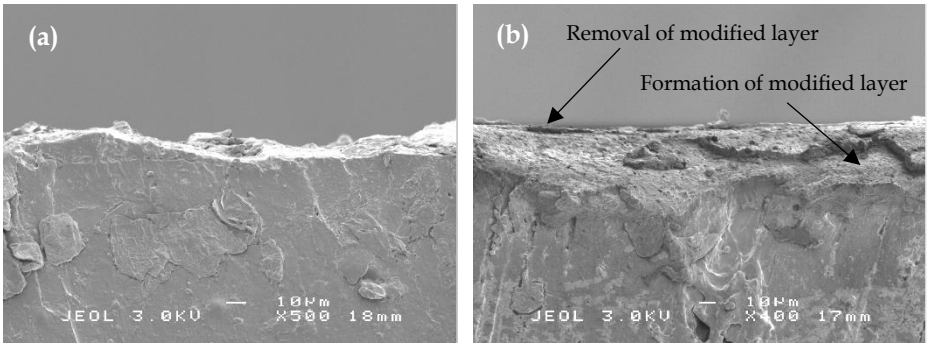

Figure 8. SEM cross-section images of the wear track: (a) at a contact pressure of 0.24 MPa and a velocity of 0.20 m/s; (b) competition between the formation and removal of the modified surface layer in the wear track.

Figure 9 shows the schematic figure of the competition between the wear depth and the formation of the modified layer thickness as a function of sliding distance. For an unworn surface, the heights of the microscopic asperities are not uniform. When two unworn surfaces are loaded for the first time and move relative to one another, the high spots of the asperities are reduced due to wear. Therefore, the wear increases quite quickly at the beginning of the test and slows down gradually because the wear surface becomes more smooth [28]. Elastomers are not an exception in this concept [29, 30].

On the other hand, the modified layer also grows with increasing sliding distance. There are several possible sources of the degradation of the mechanical properties in the top layer. Part of the frictional energy exerted in the elastomer is absorbed by heat generation. The generated heat may change the mechanical properties of the elastomer through increasing temperature [31]. The evolution of the elastomer network is another possible source of the degradation of the mechanical properties. The breakage of filler-matrix interaction due to repeated stress and strain exerted in the elastomer (Mullins and Payne effect) can be a

determining factor in mechanical degradation of elastomers [32]. The degradation of mechanical properties happens not only in tensile loading but also under compression and shear loading [33, 34]. The repeated stress during sliding contact in combination with heat generation in the elastomer may break the filler-matrix interaction, so the degradation of the mechanical properties will be found in the top layer of the elastomer. The filler-matrix interaction needs some time to be broken, therefore the formation increases marginally at early stage of the contact in comparison with the wear which increases quickly at the early stage.

There are three possible results due to the competition between the wear and the formation. Figure 9(a) shows schematically that the wear is larger than the layer formation, so no modified surface layer will be observed. As a result, the decreasing coefficient of friction phenomenon is not found. This phenomenon occurs when the energy input is too low or too high [19]. When the energy input is too low, there is not enough energy to generate a modified surface layer, for instance at a low contact pressure and/or low sliding velocity, see Figure 7 (0.24 MPa). However, the modified surface layer will be removed by wear when a high energy input is used, for instance at a high contact pressure and/or high sliding velocity, see Figure 7 (0.78 MPa).

Figure 9b shows that the coefficient of friction is constant after it reaches a maximum coefficient of friction. At the beginning of the test, the wear depth is greater than the thickness formation of the modified surface layer. As a result, no modified surface layer will be found. The coefficient of friction increases since the contact area between the elastomer and the counter surface grows due to wear. After a certain sliding distance, the wear rate will reduce because the wear surface becomes smooth and only a small amount of wear occurs. The wear and the formation rate will be approximately the same, so the coefficient of friction will reach a steady-state value. This phenomenon occurs in the test with a contact pressure of 0.66 MPa, see Figure 7.

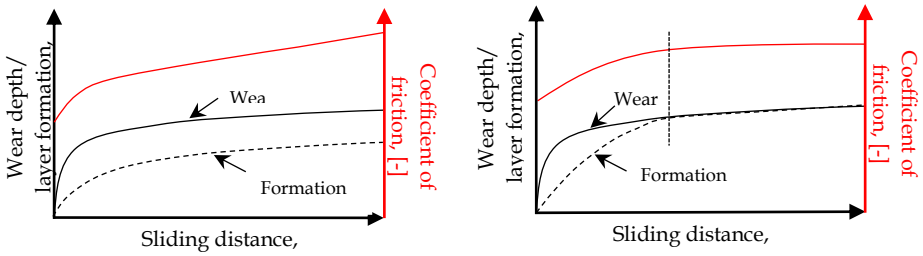

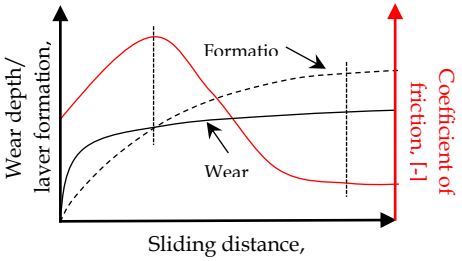

(c)

Figure 9. The schematic wear depth, layer formation and coefficient of friction as a function of sliding distance: (a) formation < wear; (b) formation ≈ wear; (c) formation > wear.

The third possibility of the competition between the wear and modified surface formation can be seen in Figure 9(c). At the beginning of the test, the wear depth is greater than the thickness of layer formation, so the coefficient of friction increases. At a certain sliding distance, the formation rate will be higher than the wear rate because the wear surface is smooth. As a result, the modified surface layer will be developed, and the coefficient of friction decreases until the minimum value is reached. The steady-state coefficient of friction will be found when the wear and the formation rate are nearly the same.

3.4 The effect of indenter roughness

The effect of the roughness of the counter surface on the coefficient of friction is depicted in Figure 10. Three values of indenter roughness were used, namely smooth (Ra = 1.16 μm), medium (Ra = 2.55 μm) and rough (Ra = 8.63 μm). The decreasing coefficient of friction occurs in all cases. The rough indenter has the lowest coefficient of friction, see Figure 10(a). This is because the real contact area between the elastomer and the rough indenter becomes smaller than that of the other indenters, while the coefficient of friction for a smooth indenter is higher than for the medium roughness of the indenter.

The normalized coefficient of friction (the ratio of the coefficient of friction and the maximum coefficient of friction for each test) of all tests can be seen in Figure 10(b). Although the coefficient of friction is different for every test, the decreasing coefficient of friction of those tests show the same behaviour. The difference between the maximum coefficient of friction and the steady-state coefficient of friction is approximately 15% for all tests. This indicates that the modified surface layer is similar under different roughness values of the counter surface.

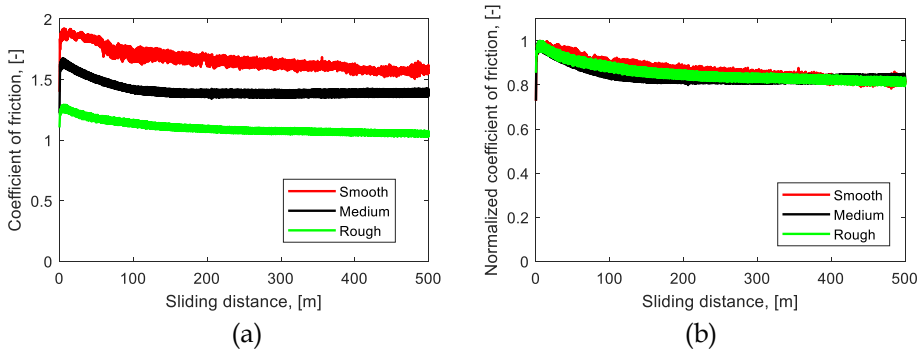

Figure 10. (a) Coefficient of friction as a function of sliding distance at different indenter roughness values; (b) normalized coefficient of friction as a function of sliding distance at different indenter roughness values, smooth (Ra = 1.16 μm), medium (Ra = 2.55 μm) and rough (Ra = 8.63 μm), P = 0.34 MPa, v = 0.2 m/s.

4. Discussion

It has been observed that the formation of a modified surface layer depends on the velocity, contact pressure and sliding distance. Based on the experimental results, a map of the modified surface layer formation is proposed, see Figure 11. The formation of a modified surface layer depends on the energy input and the sliding distance. At a short sliding distance, no modified layer will be formed because the wear rate is much larger than the surface layer formation rate. The highest wear rate occurs during the running-in phase. By increasing the sliding distance, the modified surface layer may be formed when the energy input is high enough. However, when the energy input is too low, the modified surface layer will not be developed even though the sliding distance is is long. The modified surface layer is also not observed when the energy input is too high because the wear is too high.

The effect of material properties of the elastomer is not taken into account in the present study. However, it may influence the transition lines in the map. Better mechanical properties of an elastomer for instance, will result in a low wear rate. However, at the same time, the formation of a modified surface layer is more difficult.

v [m/s] \ P [MPa]	0.24	0.46	0.66	0.78
0.05		△		
0.20	○	◊	◁	▷
0.30		□		

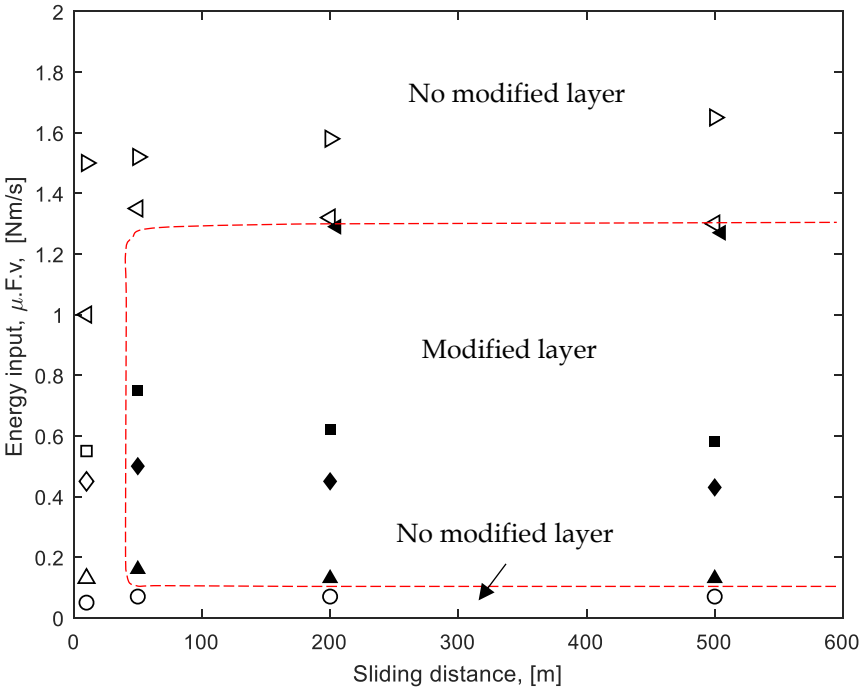

Figure 11. Schematic map of a modified surface layer formation, the existence of a modified surface layer is indicated by filled marker.

5. Conclusion

The formation of a modified surface layer on the elastomer was investigated in the present study. Three parameters were studied, namely the effect of contact pressure, velocity and counter surface roughness. The existence of a modified surface layer depends on the competition between the formation rate and the wear rate. It is influenced by the operational parameters, such as contact pressure, velocity and sliding distance. Once the modified surface layer is developed, the coefficient of friction decreases. A map of a modified surface layer formation was developed based on the experimental results.

Acknowledgement
This research forms part of the Research Programme of the Dutch Polymer Institute DPI, Project #782.

References

1. Moore, D.F., *The friction and lubrication of elastomers*. Vol. 9. 1972: Pergamon.
2. Bhushan, B., *Principles and applications of tribology*. 2013, New York: John Wiley & Sons.
3. Grosch, K.A., *Visco-elastic properties and the friction of solids: Relation between the friction and visco-elastic properties of rubber.* Nature, 1963. **197**: pp. 858-859.
4. Busse, L., I. Boubakri, and M. Klüppel, *Friction master curves for rubber on dry and wet granite: Experiments and simulations.* KGK. Kautschuk, Gummi, Kunststoffe, 2011. **64**(5): pp. 35-39.
5. Persson, B.N.J. and E. Tosatti, *The effect of surface roughness on the adhesion of elastic solids.* The Journal of Chemical Physics, 2001. **115**(12): pp. 5597-5610.
6. Momozono, S., K. Nakamura, and K. Kyogoku, *Theoretical model for adhesive friction between elastomers and rough solid surfaces.* The Journal of Chemical Physics, 2010. **132**(11): pp. 114105.
7. Lee, E.H. and J.R.M. Radok, *The contact problem for viscoelastic bodies.* Journal of Applied Mechanics, 1960. **27**(3): pp. 438-444.
8. Graham, G.A.C., *The contact problem in the linear theory of viscoelasticity.* International Journal of Engineering Science, 1965. **3**(1): pp. 27-46.
9. Ting, T.C.T., *The contact stresses between a rigid indenter and a viscoelastic half-space.* Journal of Applied Mechanics, 1966. **33**(4): pp. 845-854.
10. Ludema, K.C. and D. Tabor, *The friction and visco-elastic properties of polymeric solids.* Wear, 1966. **9**(5): pp. 329-348.
11. Arvanitaki, A., B.J. Briscoe, M.J. Adams, and S.A. Johnson, *The friction and lubrication of elastomers*, in *Tribology Series*. 1995, Elsevier. pp. 503-511.
12. Vorvolakos, K. and M.K. Chaudhury, *The effects of molecular weight and temperature on the kinetic friction of silicone rubbers.* Langmuir, 2003. **19**(17): pp. 6778-6787.
13. Khafidh, M., N.V. Rodriguez, M.A. Masen, and D.J. Schipper, *The Effect of Velocity on the Nominal Contact Area of Elastomeric Materials: Comparison between Theory and Experiment*, in *Proceedings of the 6th World Tribology Congress*. 2017: Beijing.
14. Biswas, S.K., *Some mechanisms of tribofilm formation in metal/metal and ceramic/metal sliding interactions.* Wear, 2000. **245**(1): pp. 178-189.
15. Valefi, M., M. de Rooij, M. Mokhtari, and D.J. Schipper, *Modelling of a thin soft layer on a self-lubricating ceramic composite.* Wear, 2013. **303**(1-2): pp. 178-184.

16. Rodriguez, N., M.A. Masen, and D.J. Schipper, *Tribologically modified surfaces on elastomeric materials.* Proceedings of the Institution of Mechanical Engineers, Part J: Journal of Engineering Tribology, 2013. **227**(5): pp. 398-405.
17. Deladi, E.L., *Static friction in rubber-metal contacts with application to rubber pad forming processes*, PhD Thesis. Enschede, The Netherlands: University of Twente. 2006.
18. Lorenz, B., B.N.J. Persson, S. Dieluweit, and T. Tada, *Rubber friction: comparison of theory with experiment.* The European Physical Journal E, 2011. **34**(12): pp. 129.
19. Mokhtari, M. and D.J. Schipper, *Existence of a tribo-modified surface layer of BR/S-SBR elastomers reinforced with silica or carbon black.* Tribology International, 2016. **96**: pp. 382-388.
20. Degrange, J.-M., M. Thomine, P. Kapsa, J.-M. Pelletier, L. Chazeau, G. Vigier, G. Dudragne, and L. Guerbe, *Influence of viscoelasticity on the tribological behaviour of carbon black filled nitrile rubber (NBR) for lip seal application.* Wear, 2005. **259**(1-6): pp. 684-692.
21. Martinez, L., R. Nevshupa, D. Felhös, J. De Segovia, and E. Roman, *Influence of friction on the surface characteristics of EPDM elastomers with different carbon black contents.* Tribology International, 2011. **44**(9): pp. 996-1003.
22. Karger-Kocsis, J., A. Mousa, Z. Major, and N. Békési, *Dry friction and sliding wear of EPDM rubbers against steel as a function of carbon black content.* Wear, 2008. **264**(3-4): pp. 359-367.
23. Mokhtari, M., D.J. Schipper, N. Vleugels, and J.W.M. Noordermeer, *Existence of a tribo-modified surface layer on SBR elastomers: balance between formation and wear of the modified layer.* Tribology Letters, 2015. **58**(2): pp. 22.
24. Rauline, R., *(to Compagnie Generale des Establissements Michelin) EU 0501227*. 1992.
25. Hintze, C., R. Boldt, S. Wiessner, and G. Heinrich, *Influence of processing on morphology in short aramid fiber reinforced elastomer compounds.* Journal of Applied Polymer Science, 2013. **130**(3): pp. 1682-1690.
26. Grosch, K.A., *The relation between the friction and visco-elastic properties of rubber.* Proceedings of the Royal Society A, 1963. **274**(1356): pp. 21-39.
27. Le Gal, A., X. Yang, and M. Klüppel, *Evaluation of sliding friction and contact mechanics of elastomers based on dynamic-mechanical analysis.* The Journal of Chemical Physics, 2005. **123**(1): pp. 014704.
28. Zhang, S.-W., *Tribology of elastomers*. Vol. 47. 2004: Elsevier.
29. Fukahori, Y. and H. Yamazaki, *Mechanism of rubber abrasion. Part I: Abrasion pattern formation in natural rubber vulcanizate.* Wear, 1994. **171**(1-2): pp. 195-202.

30. Liang, H., Y. Fukahori, A.G. Thomas, and J.J.C. Busfield, *Rubber abrasion at steady state.* Wear, 2009. **266**(1-2): pp. 288-296.
31. Persson, B.N.J., *Rubber friction: role of the flash temperature.* Journal of Physics: Condensed Matter, 2006. **18**(32): pp. 7789.
32. Nakazono, T. and A. Matsumoto, *Mechanical aging behavior of styrene-butadiene rubbers evaluated by abrasion test.* Journal of Applied Polymer Science, 2011. **120**(1): pp. 379-389.
33. Rickaby, S.R. and N.H. Scott, *Cyclic stress-softening model for the Mullins effect in compression.* International Journal of Non-Linear Mechanics, 2013. **49**: pp. 152-158.
34. Rickaby, S.R. and N.H. Scott, *Orthotropic cyclic stress-softening model for pure shear during repeated loading and unloading.* The IMA Journal of Applied Mathematics, 2014. **79**(5): pp. 869-888.

PAPER B

Understanding the Occurrence of a Wavy Wear Track on Elastomeric Materials

M. Khafidh[1,2*], B. Setiyana[1,3], J. Jamari[3], M.A. Masen[4], D.J. Schipper[1]

[1] Faculty of Engineering Technology, University of Twente, P.O. Box 217, 7500AE, Enschede, The Netherlands.
[2] Dutch Polymer Institute DPI, P.O. Box 902, 5600AX Eindhoven, The Netherlands.

[3] Department of Mechanical Engineering, University of Diponegoro, Jl. Prof. Soedharto SH, Tembalang, Semarang 50275, Indonesia.
[4] Department of Mechanical Engineering, Imperial College London, Exhibition Road, London, SW7 2AZ, United Kingdom.
*email: m.khafidh@utwente.nl

Abstract
Elastomeric materials are used in daily applications, such as tyres and conveyor belts. Sliding friction of elastomeric materials often produces a unique periodic wear pattern. In general, the periodic wear pattern has to be prevented because it generates surface instabilities and, as a result, vibration. Sliding contact between an elastomer and a rigid ball may cause the development of a periodic wear pattern like a wave on the elastomer surface, called a wavy wear track. The present study has investigated the occurrence of the wavy wear track on the elastomers under several operating conditions. The elastomers used were a Styrene-Butadiene Rubber (SBR) and Butadiene Rubber (BR) reinforced with two types of fillers, i.e. highly dispersible silica and short-cut aramid fiber. A pin-on-disc tribometer was used to study the wavy wear track of the materials under several operating conditions. An analytical model was used to predict the wave length of the wear pattern and to study the occurrence of the wavy wear track. The results show that the occurrence of the wavy wear track depends on the mechanical properties of the elastomer, the operating conditions (such as sliding velocity and force), the inertia mass of the counter surface frame and the circumferential length of the wear track. The analytical model is in good agreement with the experimental results.

Keywords: Styrene-Butadiene Rubber (SBR), Butadiene Rubber (BR), elastomer, sliding friction, wear, wavy wear track.

1. Introduction

Elastomeric materials are used in a wide range of applications, such as tyres [1], wiper blades [2], conveyor belts [3] and seals [4]. In these applications, the

elastomers contact with and slide against other components, which is a major source of frictional losses and wear. As a result, numerous investigations have been carried out regarding the sliding friction of elastomeric materials, focusing on topics such as the contact area [5], friction [6], wear [7] and lubrication [8]. Typically, materials that wear as the result of sliding contact with a harder counter material develop a fairly smooth, uniform wear track. However, elastomeric materials typically show a wear track that appears to have periodic features, as described in detail by [9]. In daily life, this phenomenon has been reported in several applications, such as tyres [10] and conveyor belts [11]. Such a periodic pattern often generates surface instabilities at the elastomer surface. The resulting dynamics and fluctuations reduce the performance of the rolling/sliding system significantly, especially with respect to the positional accuracy, stability [12], vibration and noise [13]. Because of these disadvantages, the development of periodic wear patterns should be prevented in practical applications.

The surface irregularities that develop in a sliding elastomer contact often correlate with the so-called Schallamach waves [14]. Schallamach investigated the development of detachment waves in the sliding contact between soft elastomers and glass and found that a periodic pattern propagates across the contact zone from the leading edge to the trailing edge. Following the work of Schallamach, many studies have investigated the Schallamach waves, see for instance [15-20].

The development of periodic features and wear patterns have been investigated previously using needle [21-24] and blade [9, 25-29] indenters. Fukahori et al. [9, 28, 29]studied the periodic wear pattern between a blade indenter and an elastomer and observed a periodic crack pattern in the elastomer. They state that the initial cracks are formed due to micro-vibrations of the elastomer, followed by stick-slip oscillation that causes propagation of the cracks. The resulting spacing of the final pattern can be correlated with the stick-slip frequency.

In the case of a rigid sphere sliding against an elastomer counter surface, a macro wear pattern so-called wavy wear track may be created on the elastomer surface. This wavy wear track generates severe vibration in the system and furthermore influences both the frictional and wear behaviour. Several experimental studies have been reported considering the stick-slip motion for the sliding contact between a rigid ball and an elastomer flat surface [14, 15, 30-32]. Maegawa and Nakano [31] investigated the mechanism of stick-slip associated with Schallamach waves and found that stick-slip will occur at certain combinations of low forces and high sliding velocities. The Schallamach waves will generate variations in the contact area, which determines the stick-slip behaviour, but the key parameters that influence the occurrence of a wavy wear track are not fully understood and, as a result, there is no method available to describe or predict the formation and the properties of the wavy wear track.

In the present study, the wavy wear track phenomenon of an elastomeric material was investigated. A pin-on-disc tribometer was used to study the occurrence of the wavy wear track, using a relatively large and smooth ball as the counter surface of the elastomeric flat. Two types of materials based on a Styrene-Butadiene Rubber (SBR) and Butadiene Rubber (BR) were used. A range of operating conditions was used to investigate the effects of the radius of sliding track, the sliding velocity and the normal force on the occurrence of a wavy wear track. A comparative study has been made between the analytical model and the experimental results.

2. Materials and Methods

2.1 Materials

Two types of elastomers were used in the present study: (1) a mixture of Styrene-Butadiene Rubber (SBR) and Butadiene Rubber (BR, high-cis-polybutadiene) with a formulation based on a silica-reinforced passenger car tire tread called 'Green Tyre' [33]. The rubber is reinforced with 80 phr (parts per hundred rubber) of highly dispersible silica using *bis*-(tri-ethoxy-silyl propyl) tetrasulfide (TESPT) as the coupling agent to provide a bond between the silica particles and the polymer; (2) a Styrene-Butadiene Rubber (SBR) reinforced with 15 phr aramid fibres supplied by Teijin Aramid B.V, Arnhem, The Netherlands. The initial length of the Aramid fibres is approximately 3 mm, with a diameter of between 10 and 12 μm. A silane coupling agent NXT S-3-(triethoxysilylpropyl)-octanethioate was used to provide chemical bonding between the fibres and the matrix. The fibres were dispersed in random directions in the matrix, meaning that the mechanical properties of the material can be assumed to be the same in all directions and the material can be regarded as being isotropic. Details of the formulation in parts per hundred rubber (phr) are given in Table 1.

Table 1. Material formulation of the elastomers.

Ingredients	SBR-BR [in phr]	SBR [in phr]	Supplier
SBR, Buna VSL VP PBR 4045 HM	-	100	Arlanxeo, Leverkusen, Germany
SBR, Buna VSL 5025-2 HM	97.3*	-	Arlanxeo, Leverkusen, Germany
BR, KBR 01	30.0	-	Kumho, Seoul, S-Korea
Silica Ultrasil VN3	80.0	-	Evonik Industries AG, Essen, Germany
Zinc oxide (ZnO)	2.5	2.5	Sigma Aldrich, St. Louis, United States

Stearic acid (SA)	2.5	1.5	Sigma Aldrich, St. Louis, United States
TDAE oil	6.7	-	Hansen & Rosenthal, Hamburg, Germany
Twaron aramid fibre	-	15	Teijin Aramid B.V, Arnhem, The Netherlands
TESPT	7.0	-	Evonik Industries AG, Essen, Germany
NXT	-	6.0	Momentive, New York, United States
6PPD	2.0	-	Flexsys, Brussels, Belgium
TMQ	2.0	-	Flexsys, Brussels, Belgium
Sulfur	1.4	2.8	Sigma Aldrich, St. Louis, United States
N-Cyclohexyl Benzothiazole Sulfenamide (CBS)	1.7	3.4	Flexsys, Brussels, Belgium
Di-Phenyl Guanidine (DPG)	2.0	4	Flexsys, Brussels, Belgium

* Containing 37.5 wt% oil

The materials were mixed in an internal mixer. Vulcanized specimens with a thickness of 2 mm were prepared for tensile tests, while vulcanized specimens with a thickness of 5 mm and a diameter of 50 mm were prepared for tribometer tests.

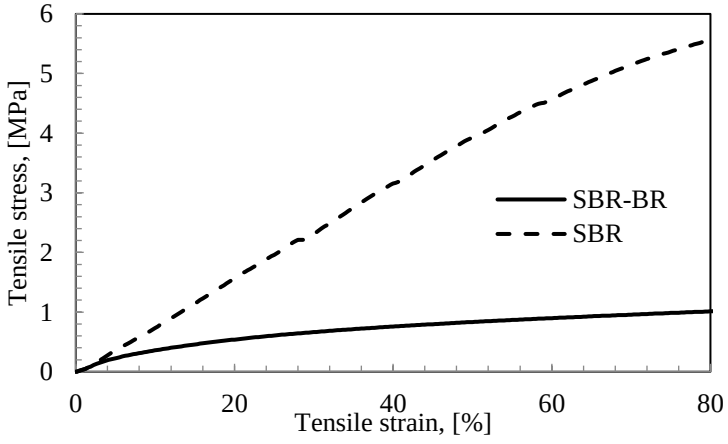

Figure 1. Stress-strain relationship of the materials listed in Table 1.

Tensile measurements were performed using an Instron tensile tester. The stress-strain relation for the two materials is depicted in Figure 1. The elastomer behaves nonlinearly at relatively high strains. The mechanical properties of the elastomer at high strains are a complex problem and are still the subject of several studies. Therefore, in the present study the elastic moduli of the materials were defined at a strain of 2%, assuming the material behaves linearly at that strain [34]. From the experimental results, the elastic moduli of the SBR-BR mix and the SBR material were 4.69 ± 0.2 MPa and 4.90 ± 0.4 MPa, respectively.

A Dynamic Mechanical Analyser (DMA) was used to determine the dynamic properties of the materials. Creep compliances of the materials were determined using a Metravib Viscoanalyser DMA+150, constant stress and at ambient temperature. Figure 2 shows that the creep compliance of the SBR-BR materials is higher than that of the SBR materials. The creep compliance results were fitted using a series of discrete exponential terms given by [35]:

$$\phi(t) = \phi_r - \sum_{i=1}^{3} \phi_i \, exp\left(\frac{-t}{\lambda_i}\right) \tag{1}$$

where ϕ_r indicates the creep at a fully relaxed state, t indicates time and λ_i indicates the retardation times. As can be seen in Figure 2, the creep compliances of the materials are well described by the equation. The parameter values of the fit equation can be found in Table 2 for both materials.

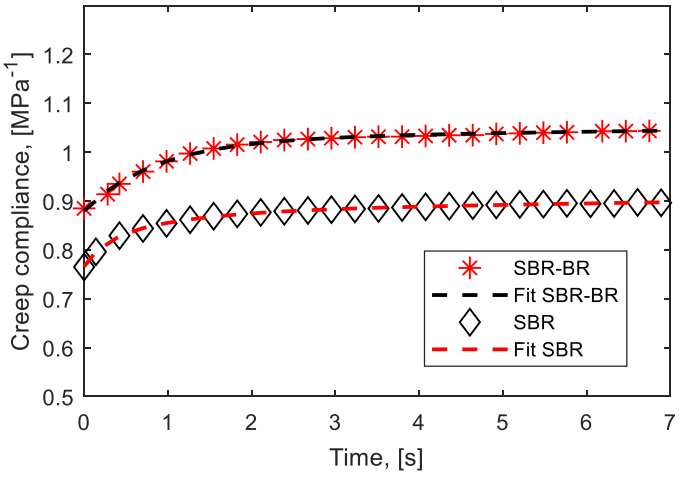

Figure 2. Experimental data and curve fitting of the creep compliances for both materials.

Table 2. Parameter values of the fit equation.

	SBR-BR	SBR
ϕ_r [Pa^{-1}]	1.07×10^{-06}	9.26×10^{-07}
ϕ_1 [Pa^{-1}]	1.42×10^{-07}	4.22×10^{-08}
ϕ_2 [Pa^{-1}]	2.11×10^{-07}	6.64×10^{-08}
ϕ_3 [Pa^{-1}]	2.87×10^{-08}	5.19×10^{-08}
λ_1 [s]	0.86	0.21
λ_2 [s]	6.79	0.94
λ_3 [s]	19.97	11.79

2.2 Methods

A schematic illustration of the pin-on-disc tester used in the present study is depicted in Figure 3. It consists of a rotating elastomer disc and a spherically shaped pin. The total force of the pin on the elastomer surface consists of a static and a dynamic component; the static force is caused by the dead weight applied on the elastomer surface, while the dynamic force is caused by the inertia force of the counter surface frame, i.e. dead weight, beam and counterweight during sliding.

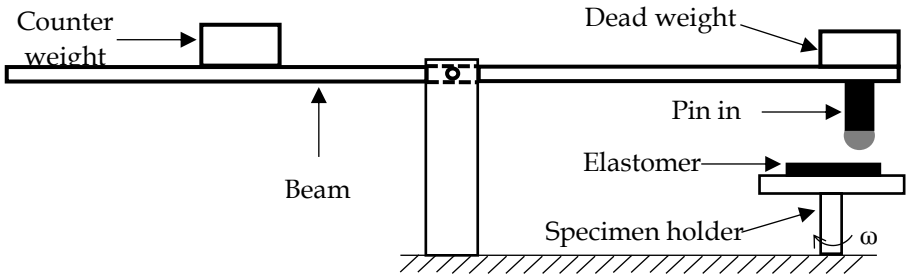

Figure 3. Pin-on-disc tribometer, shown schematically.

During sliding, oscillations can occur both in the normal and in the tangential (sliding) direction. When contact occurs between the elastomer surface and the counter surface, they oscillate together. These oscillations will be influenced by the dead weight mass (m_w), the inertia of the frame (m_f), the mechanical properties of the elastomer and the operating conditions of the test. In the appendix to this paper, a summary of the dynamical behaviour of the system is given, based on the work of Setiyana, et al. [36].

For low sliding velocities, the oscillation will take place predominantly in the tangential direction. In this case, the effect of static and kinetic friction will be important. A study of stick-slip behaviour when oscillation occurs only in the tangential direction has been done in a previous study [37]. For high sliding velocities, the normal direction oscillation of the elastomer surface dominates the total dynamic response, meaning that the vibrations in tangential direction can be neglected. This study focuses on the macro scale irregularity of the wear track due to the normal oscillation of the system. The normal oscillation frequency of the system is defined as [36]:

$$f_n = \frac{1}{2\pi}\sqrt{\frac{k_n\left(1-{\xi_f}^2\right)}{m_w+m_f}} \tag{2}$$

where f_n is the frequency of the counter surface system in the normal direction, k_n is the normal stiffness of the elastomer, ξ_f is the damping factor of the frame, m_w is the dead weight mass and m_f is the inertia of the frame. Since the materials used in the present study behave isotropic-viscoelastic, the indentation depth δ can be estimated as [38]:

$$\delta = \left(\frac{9{F_N}^2}{16{E^*}^2 R}\bar{\phi}(t)\right)^{1/3} \tag{3}$$

where δ is the indentation depth, F_N is the normal force, E^* is the reduced elastic modulus, R is the radius of the spherical counter surface, and $\bar{\phi}(t)$ is the normalized creep compliance. The stiffness in normal direction of the material is defined as the ratio of the normal force and the indentation depth:

$$k_n = \frac{F_N}{\delta} \tag{4}$$

The wave length (Δx_n) of the wavy wear pattern is the ratio of the given sliding velocity and the normal frequency of the system, which is defined as:

$$\Delta x_n = 2\pi v\sqrt{\frac{m_w+m_f}{k_n\left(1-{\xi_f}^2\right)}} \tag{5}$$

where v is the sliding velocity. A detailed explanation about this analytical dynamic model for the set-up can be found in the Appendix.

Table 3. Operating conditions of pin-on-disc tests.

Test ID	#1	#2	#3	#4	#5	#6
Disc material	SBR-BR	SBR-BR	SBR-BR	SBR	SBR	SBR
Normal force [N]	2	2	2	3	5	5
Velocity [m/s]	0.2	0.2	0.2	0.2	0.2	0.3
Radius of track [m]	0.006	0.0125	0.019	0.012	0.012	0.012

The pin-on-disc tribometer was equipped with a ball with a radius of 12.5 mm, sliding against an elastomer flat disc. The tests were performed under dry condition and at room temperature. Table 3 lists the operating conditions that were used in the present study. For the SBR-BR material, a different radius of the wear track was used, see test #1 to test #3 in Table 3. The normal force and sliding velocity were varied for the SBR material. Due to the lack of a damper in the pin-on-disc tribometer set-up, the damping factor of the counter surface frame is neglected (ξ_{nd} = 0). The inertia mass of the frame in the present study is approximately 0.26 Kg.m^2. Since the type and the dimension of the rigid ball are the same for all tests, the inertia mass of the counter surface frame (*mf*) is the same for all tests.

3. Results and Discussion

3.1 Analytical results

The analytical calculation was conducted with Equation 1 to Equation 5, in which the wave length depends on the mechanical properties of the material and the operating conditions used in the experiment, such as normal force and sliding velocity.

Figure 4 shows examples of analytical calculations for two types of materials with different elastic modulus, i.e. 5 MPa and 10 MPa. The inertia mass of frame of 0.26 Kg.m^2 and the radius of the spherical counter surface of 12.5 mm were used in the calculations. The sliding velocity was kept constant, v = 0.2 m/s, and the value of the normal force was varied. The creep compliance of the SBR material was used in these calculations. The results show that the wave length increases with increasing normal force. It is caused by the system oscillating with difficulty at a higher normal force so that the normal oscillation frequency reduces. As a result, the wave length increases when a constant sliding velocity is applied. At very high normal forces, the wave length increases marginally. On the other hand, a stiffer material shows a shorter wave length than the soft material. The stick-slip or wave motion often occurs in soft materials and diminishes in stiff materials [20, 39].

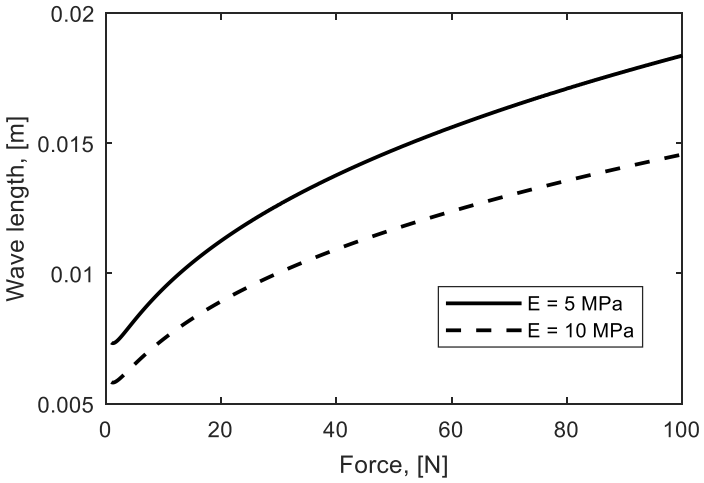

Figure 4. The wave length as a function of the normal force at a sliding velocity of 0.2 m/s.

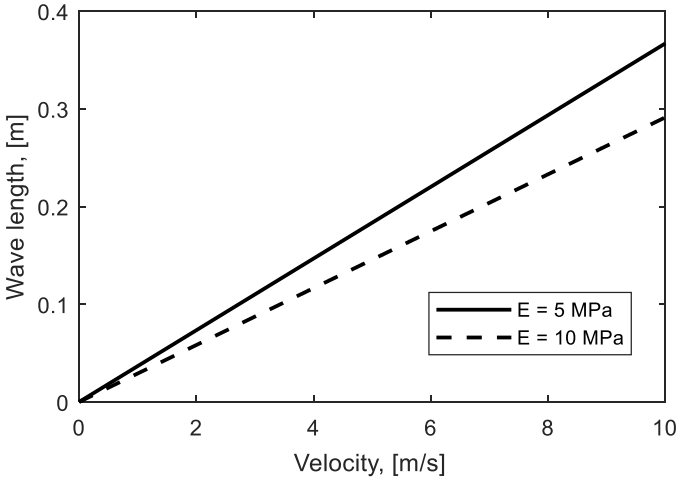

Figure 5. The wave length as a function of sliding velocity at a normal force of 1 N.

The effect of sliding velocity on the wave length is depicted in Figure 5. The materials, inertia mass of frame and radius of the spherical counter surface used in these calculations are the same as the calculations in Figure 4. A constant normal force of 1 N was used, and the sliding velocity was varied. The results show that the wave length increases linearly with increasing sliding velocity. This can be explained by the fact that a longer travelling distance in one periodic oscillation can be achieved at a higher sliding velocity when a constant normal oscillation frequency

is applied. As a result, a longer wave length is found, which is consistent with previous studies [9, 40]. Moreover, a shorter wave length is found for the stiffer material because it reduces the normal oscillation frequency. The different wave lengths between both materials become more pronounced at a high sliding velocity.

3.2 Experimental results

Pin-on-disc tribometer experiments were carried out using several materials and under various operating conditions to validate the analytical model. The tests were stopped when the coefficient of friction reached a steady-state phase. Figure 6 shows the wear track results of SBR-BR material under several operating conditions, i.e. test #1 to test #3. It is clearly seen that a wavy wear track is observed in test #1, while the wear tracks in test #2 and test #3 are relatively smooth without a wave pattern. The number of wavy wear patterns on the SBR-BR surface in test #1 is 5, with a wave length of approximately 7.54 mm, see Figure 6.

The wave length of each test was calculated based on Equation 1 to Equation 5 using the operational conditions given in Table 3, together with the inertia mass of the counter surface frame and the mechanical properties of the materials. The creep compliances of the materials can be obtained by putting the parameter values of Table 2 into Equation 1. The time used in the calculation is based on the contact time between the counter surface and the elastomer. Since the normal force and sliding velocity of test #1 to test #3 are the same, their normal oscillation frequencies are the same. As a result of the calculations, the wave length is 7.56 mm for those tests. This result is in agreement with the wave length which is observed in test #1, see Figure 6. Although test #2 and test #3 have the same wave length, the wavy wear track is not observed on the SBR-BR surface after those tests. This is because of the different locations of the waves between the different cycles, see Figure 7a. The aforementioned term 'cycle' means one revolution of the disc. When the locations of waves are at the same position in every cycle, the wavy wear track will be visible at the surface after the test. However, when the locations of the waves are different in each cycle, the wear track becomes relatively smooth after a large number of cycles, and the wavy wear track will not be visible, see Figure 7b.

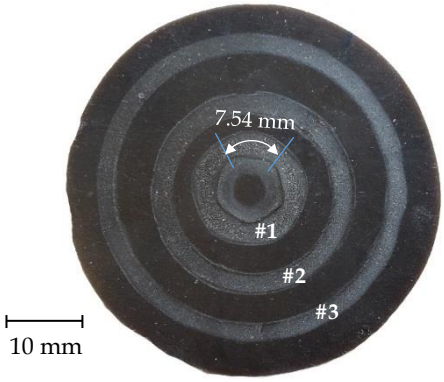

Figure 6. The wear tracks on the surface of SBR-BR material in test #1 to test #3.

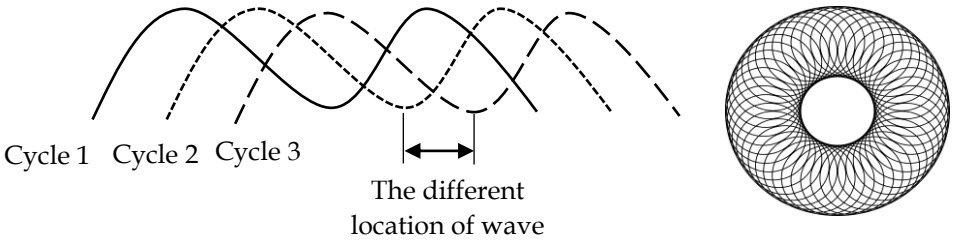

(b) (b)

Figure 7. (a) The waves at three different locations, (b) the final wear track for a large number of cycles when the locations of waves are different in each cycle, shown schematically.

The requirement of the occurrence of a wavy wear track is that the location of the waves has to be the same in each cycle. It means that the ratio between the circumferential distance of the wear track and the wave length has to be an integer. The number of wavy wear patterns in the circumferential of wear track can be expressed as:

$$n = \frac{2\pi r}{\Delta x_n} \tag{6}$$

where n is the number of the wavy wear patterns, Δx_n is the wave length and r is the radius of the wear track.

By putting the calculated result of the wave length (7.56 mm) and the radius of the wear track given in Table 3 into Equation 6, the number of wavy wear patterns

in the circumferential direction in the wear track is 4.99 ≈ 5, 10.39 and 15.80 in test #1, test #2 and test #3, respectively. The number of wavy wear patterns in test #1 was found to be an integer and in agreement with the experimental result, see Figure 6. At the same time, the non-integer numbers of wavy wear patterns in the circumferential track were found in test #2 and test #3. This is why they had smooth wear tracks at the end of the tribometer tests.

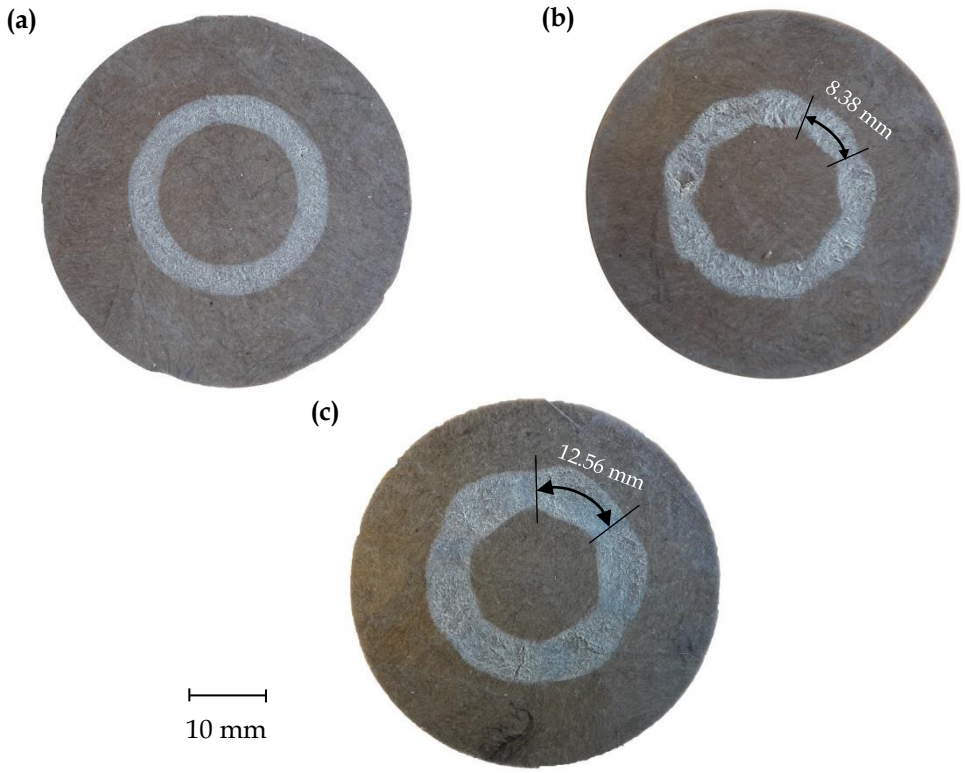

Figure 8. The wear tracks on the surface of SBR material in: (a) test #4, (b) test #5 and (c) test #6.

The effects of normal force and sliding velocity on the occurrence of a wavy wear track were investigated using SBR material, see Figure 8. It can be seen that the wavy wear track is not observed in test #4, whereas it is visible in tests #5 and #6. The number of wavy wear patterns in test #5 and test #6 is 9 and 6, respectively. By using the same calculation procedure, the number of wave patterns in the circumferential direction of the wear track can be estimated for those tests. As can be seen from the results, the number of wave patterns in test #4, test #5 and test #6

is 9.65, 9.01 ≈ 9 and 6.01≈ 6, respectively. These results are in good agreement with the experimental results, see Figure 8.

The comparison between the analytical model and the experimental results for all materials is summarized in Table 4. It can be seen that the number of wavy wear patterns in the circumferential direction in test #2, test #3 and test #4 is not an integer and, as a result, no wavy wear track is observed.

Table 4. The comparison between the analytical model and experimental results.

Tests ID	Force [N]	Velocity [m/s]	Radius of the track [mm]	Δx_n [mm] (model)	Δx_n [mm] (experiment)	$\frac{2\pi r}{\Delta x_n\ (model)}$
#1	2	0.2	6	7.56	7.54	4.99 ≈ 5
#2	2	0.2	12.5	7.56	-	10.39
#3	2	0.2	19	7.56	-	15.80
#4	3	0.2	12	7.81	-	9.65
#5	5	0.2	12	8.37	8.38	9.01 ≈ 9
#6	5	0.3	12	12.55	12.56	6.01 ≈ 6

It is shown that the analytical model that predicts the occurrence of a wavy wear track is in good agreement with the experimental results. The wave length can be estimated based on the mechanical properties of the material, the inertia mass of the counter surface frame and the operating conditions used in the experiments, such as normal force and sliding velocity. In a previous study, the stick-slip motion is likely to occur for small normal force and large sliding velocity [31]. However, the occurrence of a wavy wear track depends not only on the stick-slip motion of the system but also on the circumferential length of the wear track, as seen in test #1 to test #3.

Figure 9 shows an image of wear surface on the SBR-BR material in test #2. Although a wavy wear track is not visible in this test, crack patterns are found in the wear track. This phenomenon was also reported by many other studies, see for instance [9, 10, 22, 28, 41, 42]. These crack patterns can be associated with the wave of the system during sliding contact. Since the locations of the waves are different for each cycle, the small crack patterns are formed after a large number of cycles, see Figure 7b. For the SBR material, no specific wear pattern is formed on the wear surface. This is caused by the presence of fibres on the wear surface preventing the specific crack pattern, which is consistent with a previous study [43]. For a fibre reinforced elastomer without any filler (such as silica and carbon black), the rigid counter surface is in contact mainly with the fibres in the steady-state phase [44, 45].

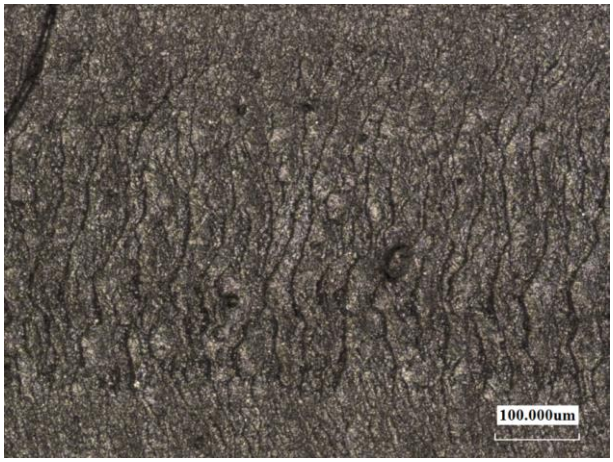

Figure 9. Crack patterns on the SBR-BR surface in test #2.

Based on the present study, a wavy wear track can be prevented by adjusting several parameters like the radius of the wear track, the sliding velocity and the normal force. The wavy wear track may generate inaccuracy of friction and wear results of pin-on-disc tribometer experiments. By preventing a wavy wear track, this inaccuracy can be avoided. In the real engineering application, not only a macro-wave has to be prevented but also a micro-wave (crack pattern). Therefore, the best way to prevent both is by adjusting the dynamics of the system in which the elastomer is operating through the application of a damper system, for instance.

4. Conclusion

The wavy wear track of elastomers as a function of several operating conditions was studied. A rigid indenter ball and two types of elastomers made of Styrene-Butadiene Rubber (SBR) and Butadiene Rubber (BR) were used. The conclusions of this study can be summarized as follows:

1. The oscillations may occur in the system during sliding friction that can cause a macro (wavy wear track) and micro (crack pattern) wear pattern on the elastomer surface.
2. The wavy wear track can be prevented by adjusting the mechanical properties of the elastomer, the operational conditions (such as sliding velocity and force), the inertia mass of the system, and the circumferential length of the wear track. While the crack pattern may be prevented by adding a damper to the system.
3. An analytical model was developed to predict the occurrence of a wavy wear track, and it shows good agreement with the experimental results.

Acknowledgement

This research forms part of the Research Programme of the Dutch Polymer Institute DPI, Project #782.

Appendix [36]

Figure A.1 shows the physical model that represents an elastomer surface in contact with a counter surface. It consists of an oscillating elastomer mass (m_e) with stiffness and damping in tangential (k_t, c_t) as well as in normal direction (k_n, c_n). The acting forces in the contacting surfaces are the driving force (F_d) of the elastomer, the tangential contact force (F_t) and the normal contact force (F_n). During sliding friction, there are two possibilities of contact interaction between the elastomer surface and the counter surface: separation and unification. The separation means no contact between the elastomer surface and the counter surface, see Figure A.1 (a). In this case, the oscillating mass of the elastomer (m_e) oscillates without the mass of the counter surface system (m_s). The unification interaction means that the elastomer surface and the counter surface are unified, and they oscillate together. The unified mass (M) is an aggregate of the oscillating elastomer mass and the inertia mass of the counter surface system ($M = m_e + m_s$), see Figure A.1 (b). The oscillating elastomer mass is assumed to be much smaller than the inertia mass of the counter surface frame, so it can be neglected. Thus, the oscillating unified mass can be written as $M \approx m_s = m_w + m_f$, where m_w is the dead weight mass and m_f is the inertia mass of the counter surface frame. An equivalent damping is denoted by c_{nd}, which is a combination of the elastomer and the apparatus dashpot. Based on Figure A.1 (b), the equation of motion in tangential direction is given in Equation (A.1) by involving the tangential force (F_t), where, v is the sliding velocity and t is time. The equation of motion in normal direction is given in Equation (A.2).

$$m_e\ddot{x} + c_t\dot{x} + k_t x = k_t vt + c_t v - F_t \tag{A.1}$$

$$M\ddot{y} + c_{nd}\dot{y} + k_n y = 0 \tag{A.2}$$

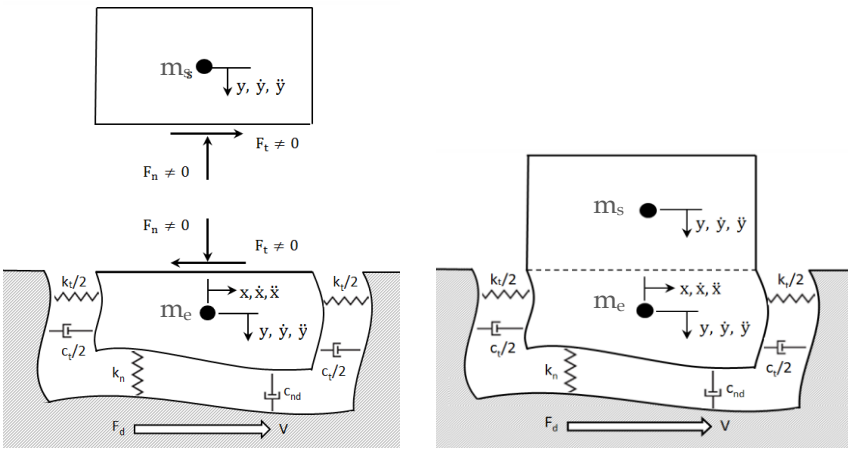

Figure A.1. The interaction during sliding contact between an elastomer surface and a counter surface, (a) separation, (b) unification [36].

For a high driving velocity, the elastomer surface oscillates predominantly in the normal direction, meaning that the oscillation in tangential direction can be neglected. The natural frequency in the normal oscillation for the undamped system (ω_n) can be defined as follows:

$$\omega_n = \sqrt{\frac{k_n}{M}} \tag{A.3}$$

When the system uses a dashpot, a damped natural frequency (ω_d) is given by:

$$\omega_d = \omega_n \sqrt{1 - \xi_f{}^2} \tag{A.4}$$

The normal oscillation period of the system (T_n) can be found by using the following equation:

$$T_n = 2\pi\omega_d \tag{A.5}$$

By putting Equation A.3 and Equation A.4 into Equation A.5, the normal oscillation period can be expressed as follows:

$$T_n = 2\pi\sqrt{\frac{M}{k_n\left(1-{\xi_f}^2\right)}} \tag{A.6}$$

The periodic displacement (Δx_n) in tangential direction due to normal oscillation is:

$$\Delta x_n = vT_n = 2\pi\sqrt{\frac{M}{k_n\left(1-{\xi_f}^2\right)}} \tag{A.7}$$

References

1. Lorenz, B., Y.R. Oh, S.K. Nam, S.H. Jeon, and B.N.J. Persson, *Rubber friction on road surfaces: Experiment and theory for low sliding speeds.* The Journal of Chemical Physics, 2015. **142**(19): pp. 194701.
2. Bódai, G. and T.J. Goda, *Friction force measurement at windscreen wiper/glass contact.* Tribology Letters, 2012. **45**(3): pp. 515-523.
3. Zhao, L.H., X.B. Wei, and X.G. Li. *The analysis on the tribological properties of CR/EPDM blends with chrome-plated steel under dry sliding*. in *Advanced Materials Research*. 2013. Trans Tech Publ.
4. Farfán-Cabrera, L.I., E.A. Gallardo-Hernández, J.B. Pascual-Francisco, C.D. Resendiz-Calderon, and C.S. de la Rosa, *Experimental method for wear assessment of sealing elastomers.* Polymer Testing, 2016. **53**: pp. 116-121.
5. Khafidh, M., N.V. Rodriguez, M.A. Masen, and D.J. Schipper, *The dynamic contact area of elastomers at different velocities.* Tribology - Materials, Surfaces & Interfaces, 2016. **10**(2): pp. 70-73.
6. Mokhtari, M., D.J. Schipper, and T.V. Tolpekina, *On the friction of carbon black- and silica-reinforced BR and S-SBR elastomers.* Tribology Letters, 2014. **54**(3): pp. 297-308.
7. Payne, N.G. and R.G. Bayer, *Friction and wear tests for elastomers.* Wear, 1991. **150**(1–2): pp. 67-77.
8. Mofidi, M., E. Kassfeldt, and B. Prakash, *Tribological behaviour of an elastomer aged in different oils.* Tribology International, 2008. **41**(9–10): pp. 860-866.
9. Fukahori, Y. and H. Yamazaki, *Mechanism of rubber abrasion. Part I: Abrasion pattern formation in natural rubber vulcanizate.* Wear, 1994. **171**(1): pp. 195-202.
10. Mané, Z., J.-L. Loubet, C. Guerret, L. Guy, O. Sanseau, L. Odoni, L. Vanel, D.R. Long, and P. Sotta, *A new rotary tribometer to study the wear of reinforced rubber materials.* Wear, 2013. **306**(1-2): pp. 149-160.

11. Molnar, W., M. Varga, P. Braun, K. Adam, and E. Badisch, *Correlation of rubber based conveyor belt properties and abrasive wear rates under 2-and 3-body conditions.* Wear, 2014. **320**: pp. 1-6.
12. Maegawa, S., F. Itoigawa, and T. Nakamura, *Dynamics in sliding friction of soft adhesive elastomer: Schallamach waves as a stress-relaxation mechanism.* Tribology International, 2016. **96**: pp. 23-30.
13. Nakano, K. and S. Maegawa, *Safety-design criteria of sliding systems for preventing friction-induced vibration.* Journal of Sound and Vibration, 2009. **324**(3-5): pp. 539-555.
14. Schallamach, A., *How does rubber slide?* Wear, 1971. **17**(4): pp. 301-312.
15. Best, B., P. Meijers, and A.R. Savkoor, *The formation of schallamach waves.* Wear, 1981. **65**(3): pp. 385-396.
16. Persson, B.N.J., *Elastic instabilities at a sliding interface.* Physical Review B, 2001. **63**(10): pp. 104101.
17. Barquins, M., *Energy dissipation in schallamach waves.* Wear, 1983. **91**(1): pp. 103-110.
18. Barquins, M., *Friction and wear of rubber-like materials.* Wear, 1993. **160**(1): pp. 1-11.
19. Koudine, A., M. Lambert, and M. Barquins, *Some new experimental results on the Schallamach waves propagation by space-time analysis.* International Journal of Adhesion and Adhesives, 1997. **17**(4): pp. 359-363.
20. Rand, C.J. and A.J. Crosby, *Insight into the periodicity of Schallamach waves in soft material friction.* Applied Physics Letters, 2006. **89**(26): pp. 261907.
21. Schallamach, A., *Abrasion of rubber by a needle.* Journal of Polymer Science, 1952. **9**(5): pp. 385-404.
22. Schallamach, A., *Friction and abrasion of rubber.* Wear, 1958. **1**(5): pp. 384-417.
23. Thomas, A.G. *Factors influencing the strength of rubbers.* in *Journal of Polymer Science: Polymer Symposia*. 1974. Wiley Online Library.
24. Champ, D.H., E. Southern, and A.G. Thomas, *Fracture mechanics applied to rubber abrasion*, in *Advances in Polymer Friction and Wear*. 1974, Springer. pp. 133-144.
25. Liang, H., Y. Fukahori, A.G. Thomas, and J.J.C. Busfield, *Rubber abrasion at steady state.* Wear, 2009. **266**(1–2): pp. 288-296.
26. Coveney, V. and C. Menger, *Initiation and development of wear of an elastomeric surface by a blade abrader.* Wear, 1999. **233–235**: pp. 702-711.
27. Fukahori, Y., H. Liang, and J.J.C. Busfield, *Criteria for crack initiation during rubber abrasion.* Wear, 2008. **265**(3–4): pp. 387-395.
28. Fukahori, Y. and H. Yamazaki, *Mechanism of rubber abrasion. Part 2: General rule in abrasion pattern formation in rubber-like materials.* Wear, 1994. **178**(1-2): pp. 109-116.

29. Fukahori, Y. and H. Yamazaki, *Mechanism of rubber abrasion. Part 3: how is friction linked to fracture in rubber abrasion?* Wear, 1995. **188**(1–2): pp. 19-26.
30. Barquins, M. and R. Courtel, *Rubber friction and the rheology of viscoelastic contact.* Wear, 1975. **32**(2): pp. 133-150.
31. Maegawa, S. and K. Nakano, *Mechanism of stick-slip associated with Schallamach waves.* Wear, 2010. **268**(7–8): pp. 924-930.
32. Koudine, A.A. and M. Barquins, *Formation of micro-ridges on the surface of Schallamach waves propagating in the contact area between a moving rubber sample and a glass lens.* Journal of Adhesion Science and Technology, 1996. **10**(10): pp. 951-961.
33. Rauline, R., *(to Compagnie Generale des Establissements Michelin) EU 0501227.* 1992.
34. Hintze, C., R. Boldt, S. Wiessner, and G. Heinrich, *Influence of processing on morphology in short aramid fiber reinforced elastomer compounds.* Journal of Applied Polymer Science, 2013. **130**(3): pp. 1682-1690.
35. Ferry, J.D. and J.D. Ferry, *Viscoelastic properties of polymers*. 1980: John Wiley & Sons.
36. Setiyana, B., R. Ismail, J. Jamari, and D.J. Schipper, *An analytical study of the wear pattern of an abraded rubber surface: the interaction model.* Tribology-Materials, Surfaces & Interfaces, 2018: pp. 1-7.
37. Setiyana, B., R. Ismail, J. Jamari, and D.J. Schipper, *Stick-slip behaviour of a viscoelastic flat sliding along a rigid indenter.* Tribology Online, 2016. **11**(4): pp. 512-518.
38. Rodriguez, N.V., M.A. Masen, and D.J. Schipper, *A contact model for orthotropic-viscoelastic materials.* International Journal of Mechanical Sciences, 2013. **74**: pp. 91-98.
39. Maegawa, S. and K. Nakano, *Dynamic behaviors of contact surfaces in the sliding friction of a soft material.* Journal of Advanced Mechanical Design, Systems, and Manufacturing, 2007. **1**(4): pp. 553-561.
40. Nakano, K. and S. Maegawa, *Occurrence limit of stick-slip: dimensionless analysis for fundamental design of robust-stable systems.* Lubrication Science, 2010. **22**(1): pp. 1-18.
41. Kopchenkov, V., *Modeling elastomer wear under the effects of solid particles at an angle to the surface.* Journal of Friction and Wear, 2017. **38**(2): pp. 162-167.
42. Muhr, A. and A. Roberts, *Rubber abrasion and wear.* Wear, 1992. **158**(1-2): pp. 213-228.
43. Wada, N. and Y. Uchiyama, *Friction and wear of short-fibre-reinforced rubber composites under various sliding speeds and loads.* Wear, 1993. **162**: pp. 930-938.

44. Khafidh, M., D.J. Schipper, M.A. Masen, N. Vleugels, and J.W.M. Noordermeer, *Friction of short-cut aramid fiber reinforced elastomer*, in *Proceedings of the 6th World Tribology Congress*. 2017: Beijing.
45. Khafidh, M., D.J. Schipper, M.A. Masen, N. Vleugels, and J.W.M. Noordermeer, *Tribological behavior of short-cut aramid fiber reinforced SBR elastomers: the effect of fiber orientation.* Journal of Mechanical Engineering and Sciences, 2018. **12**(2): pp. 3700-3711.

PAPER C

Friction and Wear Mechanism of Short-cut Aramid Fiber and Silica Reinforced Elastomers

M. Khafidh[1,2*], D.J. Schipper [1], M.A. Masen[3], N. Vleugels[1,2], W.K. Dierkes[1], J.W.M. Noordermeer[1]

[1] Faculty of Engineering Technology, University of Twente, P.O. Box 217, 7500AE, Enschede, The Netherlands.

[2] Dutch Polymer Institute DPI, P.O. Box 902, 5600AX Eindhoven, The Netherlands.

[3] Department of Mechanical Engineering, Imperial College London, Exhibition Road, London, SW7 2AZ, United Kingdom.

*email: m.khafidh@utwente.nl.

Abstract

Important phenomena during sliding contact of elastomeric materials are friction and wear. Wear reduction of elastomers can be achieved by minimizing the propagation of cracks in the elastomer during sliding contact. Adding fillers like silica and fibres is a way to reduce the propagation of cracks and as a result reduction of wear. In the present study, the wear processes of short-cut aramid fibre reinforced elastomers as a function of sliding distance and their relation to friction are investigated. Two different types of systems are considered: (1) elastomers reinforced by solely short-cut aramid fibres and (2) elastomers reinforced by short-cut aramid fibres and silica. A pin-on-disc tribometer and a microscope are used to analyse the friction and wear mechanism of the elastomeric composites during sliding contact. The results show that the coefficient of friction of the composites consists of different stages, these stages are influenced by the wear processes during sliding. For elastomers which are reinforced by short-cut aramid fibres and silica, a higher energy input is needed to achieve all stages since the presence of silica in the elastomer matrix increases the matrix pull-out resistance. A general friction behaviour of short-cut aramid fibre and silica reinforced elastomers is proposed.

Keywords: elastomer; friction; short-cut aramid fibre; wear.

1. Introduction

Elastomers are polymers which have both viscous and elastic behaviour at room temperature. Generally, they have very weak inter-molecular forces, resulting in a lower Young's modulus than other materials. Elastomeric materials are used in daily applications such as tyres [1] and wiper blades [2]. The capability to withstand large

deformations without permanent loss of shape and mechanical properties is one of the reasons for their use. However, a single elastomer usually cannot fulfil all of the required properties which are needed in the applications. Adding reinforcing material such as silica and fibres is a way to improve the mechanical and tribological properties of elastomers.

Several possible mechanisms of the initiation of elastomer wear have been proposed [3-8]. Schallamach [3] suggested that the initiation of elastomer wear is caused by stick-slip. The stress concentration at the rear of the contact area between an elastomer and a counter surface results in crack formation in the elastomer surface. Gent et al. suggested [4] that the elastomer wear is caused by the detachment of small particles which are the results of small surface cracks. These cracks are developed by the unbounded elastic expansion of voids when they open the cracks under high internal pressure. Later, Fukahori et al. [5-7] concluded that the initial cracks are formed due to micro-vibration of the elastomer and that the stick-slip oscillation will propagate the cracks. Another study concluded that the intrinsic defects on the elastomer surface are the initiation points for the wear of the elastomer [8].

Carbon black and silica have been used as the main reinforcing materials for elastomeric composites in the past few decades. It is caused by their ability to improve the tribological behaviour by, for example, reducing abrasion wear [4]. Studies regarding wear and friction of carbon black/silica reinforced elastomers have been intensively conducted [9-11]. Later, fibres become popular for use as a reinforcing filler of elastomers because of the processing advantages and increase in strength, stiffness, modulus and damping [12].

Several types of fibres have been added into elastomers to improve the mechanical and tribological properties. The study of fiber reinforced elastomer composites on the tribological behaviour have been conducted by using several types of fibres, such as carbon fibre [13], cellulose fibre [14], polyamide fibre [15] and short-cut aramid fibre [16-18]. Khasani [16] studied the abrasion wear of elastomer reinforced with 1 phr (part per hundred rubber) short-cut aramid fibres and concluded that wear of the reinforced elastomer is slightly lower than that of the unreinforced elastomer. The low amount of short-cut aramid fibres also reduces the hysteresis and the abrasion wear of the truck tread composite [17]. Later, Rodriguez [18] showed that by adding short-cut aramid fibres into the elastomers leads to the reduction of the coefficient of friction. In a previous study, the effect of fibre orientation on the tribological behaviour of short-cut aramid fibre reinforced elastomers has been reported [19]. It is concluded that the steady-state coefficient of friction are the same for all reinforcement directions due to the presence of fibres on the wear surface. Although several studies of short-cut aramid fibre reinforced elastomers have been conducted, the wear processes of short-cut aramid fibre

reinforced elastomers as a function of sliding distance and their relation to friction is still not fully understood. The present study aims to investigate the friction and wear mechanism of elastomers that are reinforced solely by short-cut aramid fibers and elastomers that are reinforced by short-cut aramid fibres and silica. By employing a sliding contact between an elastomeric composite and a rigid counter surface, the friction behaviour and its relation to the wear process are investigated.

2. Materials and Methods

2.1. Materials

The studied materials are elastomers based on a styrene butadiene rubber (SBR) and a butadiene rubber (BR) with two types of reinforcing systems: highly dispersible silica and non-treated short-cut aramid fibres. The initial length of the short-cut aramid fibres is approximately 3 mm and their diameter is 10-12 μm, supplied by Teijin Aramid B.V, Arnhem, The Netherlands. The friction and wear mechanism are studied in two different types of systems. The first system is composed of elastomers reinforced by solely short-cut aramid fibres and the second system is composed of elastomers reinforced by short-cut aramid fibres and silica. Details of the formulation in parts per hundred rubber (phr) are given in Table 1. The formulation of the first system is based on the optimum formulation in a previous study [20], whereas the formulation of the second system is based on a silica-reinforced passenger car tire tread, called 'Green Tyre' [21]. The fibre direction of all composites is randomly oriented. Therefore, the composites can be assumed to be isotropic materials. This means that the mechanical properties of the composites are the same in all directions. The composites with a thickness of 2 mm and 5 mm were prepared for tensile and tribometer tests respectively.

Table 1. Material formulation of the composites.

Ingredients	Composite's ID		Supplier
	1 [in phr]	2 [in phr]	
SBR, Buna VSL VP PBR 4045 HM	100	-	Arlanxeo, Leverkusen, Germany
SBR, Buna VSL 5025-2 HM	-	97.3*	Arlanxeo, Leverkusen, Germany
BR, KBR 01	-	30.0	Kumho, Seoul, S-Korea
Silica Ultrasil VN3	-	80.0	Evonik Industries AG, Essen, Germany
Zinc oxide (ZnO)	2.5	2.5	Sigma Aldrich, St. Louis, United States

Stearic acid (SA)	1.5	2.5	Sigma Aldrich, St. Louis, United States
TDAE oil	-	6.7	Hansen & Rosenthal, Hamburg, Germany
Twaron aramid fibre	15	20	Teijin Aramid B.V, Arnhem, The Netherlands
Bis-triethoxysilylpropyl-tetrasulfide (TESPT)	-	7.0	Evonik Industries AG, Essen, Germany
S-3-triethoxysilylpropyl-octanethioate (NXT)	6.0	-	Momentive, New York, United States
6PPD stabilizer	-	2.0	Flexsys, Brussels, Belgium
TMQ stabilizer	-	2.0	Flexsys, Brussels, Belgium
Sulfur	2.8	1.4	Sigma Aldrich, St. Louis, United States
N-Cyclohexyl Benzothiazole Sulfenamide (CBS)	3.4	1.7	Flexsys, Brussels, Belgium
Di-Phenyl Guanidine (DPG)	4	2.0	Flexsys, Brussels, Belgium

* Containing 37.5 wt% oil

2.2. Experimental method

The mechanical properties of the composites were evaluated using tensile tests. An Instron tensile tester 3343 series was used, according to ISO 37 at a crosshead speed of 500 mm/min. A pin-on-disc tribometer was used for investigating the friction behaviour of the elastomeric composites. The pin-on-disc tribometer was equipped with a rigid ball, sliding against an elastomeric composite flat disc. The tribometer tests were performed under dry sliding and at room temperature. A Keyence VHX-5000 microscope and a Jeol JSM 6400 Scanning Electron Microscope (SEM) were used to scan the wear surface of the elastomeric composites.

In a previous study, it was reported that the steady-state coefficients of friction of 15 phr short-cut aramid fiber reinforced elastomer (composite 1) for several reinforcement directions show the same values although the mechanical properties of these composites are different [19]. To gain a better understanding of that finding, the wear processes of composite 1 and its relation to friction during sliding contact is studied here. The operating conditions used in the experiments are the same as applied in [19], i.e. a contact pressure of 0.2 MPa, a velocity of 0.2 m/s, and at ambient temperature.

The friction and wear mechanism of silica and short-cut aramid fibre reinforced elastomers was studied by using composite 2. Two levels of energy input were used: high energy input (a contact pressure of 2.4 MPa and a velocity of 0.3 m/s) and low energy input (a contact pressure of 0.8 Mpa and a velocity of 0.2 m/s).

3. Results and discussion

3.1. Mechanical properties of the composites

The mechanical properties of the composites are an important factor in analysing the tribological behaviour. The stress-strain relations of the composites 1 and 2 are depicted in Figure 1. As expected, the curve of the elastomer which is reinforced by short-cut aramid fibres and silica is steeper than that of the elastomer which is reinforced by solely short-cut aramid fibres. Elastomer behaves in a nonlinear manner at relatively high strains. Mechanical properties of the elastomer at high strain are complex. Therefore, in the present study, the elastic moduli of the composites were defined at a strain of 2%, assuming the material behaves linearly at that strain [22]. The elastic moduli of the composites 1 and 2 are 2.34 MPa and 13.7 MPa, respectively.

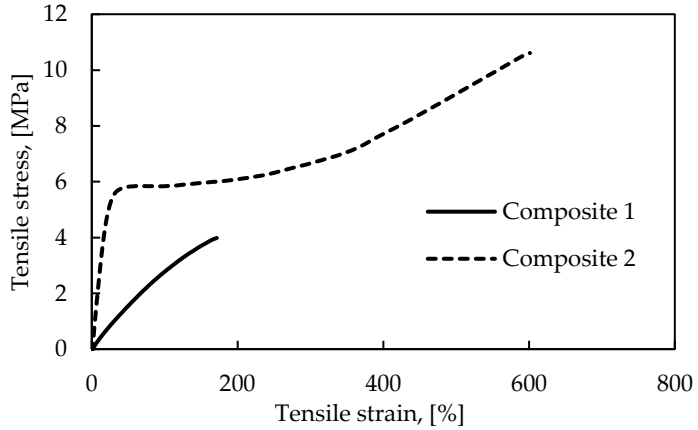

Figure 1. Stress-strain relations of the composites 1 and 2.

3.2. Friction and wear mechanism of short-cut aramid fiber reinforced elastomers

Figure 2 shows the coefficient of friction of composite 1 for several reinforcement directions, namely random, longitudinal (the fibres are oriented in the sliding direction), transverse (the fibres are oriented perpendicularly to the sliding direction) and normal (the fibres are oriented perpendicularly to the compound's surface). This shows that the coefficient of friction values are different in the running-in phase (0-700 m) and the values become similar in the steady-state phase

while these composites have different mechanical properties. The reason of this phenomenon is that the fibres are present on the wear surface and align in the direction of sliding in the steady-state phase. As a result, the rigid counter surface is mainly in contact with the fibres [19]. The wear processes during sliding contact is investigated using composite 1 with randomly oriented fibres.

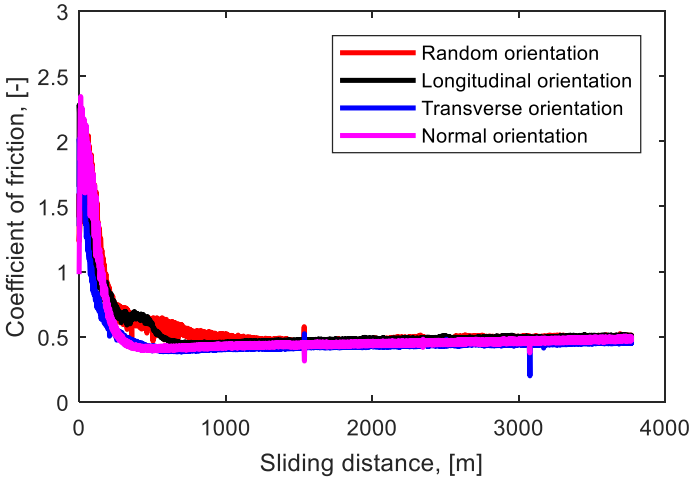

Figure 2. Coefficient of friction as a function of sliding distance of composite 1 for several fibre orientations, adapted from [19].

Figure 3 shows that the coefficient of friction of short-cut aramid fibre reinforced elastomers consists of four stages: (1) the coefficient of friction increases, (2) the coefficient of friction reaches a maximum, (3) the coefficient of friction decreases drastically, and (4) the coefficient of friction reaches a steady-state value. The wear processes of short-cut aramid fibre reinforced elastomer at every stage is studied by using a Keyence VHX-5000 Microscope.

Figure 4 shows the wear track images of composite 1 during sliding friction. At the first stage of the coefficient of friction curve, initiation of cracks occurs in the elastomer matrix because of its poor mechanical properties, see Figure 4a. Because of wear, the contact area between the composite and the counter surface increases. Therefore, the coefficient of friction increases in this stage, see Figure 3.

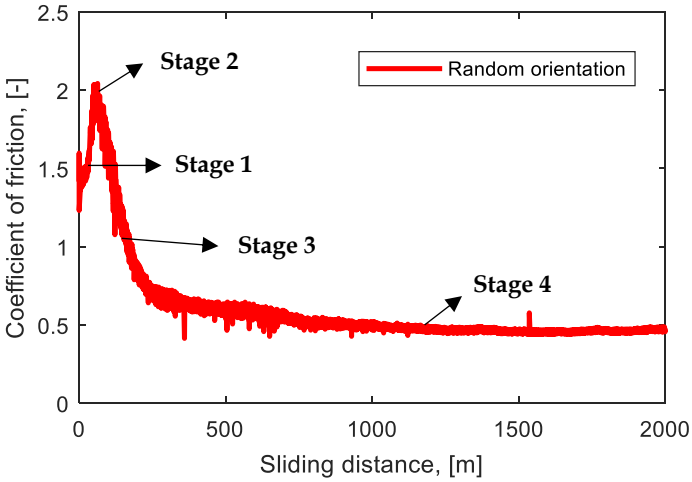

Figure 3. The coefficient of friction as a function of sliding distance of composite 1 with randomly oriented fibres, a velocity of 0.2 m/s and a contact pressure of 0.2 MPa.

At the second stage of the coefficient of friction curve, the coefficient of friction reaches a maximum value. The wear mechanism in this stage is depicted in Figure 4b. Some elastomer matrix pull out from the composite and exist on the surface. When many elastomer particles are pulled out from the matrix, a certain part of the fibres stick out from the composite, see Figure 4c. They are present on the wear surface and align in the direction of sliding. The existence of fibres on the wear surface will result in the increasing surface roughness which leads to the reduction of the real contact area between the elastomer and the counter surface. Hence, the coefficient of friction decreases approximately 4 times lower than that of the maximum value, see the third stage in Figure 3.

Due to the repeated sliding contact, the processes of initiation and propagation of cracks occur continuously. After a certain sliding distance, many fibres cover the wear surface, see Figure 4d. They orient in the direction of sliding and prevent the composite from the initiation and the propagation of cracks. As a result, wear of the composite is reduced. Since the counter surface is mainly in contact with the fibres, the coefficient of friction is controlled by the fibres and reaches a steady-state value. The specific wear pattern is not visible. This is due to the presence of fibers on the wear surface. It is consistent with the previous research that the specific wear pattern does not develop for the fibre reinforced elastomeric composites [15].

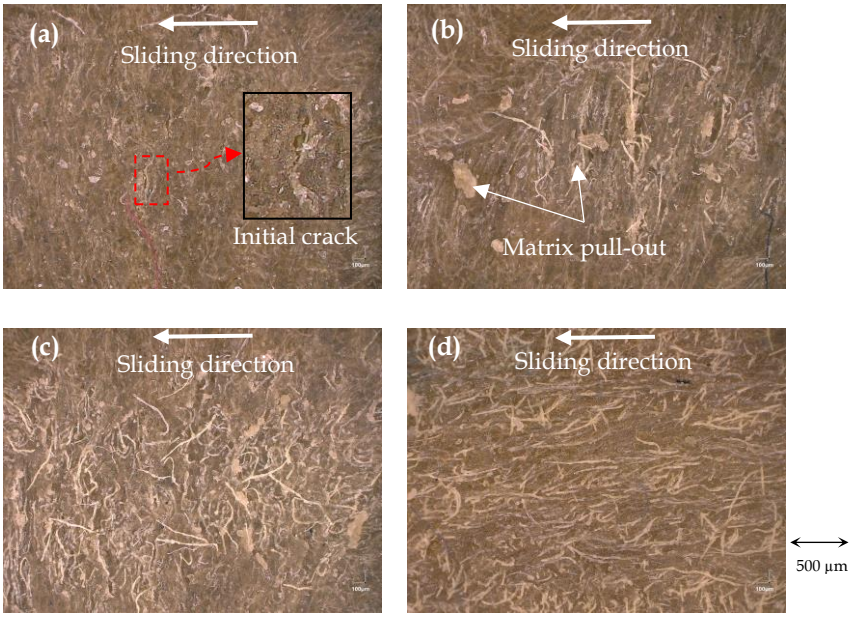

Figure 4. Wear processes of short-cut aramid fibre reinforced elastomers: a) the first stage; b) the second stage; c) the third stage; and d) the fourth stage of the coefficient of friction curve (see Figure 3).

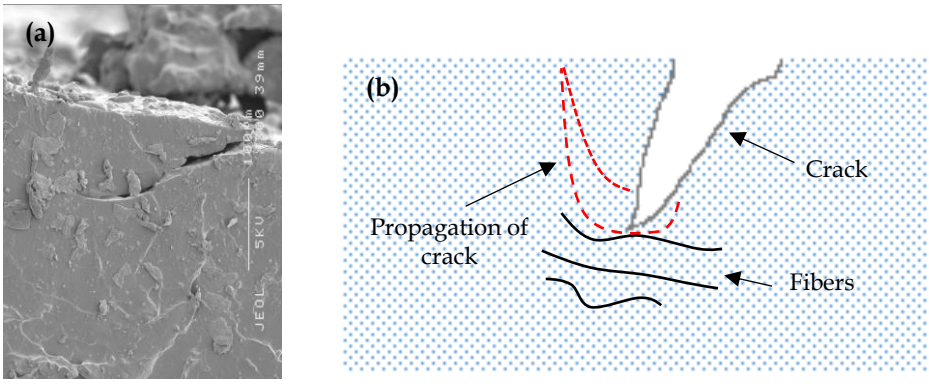

Figure 5. (a) Crack of an unreinforced elastomer, cross-section view of the wear track, (b) Crack is stopped by fibres and it bends to the elastomer surface, shown schematically.

Studying how to minimize the wear of elastomers is of importance because it will increase the lifetime of the components made of an elastomer. Basically, the

wear of elastomer can be minimized if the crack mean free path is reduced [23]. Figure 5a shows the crack propagated of unreinforced elastomer from the cross-section view of the wear track. The wear of the composite can be minimized if this crack is avoided or stopped. Adding fibres is a way to stop this crack. Instead of penetrating further into the composite, the crack will be stopped and it bends to the composite surface when the crack reaches these fibres, see Figure 5b.

Based on the experimental results, the wear processes of short-cut aramid fibre reinforced elastomers can be explained by Figure 6. In the initial part of the sliding distance, cracks are formed in the elastomer matrix because its mechanical properties are worse than those of the fibre. The cracks are initiated at the trailing edge of the contact because the strain is concentrated at that area [3], see Figure 6a.

The propagation of crack occurs in the direction of sliding. When the crack reaches the fibre, it will be stopped and it bends to the elastomer surface, instead of penetrating further into the composite, see Figure 6b. Due to the repeated sliding contact, a part of the elastomer matrix will be pulled out from the composite, see Figure 6c. Depending on the orientation of the fibres and the fibre-matrix bonds, some fibres will be pulled out completely or only a part of the fibres which stick out from the composite will be present on the wear surface and align in the sliding direction, see Figure 6d.

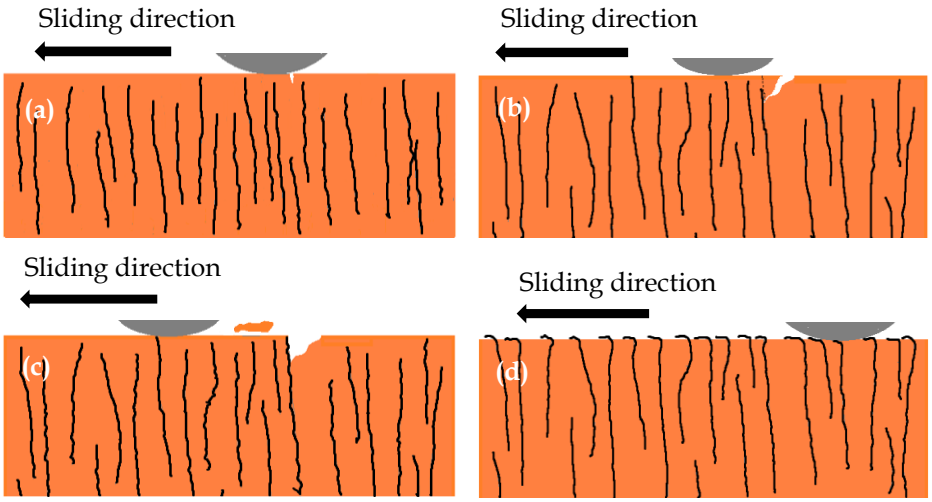

Figure 6. Wear process of short-cut aramid fiber reinforced elastomers, schematically: (a) initiation of the crack in the elastomer matrix; (b) propagation of the crack; (c) the elastomer matrix is pulled-out because the crack bends to the elastomer surface; (d) the part of the fibers that protrude above the surface bend and align in the direction of sliding.

Persson [23] suggested that there are three possible wear mechanisms that may occur between an elastomer and a counter surface: (1) elastomer wear resulting from the formation and propagation of cracks, (2) elastomer wear due to a very sharp counter surface and (3) elastomer surface modifications in the wear surface that will reduce the wear rate by protecting the underlying elastomer. For the short-cut aramid fibre reinforced elastomers, mechanism 1 occurs at the beginning of the test, in which the cracks occur in the elastomer matrix due to cyclic loading. After a certain sliding distance, a part of the fibres will be present on the wear surface, thereby reducing the wear. This process corresponds to the third mechanism of wear, in which the modification of the surface is developed. Therefore, the wear processes of a short-cut aramid fibre reinforced elastomer appear to be a combination of mechanisms 1 and 3.

3.3. Friction and wear mechanism of silica and short-cut aramid fiber reinforced elastomers

Adding silica into a short-cut aramid fibre reinforced elastomers increases the mechanical properties of the composite drastically, see Figure 1. It may also change the tribological behaviour of the composite. Figure 7 shows the tribometer results of composite 2 with two sets of operating conditions, i.e. low energy input and high energy input. The results show that at low energy input the coefficient of friction increases at the beginning of the test. After a certain sliding distance, the coefficient of friction shows a constant value once a maximum coefficient of friction has been reached. Regarding the stage of the coefficient of friction curve in Figure 3, the result of low energy input indicated that only the second stage is reached. The decreasing coefficient of friction is not found in this case. For high energy input, the coefficient of friction increases at a short sliding distance (first stage). Then it reaches a maximum coefficient of friction (second stage). After a sliding distance of approximately 1250 m, the coefficient of friction decreases until the end of the test (third stage). For a very long test duration, the coefficient of friction may reach the fourth stage once the rigid counter surface is mainly in contact with the short-cut aramid fibres.

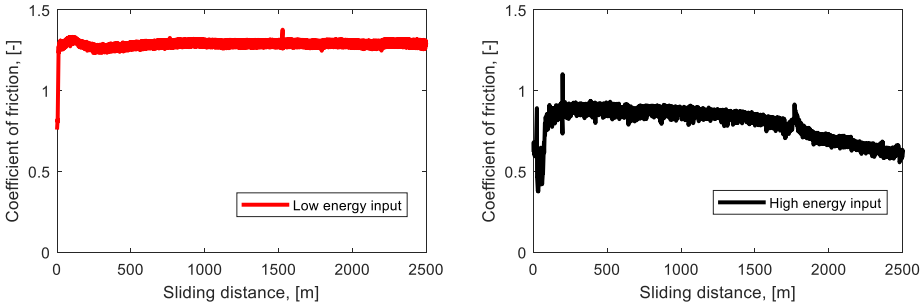

Figure 7. The coefficient of friction as a function of sliding distance of composite 2: (a) low energy input, Pv = 0.16 MPa.m/s; (b) high energy input, Pv = 0.72 MPa.m/s.

The wear surfaces of both composites after the tribometer tests are shown in Figure 8. For the composite at low energy input, a relatively smooth wear track is found on the wear surface, see Figure 8a. The fibres which align parallel to the sliding surface are pulled out. Some grooves on the wear surface are found due to fibre pull-out, while the fibres which are deeply embedded in the matrix show greater resistance to detachment. Only a small part of the fibres which stick out from the matrix are present on the wear surface. Figure 8a corresponds with the wear process of Figure 4b, at which the coefficient of friction reaches a maximum coefficient of friction (second stage).

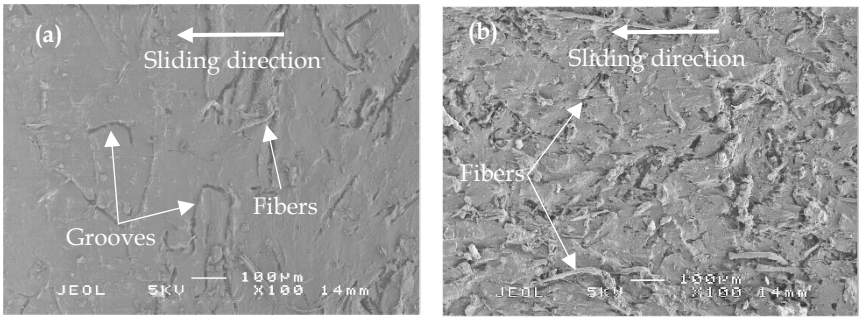

Figure 8. Wear surfaces of elastomers after tests: (a) low energy input; (b) high energy input.

Figure 8b shows the wear surface at high energy input after the test. It can be seen that many fibres exist on the wear surface. Since part of the elastomer matrix is pulled out, fibres which stick out from the elastomer matrix align to the direction

of sliding. A rough surface is found at the high energy input test. Figure 8b corresponds to the wear process in Figure 4c. This wear process causes the coefficient of friction to decrease.

For an elastomer which is reinforced by solely short-cut aramid fibres, the propagation of cracks will be stopped after rather long cracks because the distance between those fibres is relatively far, see Figure 9a. As a result, the composite has a high wear loss. By adding silica to the composite, the cracks can be stopped more effectively. Since the size of silica is very small (in the order of nanometres) and dispersed in the whole elastomer matrix, they will stop the cracks at short length. A previous study reported that by adding filler particles such as carbon black and silica, the wear resistance will increase strongly because the cracks are stopped by filler clusters at a length of a few micrometres [23].

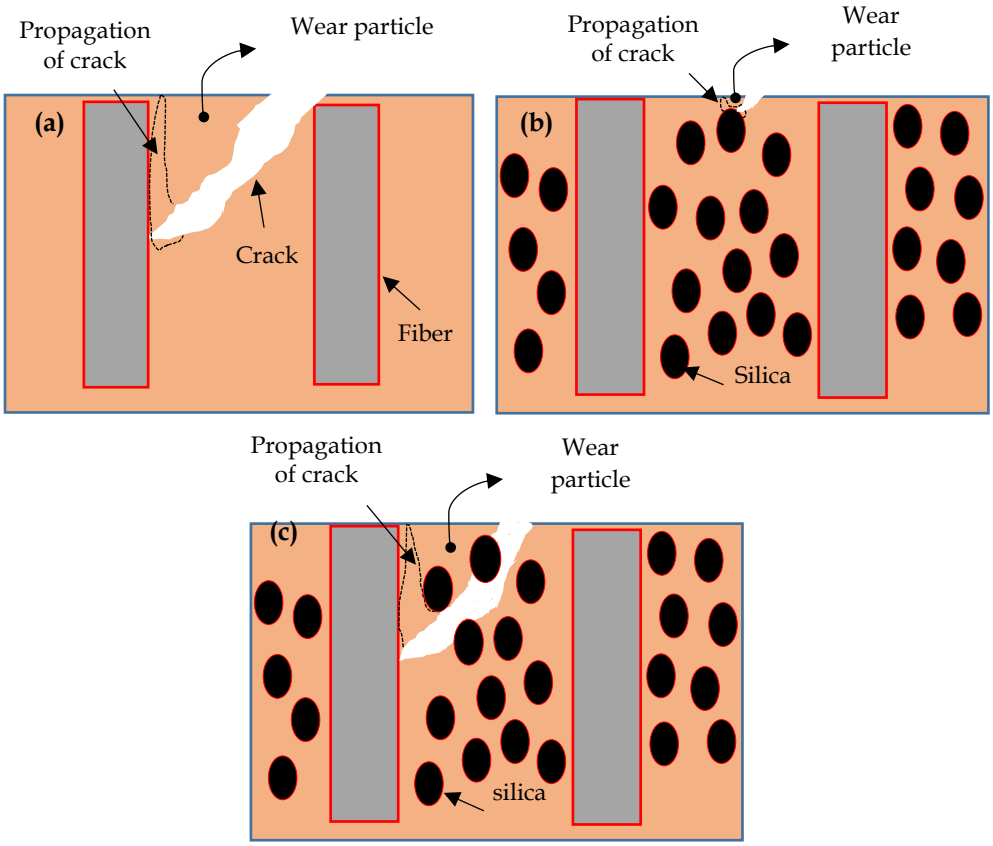

Figure 9. The process of crack propagation: (a) elastomer is reinforced by solely short-cut aramid fibres; (b) elastomer is reinforced by short-cut aramid fibres and silica at low energy input; and (c) high energy input, shown schematically.

There are two possible wear processes which may occur for an elastomer which is reinforced by short-cut aramid fibres and silica: (1) when a low energy input is applied, the crack reaches the inhomogeneous particle (silica) at a very short propagation length, see Figure 9b. Therefore, the wear particles of the elastomer matrix are rather small, and the wear track is relatively smooth, see Figure 8a. Since only a few fibres exist on the wear surface, a decreasing coefficient of friction does not occur for this composite. (2) When a high energy input is used, the silica-matrix bonds will be broken, then the propagation of cracks extends to reach the fibre. It leads to irregularities of wear, so the wear surface becomes rough. Since several fibres are sticking out from the composite and exist on the wear surface, the coefficient of friction reduces, as found in the third stage of the friction curve in Figure 3. The presence of fibres in the composite increases the wear resistance because it is more difficult to pull out the fibre than the the silica. The decreasing coefficient of friction is caused by the reduction of the real contact area between the composite and the counter surface.

A high concentration of silica and fibre leads to reduction of the distance between these fillers in the composite. It will increase the wear resistance because the crack is reduced to a short length. However, too high a concentration of silica and/or fibre will lead to agglomeration of filler networks and will reduce the bond between the filler surface and elastomer matrix. As a result, the filler-matrix bond may be easily broken by propagation of cracks, hence the wear increases. A strong bond between the matrix and fillers also increases the wear resistance of the composite.

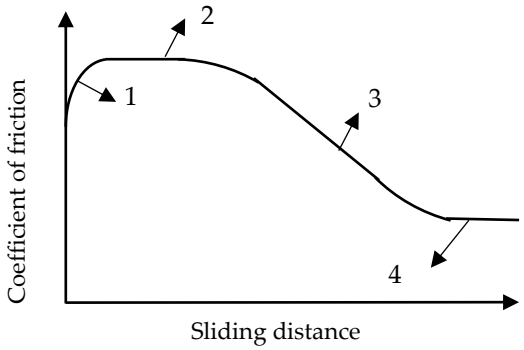

Figure 10. General friction behaviour of short-cut aramid fibre (and silica) reinforced elastomers, shown schematically.

Based on the experimental results, a general friction behaviour of short-cut aramid fibre and silica reinforced elastomers is proposed, see Figure 10. The coefficient of friction consists of four stages:

1. At the initial part of sliding distance, the contact area increases due to wear. As a result, the coefficient of friction increases.
2. The coefficient of friction reaches a maximum value. When the wear loss is low, and only a few fibere exist on the wear surface, the coefficient of friction will be constant.
3. Once many elastomer matrix pull out from the composite, and fibres exist on the wear surface, the coefficient of friction decreases drastically. This is caused by the reduction of the real contact area between the contacting surfaces.
4. The coefficient of friction reaches a steady-state value when many fibres cover the wear surface, and the counter surface is in contact mainly with the fibres.

5. Conclusion

Friction and wear mechanisms of short-cut aramid fibre (and silica) reinforced elastomers as a function of sliding distance were studied. The coefficient of friction of short-cut aramid fibre reinforced elastomer comprises four stages. Every stage of the coefficient of friction is influenced by the actual wear process of the composite. The presence of fibres on the wear surface reduces the coefficient of friction drastically. For an elastomer that is reinforced by short-cut aramid fibres and silica, a higher energy input is needed to achieve stages 3 and 4. This is because the presence of silica in the elastomer matrix increases the matrix pull-out resistance. As a result, only a small number of fibres exist on the wear surface. A mechanism of wear process of short-cut aramid fibre and silica reinforced elastomers and its relation to friction behaviour was proposed.

Acknowledgement
This research forms part of the Research Programme of the Dutch Polymer Institute DPI, Project #782.

References

1. Lorenz, B., Y.R. Oh, S.K. Nam, S.H. Jeon, and B.N.J. Persson, *Rubber friction on road surfaces: Experiment and theory for low sliding speeds.* The Journal of Chemical Physics, 2015. **142**(19): pp. 194701.
2. Bódai, G. and T.J. Goda, *Friction force measurement at windscreen wiper/glass contact.* Tribology Letters, 2012. **45**(3): pp. 515-523.
3. Schallamach, A., *Friction and abrasion of rubber.* Wear, 1958. **1**(5): pp. 384-417.
4. Gent, A.N., *A hypothetical mechanism for rubber abrasion.* Rubber Chemistry and Technology, 1989. **62**(4): pp. 750-756.

5. Fukahori, Y. and H. Yamazaki, *Mechanism of rubber abrasion. Part I: Abrasion pattern formation in natural rubber vulcanizate.* Wear, 1994. **171**(1): pp. 195-202.
6. Fukahori, Y. and H. Yamazaki, *Mechanism of rubber abrasion. Part 2: General rule in abrasion pattern formation in rubber-like materials.* Wear, 1994. **178**(1-2): pp. 109-116.
7. Fukahori, Y. and H. Yamazaki, *Mechanism of rubber abrasion. Part 3: How is friction linked to fracture in rubber abrasion?* Wear, 1995. **188**(1–2): pp. 19-26.
8. Kashani, M.R. and J. Padovan, *Simulation of surface flaw propagation associated with the mechanical fatigue wear of elastomers.* Rubber Chemistry and Technology, 1998. **71**(2): pp. 214-233.
9. Mokhtari, M., D.J. Schipper, and T.V. Tolpekina, *On the friction of carbon black-and silica-reinforced BR and S-SBR elastomers.* Tribology letters, 2014. **54**(3): pp. 297-308.
10. Le Gal, A., X. Yang, and M. Klüppel, *Evaluation of sliding friction and contact mechanics of elastomers based on dynamic-mechanical analysis.* Journal of Chemical Physics, 2005. **123**(1).
11. Busse, L., A. Le Gal, and M. Klüppel, *Modelling of dry and wet friction of silica filled elastomers on self-affine road surfaces*, in *Lecture Notes in Applied and Computational Mechanics*. 2010. pp. 1-26.
12. Goettler, L. and K. Shen, *Short fiber reinforced elastomers.* Rubber Chemistry and Technology, 1983. **56**(3): pp. 619-638.
13. Wang, X., J. Zhang, H. Zhang, and L. Qin, *Tensile and friction properties of carbon fiber/nitrile rubber composites: influence of carbon fiber content and orientation.* Gaofenzi Cailiao Kexue Yu Gongcheng/Polymeric Materials Science and Engineering, 2015. **31**(8): pp. 92-95 and 101.
14. Shojaei, A., M. Arjmand, and A. Saffar, *Studies on the friction and wear characteristics of rubber-based friction materials containing carbon and cellulose fibers.* Journal of Materials Science, 2011. **46**(6): pp. 1890-1901.
15. Wada, N. and Y. Uchiyama, *Friction and wear of short-fibre-reinforced rubber composites under various sliding speeds and loads.* Wear, 1993. **162**: pp. 930-938.
16. Kashani, M.R., *Aramid-short-fiber reinforced rubber as a tire tread composite.* Journal of Applied Polymer Science, 2009. **113**(2): pp. 1355-1363.
17. Datta, R.N., *Reduced hysteresis in truck tread compounds by using aramid short fibers.* Rubber Chemistry and Technology, 2006. **79**(1): pp. 26-38.
18. Rodriguez, N.V., *Contact and friction in systems with fibre reinforced elastomers*, PhD Thesis. Enschede, The Netherlands: University of Twente. 2012.
19. Khafidh, M., D.J. Schipper, M.A. Masen, N. Vleugels, and J.W.M. Noordermeer, *Tribological behavior of short-cut aramid fiber reinforced SBR elastomers: the effect of fiber orientation.* Journal of Mechanical Engineering and Sciences, 2018. **12**(2): pp. 3700-3711.

20. Vleugels, N., *Short fibre-reinforced elastomeric composites, fundamental routes towards improvement of the interfacial interaction of short-cut aramid fibres in a SBR compound, to improve friction and wear properties*, PhD Thesis. Enschede, The Netherlands: University of Twente. 2017.
21. Rauline, R., *(to Compagnie Generale des Establissements Michelin) EU 0501227*. 1992.
22. Hintze, C., R. Boldt, S. Wiessner, and G. Heinrich, *Influence of processing on morphology in short aramid fiber reinforced elastomer compounds.* Journal of Applied Polymer Science, 2013. **130**(3): pp. 1682-1690.
23. Persson, B.N.J., *Theory of powdery rubber wear.* Journal of Physics: Condensed Matter, 2009. **21**(48): pp. 485001.

PAPER D

The Validity of Amontons' Law for Short-cut Aramid Fibre Reinforced Elastomers: The Effect of Epoxy Coated Fibres

M. Khafidh[1,2*], D.J. Schipper [1], M.A. Masen[3], N. Vleugels[1,2], W.K. Dierkes[1], J.W.M. Noordermeer[1]

[1] Faculty of Engineering Technology, University of Twente, P.O. Box 217, 7500AE, Enschede, The Netherlands.
[2] Dutch Polymer Institute DPI, P.O. Box 902, 5600AX Eindhoven, The Netherlands.
[3] Department of Mechanical Engineering, Imperial College London, Exhibition Road, London, SW7 2AZ, United Kingdom.
[*] Email: m.khafidh@utwente.nl.

Abstract
Friction between two contacting surfaces is studied extensively. One of the known friction theories is Amontons' law which states that the friction force is proportional to the normal force. However, Amontons' law has been found to be invalid for elastomers. In the present study, the validity of Amontons' law for short-cut aramid fibre reinforced elastomers is studied. Two types of fillers are used to reinforce the elastomers, namely highly dispersible silica and short-cut aramid fibres. Short-cut aramid fibres with two different surface treatments are used, namely non-reactive fibres with standard oily finish (NF-fibres) and fibres treated with an epoxy coating (EF-fibres). A pin-on-disc tribometer is used to investigate the frictional behaviour of the composites in sliding contact with a granite counter surface. The results show that Amontons' law is valid for those composites that are reinforced by short-cut aramid fibres (without reinforcing filler, i.e. silica) if the contact pressure is below a threshold value. However, once the contact pressure exceeds this threshold value, Amontons' law will be invalid. The threshold contact pressure of the composites containing EF-fibres is higher than that of the composites containing NF-fibres. The composites that are reinforced by silica and short-cut aramid fibres do not follow Amontons' law. The surface roughness of the wear track seems to be a key factor that influences the validity of Amontons' law.

Keywords: Amontons' law, elastomer, epoxy coated fibre, short-cut aramid fibre.

1. Introduction

The sliding friction between two contacting materials has been extensively studied for many centuries. Amontons' law from the late 1600s states that the friction force,

F_f, is proportional to the normal force, F_N [1]. The ratio of friction force and normal force is called coefficient of friction, μ. According to Amontons' law, the coefficient of friction does not depend on the normal force. It is also independent of the apparent (macroscopic) contact area and the relative velocity between the two contacting materials.

There are several explanations for Amontons' law, one of the explanations is the linear dependence of the frictional shear stress on the normal force. However, this explanation is invalid when surface roughness occurs on many different length scales [2]. Another explanation for Amontons' law is the proportionality of the contact area and the normal force, while the frictional shear stress is assumed to be independent of the normal force. Tabor and Bowden [3] suggested that, in many cases, only a small fraction of the surfaces are actually in contact with the contacting material because of the surface roughness. This surface roughness is assumed to be the other explanation for Amontons' law [3-5]. Amontons' law was found to be invalid under several conditions, such as the absence of multiple real contact points, the presence of strong adhesion, under nonlinear dependence of the real contact area with normal force, under conditions of surface detachment, and in response to a change in surface conditions [6]. Later, an analytical model to predict the dependence of coefficient of friction on normal force has also been studied [7].

Elastomers are used in many common applications, such as tyres and conveyor belts. However, a single elastomeric material usually cannot deliver all the required properties that are needed in the aforementioned applications. Adding fibres into an elastomer is one way to improve the mechanical and tribological properties of the composite. For an elastomeric material in contact with a counter surface, Amontons' law is known to be invalid [8]. Instead of following Amontons' law, the coefficient of friction of elastomeric materials depends on the contact pressure, sliding velocity, temperature and lubrication regime [9]. Although Amontons' law has been investigated by many researchers, the mechanisms behind and validity of Amontons' law are still being discussed [2, 10, 11].

In the present study, the validity of Amontons' law for short-cut aramid fibre reinforced elastomers is investigated. Four types of composite materials that are reinforced by silica and short-cut aramid fibres are used. Two types of short-cut aramid fibres with different surface treatments are used in the present study. The wear surface and the wear particles of the composites are studied to investigate the validity of Amontons' law for short-cut aramid fibre reinforced elastomers.

2. Materials and methods

Four types of elastomers based on a styrene butadiene rubber (SBR) and a butadiene rubber (BR) were prepared in the present study. The elastomers were reinforced by two types of reinforcing systems: highly dispersible silica and short-cut aramid

fibres. Two types of poly-p-phenylene-terephtalamide (aramid) fibres were provided by Teijin Aramid B.V., Arnhem, The Netherlands: non-reactive short-cut aramid fibres with standard oily finish (NF-fibres) and short-cut aramid fibres treated with an epoxy coating (EF-fibres). The initial length of the short-cut aramid fibres was approximately 3 mm with a diameter of 10-12 μm.

The interfacial strength between a short-cut aramid fibre and an elastomer matrix can be influenced by two elements: an adhesive coating and a coupling agent that can interact with this coating. In the present study, an epoxy coating on the fibre surface was used, which has the ability to chemically react with a coupling agent. Silane coupling agents S-3-(triethoxysilylpropyl)-octanethioate (NXT) and *bis*-(tri-ethoxy-silyl propyl) tetrasulfide (TESPT) were used to improve the interfacial interaction between the fibres and matrix. Details of the formulation in parts per hundred rubber (phr) are given in Table 1. The formulation of composites 1 and 2 is an optimized formulation of a previous study [12], while the formulation of composites 3 and 4 is based on a silica-reinforced passenger car tyre tread, branded the 'Green Tyre' [13].

Table 1. Material formulation of the composites.

Ingredients	Composite's ID				Supplier
	1 [in phr	2 [in phr]	3 [in phr]	4 [in phr]	
SBR, Buna VSL VP PBR 4045 HM	100	100	-	-	Arlanxeo, Leverkusen, Germany
SBR, Buna VSL 5025-2 HM	-	-	97.3*	97.3*	Arlanxeo, Leverkusen, Germany
BR, KBR 01	-	-	30.0	30.0	Kumho, Seoul, S-Korea
Silica Ultrasil VN3	-	-	80.0	80.0	Evonik Industries AG, Essen, Germany
Zinc oxide (ZnO)	2.5	2.5	2.5	2.5	Sigma Aldrich, St. Louis, United States
Stearic acid (SA)	1.5	1.5	2.5	2.5	Sigma Aldrich, St. Louis, United States
TDAE oil	-	-	6.7	6.7	Hansen & Rosenthal, Hamburg, Germany
Twaron aramid fibre	15 NF	15 EF	20 NF	20 EF	Teijin Aramid B.V, Arnhem, The Netherlands
TESPT	-	-	7.0	7.0	Evonik Industries AG, Essen, Germany

NXT	6.0	6.0	-	-	Momentive, New York, United States
6PPD stabilizer	-	-	2.0	2.0	Flexsys, Brussels, Belgium
TMQ stabilizer	-	-	2.0	2.0	Flexsys, Brussels, Belgium
Sulfur	2.8	2.8	1.4	1.4	Sigma Aldrich, St. Louis, United States
N-Cyclohexyl Benzothiazole Sulfenamide (CBS)	3.4	3.4	1.7	1.7	Flexsys, Brussels, Belgium
Di-Phenyl Guanidine (DPG)	4	4	2.0	2.0	Flexsys, Brussels, Belgium
Orientation relative to the sliding contact	Random, longitudinal, transverse, normal		Random		

* Containing 37.5 wt% oil.

To investigate the effect of fibre orientation of the composites containing NF-fibres and EF-fibres, four types of reinforcement directions were prepared for composites 1 and 2, namely randomly oriented, longitudinally oriented (meaning that the fibres are aligned in the sliding direction), transversely oriented (meaning that the fibres are aligned perpendicularly to the sliding direction) and normally oriented (meaning that the fibres are aligned perpendicularly to the composite's contact surface). The fibres of composites 3 and 4 are oriented in random direction.

When the fibres are aligned in random direction, the composite can be assumed to be an isotropic material. This means that the mechanical properties of the composite are the same in all directions. When the fibres are aligned in a certain direction, the mechanical properties are different in each direction, so the composite has an anisotropic behaviour. Fibres in the composite are oriented during the production of the composite by using a two-roll mill. Composites with thickness of 2 mm and 5 mm were prepared for tensile and tribometer tests, respectively.

A pin-on-disc tribometer was used for measuring the friction force of the composites. A rigid ball with a diameter of 35 mm was used as a counter surface. The tests were stopped once the coefficient of friction reached a steady-state value. Three types of investigations were performed in the present study: (1) the effect of contact pressure on the frictional behaviour; (2) the effect of epoxy coated fibres on

the friction behaviour; and (3) the breakdown of Amontons' law when applied to the short-cut aramid fibres reinforced elastomers.

A velocity of 0.2 m/s was used for all tribometer tests. The effect of contact pressure was investigated by using two types of reinforcement system: (1) short-cut aramid fibre reinforced elastomers; and (2) silica and short-cut aramid fibre reinforced elastomers. The composites used for this investigation were composites 1 and 3. Two contact pressures were used for every composite, namely 0.15 MPa and 0.20 MPa for composite 1 and 0.68 MPa and 0.80 MPa for composite 3. The effect of epoxy coated fibres was evaluated by comparing those composites that are reinforced by EF-fibres and NF-fibres for both formulations. A contact pressure of 0.2 MPa was used to compare the friction behaviour between composites 1 and 2, while the comparison between composites 3 and 4 was conducted using a contact pressure of 0.68 MPa. Based on the results of those investigations, the breakdown of Amontons' law was investigated by further varying the contact pressure. The normal load was adapted, depending on the reinforcement direction of the fibres based on the anisotropic-viscoealastic contact model [14].

A Keyence VHX-5000 microscope and a Jeol JSM 6400 Scanning Electron Microscope (SEM) were used to scan images of the wear surfaces and the wear particles. Tensile measurements were performed with an Instron tensile tester 3343 series, according to ISO 37 at a crosshead speed of 500 mm/min.

3. Results

3.1 Mechanical properties of the materials

One of the important factors that influences the mechanical properties of short-cut aramid fibre reinforced elastomers is the interfacial interaction between the fibres and the elastomer matrix. An epoxy coating on the fibre surface, in combination with a silane coupling agent, may improve that interaction. The stress-strain relations of composites 1 to 4 with randomly oriented fibres are shown in Figure 1. The lack of silica as reinforcing filler in the composite leads to a large reduction in the failure point of the tensile stress-strain test. A yield point is observed for the composites containing silica and short-cut aramid fibres (composites 3 and 4) at a strain of approximately 30%. At the strain below the yield, the composites containing silica and short-cut aramid fibres show a steeper curve than those composites containing solely short-cut aramid fibres. Moreover, a steeper curve is found for the composites containing EF-fibres than for those containing NF-fibres. It confirms that an epoxy coating on the fibre surfaces in combination with a coupling agent is effective in improving the mechanical properties of the composites.

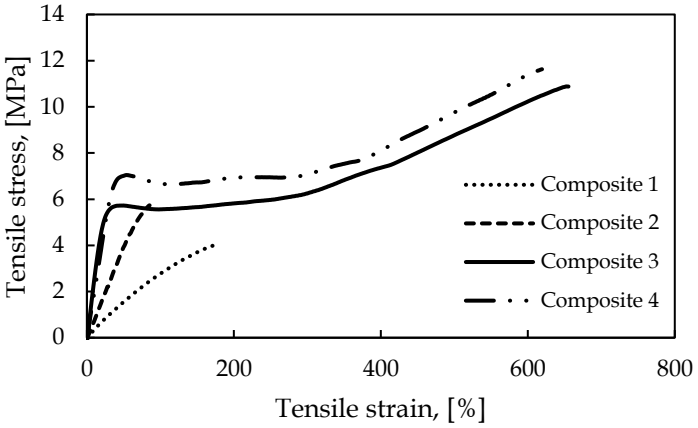

Figure 1. Stress-strain relations of all composites with randomly oriented fibres.

Figure 2 shows the stress-strain relations of composites 1 and 2 for several reinforcement directions. As expected, the composite reinforced in the *z*-direction (the fibres are aligned longitudinally to the applied force) has the steepest curve whereas the composite reinforced in the *x*-direction (the fibres are aligned perpendicularly to the applied force) shows the shallowest curve, while the composite with randomly oriented fibres shows an intermediate slope. The composites containing EF-fibres have a steeper curve than that for the composites containing NF-fibres for all reinforcement directions. The elastic moduli were defined at a strain of 2%, assuming the material behaves linearly below that strain value [15].

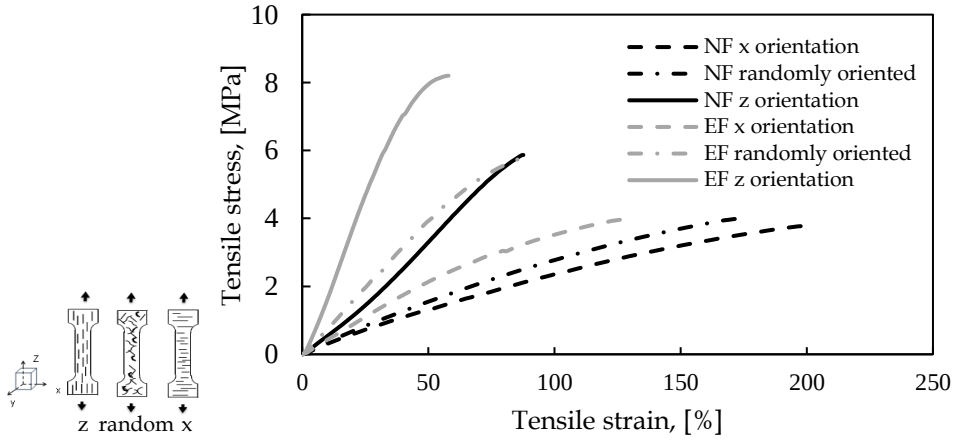

Figure 2. Stress-strain relations of composites 1 and 2 for several reinforcement directions.

3.2 *The effect of contact pressure*

As mentioned previously, the coefficient of friction of rubber-like materials depends on the contact pressure. Figure 3a shows the coefficient of friction as a function of sliding distance for composite 1 at two different contact pressures. It can be seen that the steady-state coefficient of friction of those composites decreases to approximately four times lower than that at the beginning of the tests. This is because a certain part of the fibres are sticking out of the composite while remaining present on the wear surface [16]. This leads to a reduction of the real contact area between the counter surface and the composite. Although the coefficients of friction are different at the beginning of the tests, the steady-state coefficients of friction values are the same for both contact pressures. This confirms that composite 1 follows Amontons' law.

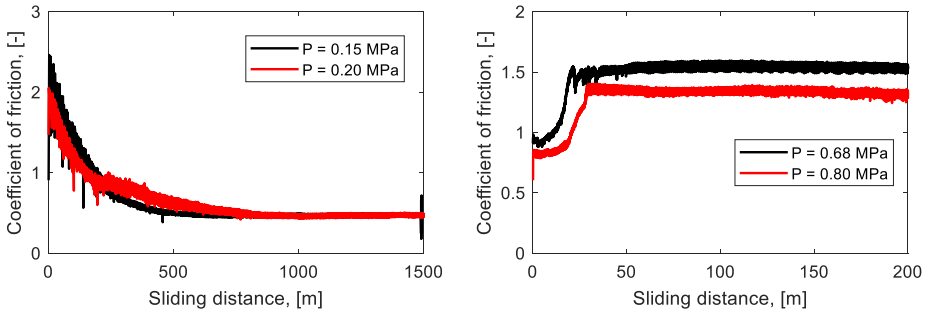

(a) (b)

Figure 3. Coefficient of friction as a function of sliding distance for different contact pressures: (a) composite 1; and (b) composite 3. All composites have randomly oriented fibres.

Figure 3b shows the coefficient of friction as a function of sliding velocity for composite 3 at two different contact pressures, namely 0.68 MPa and 0.80 MPa. A higher contact pressure results in a lower coefficient of friction, meaning that Amontons' law is invalid for composite 3. The decreasing coefficient of friction as seen in Figure 3a does not feature in these tests. Moreover, the coefficient of friction reaches a steady-state signal at a short sliding distance of ~ 30 m.

The wear surfaces of the composites after the tribometer tests are shown in Figure 4. The wear surfaces of composite 1 at both contact pressures have the same characteristic, in which many fibres exist on the wear surface and align in the direction of sliding, see Figure 4a. In a previous study [16], it was shown that the coefficient of friction of elastomers that are reinforced with a high amount of short-cut aramid fibres is controlled by the fibres on the wear surface rather than by the bulk properties. Since the counter surface is in contact mainly with the fibres, the

steady-state coefficients of friction of composite 1 at both contact pressures have a uniform value.

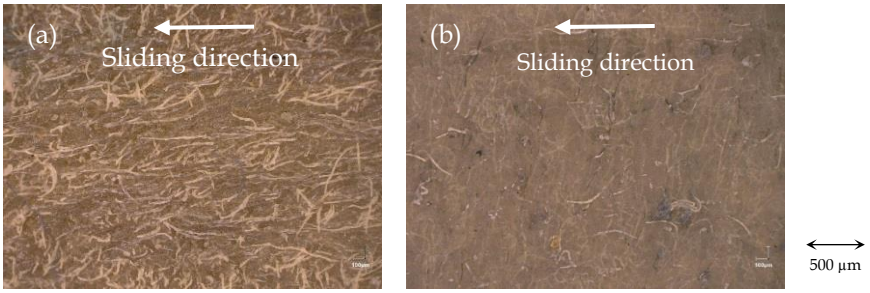

Figure 4. Wear surfaces after tribometer tests: (a) composite 1 at a contact pressure of 0.2 MPa; (b) composite 3 at a contact pressure of 0.80 MPa.

The wear surface of composite 3 at a contact pressure of 0.80 MPa has the same characteristic as that at a contact pressure of 0.68 Mpa, where only a few fibres are observed on the wear surface. Figure 4b shows the wear surface of composite 3 at a contact pressure of 0.80 MPa. Since only a few fibres are present on the wear surface, the counter surface is in contact mainly with the bulk material. Hence, the coefficient of friction is influenced predominantly by the bulk properties of the composite.

3.3 The effect of epoxy coating

Interfacial interaction between the short-cut aramid fibre and the elastomer matrix plays an important role in reinforcing the composite and controls the mechanical properties. Therefore, an investigation into the effects of surface treatment on the fibre surface is important in improving the mechanical properties and also the tribological behaviour of the composites. Figures 1 and 2 show that by adding EF-fibres to the composite leads to an improvement of the mechanical properties in comparison with those composites containing NF-fibres.

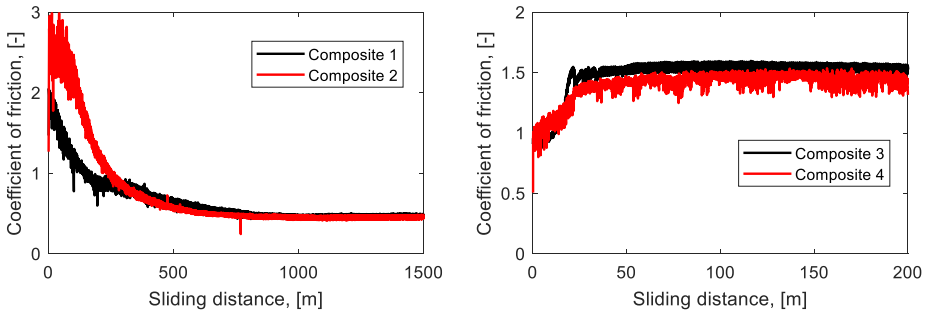

Figure 5. Coefficient of friction as a function of sliding distance for: (a) composite 1 vs. composite 2 at a contact pressure of 0.2 MPa; (b) composite 3 vs. composite 4 at a contact pressure of 0.68 MPa. All composites have randomly oriented fibres.

The coefficient of friction as a function of sliding distance for composites 1 and 2 in random orientation at a contact pressure of 0.2 MPa are shown in Figure 5a. It can be seen that after a sliding distance of approximately 800 m, the coefficients of friction reach the same steady-state values, namely ~ 0.5. Figure 5b shows the coefficient of friction as a function of sliding distance for composites 3 and 4 in random orientation at a contact pressure of 0.68 MPa. The coefficients of friction reach a steady-state phase after a short sliding distance, namely ~ 30 m. The composite containing EF-fibres (composite 4) has a slightly lower steady-state coefficient of friction compared to that containing NF-fibres (composite 3). This may be attributed to the fact that the mechanical properties of composite 4 are better than that of composite 3. Therefore, the contact area of composite 4 is smaller than that of composite 3. These results show that the coefficient of friction of the short-cut aramid fibre reinforced elastomer (without silica reinforcement) is independent of the mechanical properties of the composite, while the mechanical properties of silica and short-cut aramid fibre reinforced elastomer influence the coefficient of friction.

The wear surfaces of all composites after tribometer tests are shown in Figure 6. It can be seen that the wear surfaces of composites 1 and 2 are dominated by fibres. However, there are more fibres on the wear surface of composite 1 than of composite 2, see Figures 6a and 6b. This can be an indication that EF-fibre is more effective in minimizing wear loss than NF-fibre. However, the steady-state coefficient of friction value of composites 1 and 2 are the same since the counter surface is in contact mainly with the fibres on the wear surface.

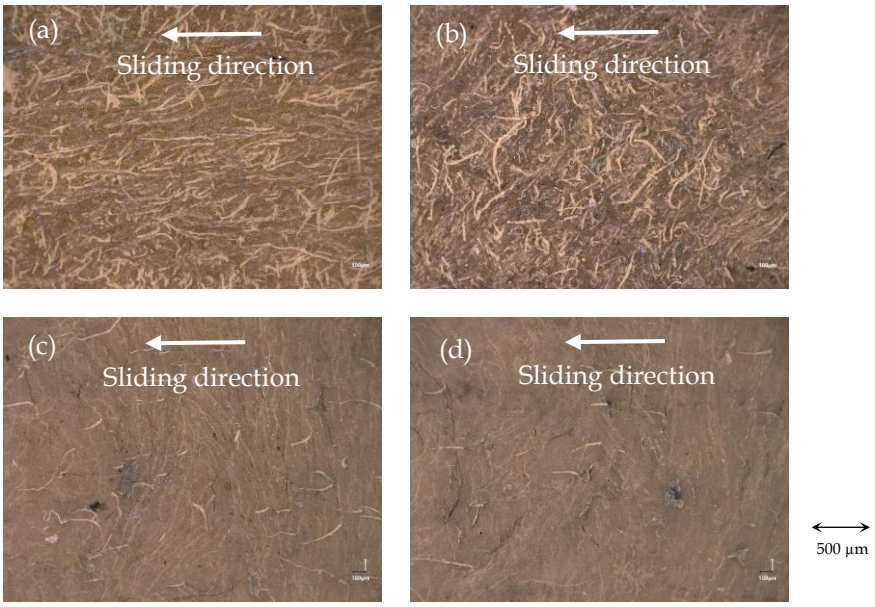

Figure 6. Wear surfaces after tribometer tests: (a) composite 1 at a contact pressure of 0.2 MPa; (b) composite 2 at a contact pressure of 0.2 MPa; (c) composite 3 at a contact pressure of 0.68 MPa; (d) composite 4 at a contact pressure of 0.68 MPa.

Figures 6c and 6d show the wear surfaces of composites 3 and 4, respectively. Although the number of fibres in composites 3 and 4 are higher than in composites 1 and 2, there are far fewer fibres on the wear surface. This suggests that the composites containing silica and short-cut aramid fibres can avoid the elastomer matrix pull-out and fibre detachment effectively. Since the contact occurs mainly between the counter surface and the bulk material, the coefficient of friction depends on the bulk properties of the composite. Hence, the coefficient of friction of the 'stiffer' material (composite 4) is lower than that of the weaker material (composite 3).

3.4 The breakdown of Amontons' law

It was observed that the short-cut aramid fibre reinforced elastomers (without silica reinforcement) in random orientation follow Amontons' law. Figure 7 shows the coefficient of friction as a function of sliding distance for composites 1 and 2 for several reinforcement directions at a contact pressure of 0.2 MPa. It can be seen that the coefficients of friction of all the composites show different values at the beginning of the test. After a certain sliding distance, the coefficients of friction show

the same value, namely ~ 0.5. This suggests that the coefficient of friction is independent of the reinforcement direction.

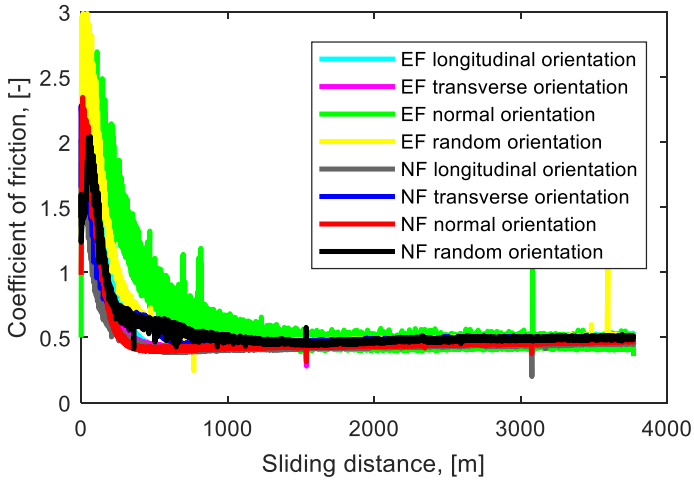

Figure 7. Coefficient of friction as a function of sliding distance for composites 1 and 2 for several reinforcement directions.

The coefficient of friction of short-cut aramid fibre reinforced elastomer (without silica reinforcement) has been observed to be independent of the contact pressure (see Figure 3a), the mechanical properties (see Figure 5a) and the fibre reinforcement direction (see Figure 7). In other words, the short-cut aramid fibre reinforced elastomers follow Amontons' law. However, those composites that are reinforced by silica and short-cut aramid fibres (composites 3 and 4) do not follow Amontons' law. The coefficient of friction of those composites depend on the contact pressure (see Figure 3b) and the mechanical properties of the composite (see Figure 5b).

The investigation of the breakdown of Amontons' law for the short-cut aramid fibre reinforced elastomers was conducted by further varying the contact pressure. Figure 8 shows the coefficient of friction as a function of sliding distance for the EF-fibre reinforced elastomers (composite 2) at various contact pressures. It can be seen that the steady-state coefficient of friction are uniform whether contact pressures of 0.2 MPa, 0.25 MPa or 0.29 MPa are applied, while the steady-state coefficient of friction changes when a contact pressure of 0.4 MPa is applied. Therefore, short-cut aramid fibre reinforced elastomers follow Amontons' law as long as the contact pressure does not exceed a threshold value. Once the contact pressure exceeds that threshold, Amontons' law is not valid anymore.

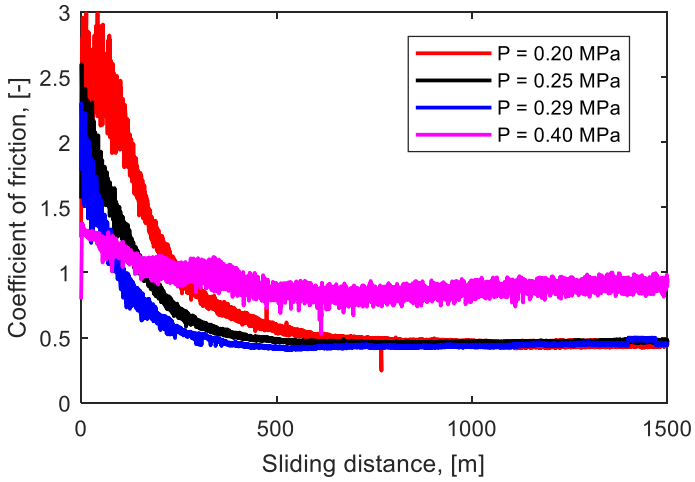

Figure 8. Coefficient of friction as a function of sliding distance for the composite 2 at different contact pressures.

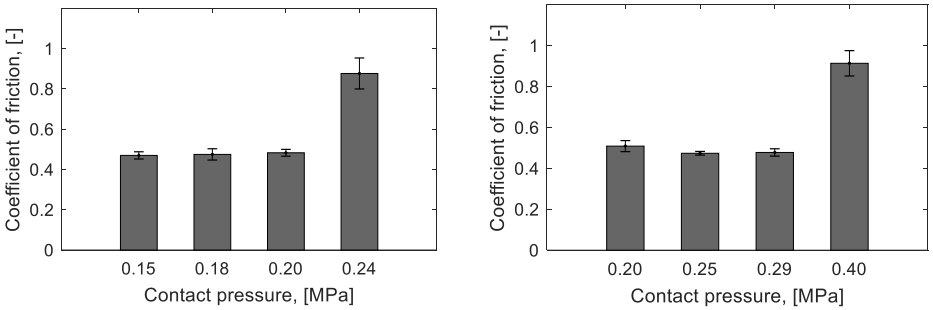

Figure 9. Steady-state coefficient of friction at various contact pressures: (a) composite 1; (b) composite 2.

Similarly, pin-on-disc tribometer tests at various contact pressures were also conducted for the NF-fibre reinforced elastomers (composite 1). Figure 9 shows the coefficient of friction at the steady-state phase for composites 1 and 2. It can be seen that both composites have a threshold contact pressure, at which Amontons' law is not valid when the contact pressure exceeds that threshold. For composite 1, Amontons' law is not valid when a contact pressure of 0.24 MPa is applied, whereas Amontons' law is not valid when a contact pressure of 0.40 MPa is applied to composite 2.

The wear surfaces of the composites at the end of the tribometer tests in which Amontons' law is valid and invalid are shown in Figure 10. When many fibres

are present on the wear surface and align in the direction of sliding, the coefficient of friction follows Amontons' law, see Figure 10a. Once the contact pressure exceeds the threshold, many fibres are pulled out from the composite, and severe wear is found. Hence, fewer fibres are present on the wear surface, see Figure 10b. It was observed that the threshold contact pressure of composite 2 is higher than that of composite 1. This can be explained by the different interfacial interaction between the fibres and elastomer matrix of those composites. The interfacial interaction with an elastomer matrix is better with EF-fibres than with NF-fibres, as shown in the mechanical properties of these composites, see Figures 1 and 2. Therefore, a higher contact pressure is required to pull out many fibres from the composite as shown in Figure 10b.

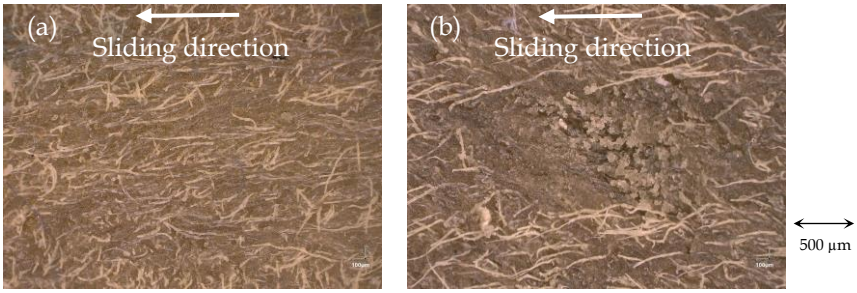

Figure 10. Wear surfaces after tribometer tests: (a) composite 1 when Amontons' law is valid; (b) composite 1 when Amontons' law is not valid.

Studying the wear particles of the composites in cases where Amontons' law is valid or invalid shows no clear difference. The fibres are sticking together with the elastomer matrix, while only a small part of the fibres stay apart from the elastomer matrix, see Figures 11a and 11b. Furthermore, the wear particles of the composites that are reinforced by silica and short-cut aramid fibres are dominated by fibres, while only a small amount of the elastomer matrix is observed in the wear particles, see Figure 11c. By adding silica to the composite, the propagation of cracks will be stopped when it reaches the silica particle [17]. Since the propagation of cracks is stopped at short propagation and it bends to the elastomer surface, only a small amount of the elastomer matrix is pulled out from the composite. Furthermore, the fibres that align parallel to the elastomer surface can easily be pulled out, whereas the fibres which are deeply embedded in the matrix give greater resistance to detachment; only a small part of the fibres which stick out from the matrix are present on the wear surface, see Figure 4b. Many fibres in the wear particles of the silica and short-cut aramid fibre reinforced elastomers are generated by the fibre pull-out from the composite.

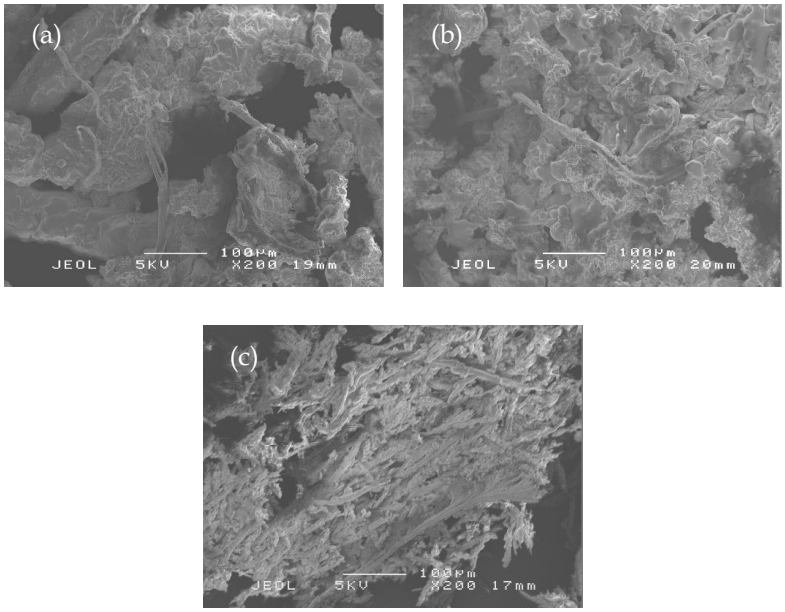

Figure 11. SEM images of wear particles: (a) composite 1 when the Amontons' law is valid; (b) composite 1 when the Amontons' law is invalid; (c) Composite 3 at a contact pressure of 0.80 MPa.

4. Discussion

It was known that Amontons' law is invalid for rubber-like materials [8]. However, Amontons' law was found to be valid for short-cut aramid fibre reinforced elastomers (without silica reinforcement) below a threshold contact pressure. The proportionality between the real contact area and the normal force may be the source of this phenomenon. For plastic materials, plastic flow in the asperity contact region explains the proportionality between the real contact area and the normal force. However, for elastomers the local pressure in the asperity contact regions reaches the rupture stress [2]. Therefore, plastic flow is not the explanation of Amontons' law in the case of short-cut aramid fibre reinforced elastomers without further silica reinforcement.

The proportionality between the real contact area and the normal force of short-cut aramid fibre reinforced elastomers may be caused by the small ratio of the real and the apparent contact area. Persson suggested that the normal force is proportional to the real contact area when the ratio between the real and the apparent contact area is less than 10% [18]. Figure 12 shows the height of wear

surfaces of short-cut aramid fibre reinforced elastomer when Amontons' law is both valid and invalid. It shows that a rough wear surface is found when Amontons' law is valid. However, a relatively smooth surface is found when the Amontons' law is invalid. Amontons' law is generally valid for a multi-contact situation, even in the case of elastomers [7, 19]. However, Amontons' law is not valid for a contact situation of mono-contact because the friction force is usually not proportional to the normal force, for example in the JKR sphere-plane contact [20].

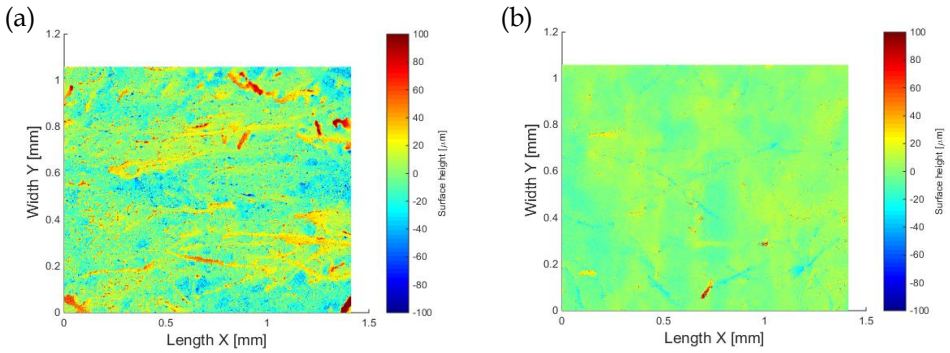

Figure 12. Height of wear surfaces: (a) when Amontons' law is valid; (b) when Amontons' law is invalid (composite 3 at a contact pressure of 0.80 MPa).

It has been observed that Amontons' law is invalid for composites that are reinforced by silica and short-cut aramid fibres. For smooth surfaces and soft materials, the relation between the contact area and the normal force follows the Hertz theory, $A \sim F^{2/3}$ or $\mu \sim F^{-1/3}$. For silica and short-cut aramid fibre reinforced elastomers, the relation is located somewhere in between the Hertz theory ($\mu \sim F^{-1/3}$) and Amonton's theory ($\mu \sim F$). For example, composite 3 has a steady-state coefficient of friction of 1.53 ± 0.04 at a contact pressure of 0.68 MPa (F = 5 N). When a contact pressure of 0.80 MPa (F = 8.2 N) is used, the steady-state coefficient of friction decreases to 1.35 ± 0.05, see Figure 3b. These results show that the coefficient of friction decreases with increasing normal force, but the reduction of the coefficient of friction is lower than predicted by the Hertz theory.

Although the decreasing coefficient of friction phenomenon does not occur in composites that are reinforced by silica and short-cut aramid fibres, this phenomenon may occur when a high energy input (high contact pressure and high velocity) is applied. In that situation, the propagation of cracks can break the silica-matrix bond. As a result, a high amount of elastomer matrix will pull out from the composite, and many fibres are present on the wear surface. The decreasing coefficient of friction is caused by the presence of many fibres on the wear surface.

Therefore, the composites that are reinforced by silica and short-cut aramid fibre may follow Amontons' law when a high enough energy input is applied.

5. Conclusion

The validity of Amontons' law for short-cut aramid fibre reinforced elastomer has been investigated. Two types of fibres were evaluated: NF-fibres and EF-fibres. Amontons' law was found to be valid for the short-cut aramid fibre reinforced elastomer (without silica reinforcement) at contact pressures below a certain threshold value. Once the contact pressures exceed the threshold, Amontons' law is not valid anymore. Amontons' law was found to be invalid for composites that are reinforced by silica and short-cut aramid fibres. The EF-fibre reinforced elastomer has a higher threshold contact pressure than that for NF-fibre reinforced elastomers. This is because the surface interaction of the EF fibre-elastomer matrix is better than that of NF the fibre-elastomer matrix. Therefore, a higher contact pressure is needed to pull out many fibres from the composite containing EF-fibres. The real contact area between the counter surface and the composite is a key factor that influences the validity of Amontons' law for short-cut aramid fibre reinforced elastomer.

Acknowledgement

This research forms part of the Research Programme of the Dutch Polymer Institute DPI, Project #782.

References

1. Popova, E. and V.L. Popov, *The research works of Coulomb and Amontons and generalized laws of friction.* Friction, 2015. **3**(2): pp. 183-190.
2. Persson, B.N.J., I.M. Sivebæk, V.N. Samoilov, K. Zhao, A.I. Volokitin, and Z. Zhang, *On the origin of Amonton's friction law.* Journal of Physics: Condensed Matter, 2008. **20**(39): pp. 395006.
3. Bowden, F.P. and D. Tabor, *The friction and lubrication of solids the friction and lubrication of solids clarendon*. 1950, Oxford.
4. Burton, Z. and B. Bhushan, *Hydrophobicity, adhesion, and friction properties of nanopatterned polymers and scale dependence for micro-and nanoelectromechanical systems.* Nano Letters, 2005. **5**(8): pp. 1607-1613.
5. Baumberger, T. and C. Caroli, *Solid friction from stick–slip down to pinning and aging.* Advances in Physics, 2006. **55**(3-4): pp. 279-348.
6. Otsuki, M. and H. Matsukawa, *Systematic breakdown of Amontons' law of friction for an elastic object locally obeying Amontons' law.* Scientific Reports, 2013. **3**: pp. 1586.

7. Maegawa, S., F. Itoigawa, and T. Nakamura, *Effect of normal load on friction coefficient for sliding contact between rough rubber surface and rigid smooth plane.* Tribology International, 2015. **92**: pp. 335-343.
8. Schallamach, A., *Friction and abrasion of rubber.* Wear, 1958. **1**(5): pp. 384-417.
9. Jiménez, M.A., J.M. Bielsa, R. Rodríguez, and S. Dobón. *The influence of contact pressure on the dynamic friction coefficient in cylindrical rubber-metal contact geometries*. in *IUTAM Symposium on Computational Methods in Contact Mechanics*. 2007. Springer.
10. Gao, J., W.D. Luedtke, D. Gourdon, M. Ruths, J.N. Israelachvili, and U. Landman, *Frictional forces and Amontons' law: from the molecular to the macroscopic scale*. 2004: ACS Publications.
11. Müser, M.H., L. Wenning, and M.O. Robbins, *Simple microscopic theory of Amontons's laws for static friction.* Physical Review Letters, 2001. **86**(7): pp. 1295.
12. Vleugels, N., *Short fibre-reinforced elastomeric composites, fundamental routes towards improvement of the interfacial interaction of short-cut aramid fibres in a SBR compound, to improve friction and wear properties*, PhD Thesis. Enschede, The Netherlands: University of Twente. 2017.
13. Rauline, R., *(to Compagnie Generale des Establissements Michelin) EU 0501227*. 1992.
14. Rodriguez, N., M.A. Masen, and D.J. Schipper, *A contact model for orthotropic-viscoelastic materials.* International Journal of Mechanical Sciences, 2013. **74**: pp. 91-98.
15. Hintze, C., R. Boldt, S. Wiessner, and G. Heinrich, *Influence of processing on morphology in short aramid fibre reinforced elastomer compounds.* Journal of Applied Polymer Science, 2013. **130**(3): pp. 1682-1690.
16. Khafidh, M., D.J. Schipper, M.A. Masen, N. Vleugels, and J.W.M. Noordermeer, *Tribological behavior of short-cut aramid fibre reinforced SBR elastomers: the effect of fibre orientation*. Journal of Mechanical Engineering and Sciences, 2018. **12**(2): pp. 3700-3711.
17. Persson, B.N.J., *Theory of powdery rubber wear.* Journal of Physics: Condensed Matter, 2009. **21**(48): pp. 485001.
18. Persson, B.N.J., *Contact mechanics for randomly rough surfaces.* Surface Science Reports, 2006. **61**(4): pp. 201-227.
19. Ronsin, O. and K.L. Coeyrehourcq, *State, rate and temperature–dependent sliding friction of elastomers.* Proceedings of the Royal Society of London. Series A: Mathematical, Physical and Engineering Sciences, 2001. **457**(2010): pp. 1277-1294.

20. Chateauminois, A. and C. Fretigny, *Local friction at a sliding interface between an elastomer and a rigid spherical probe.* The European Physical Journal E: Soft Matter and Biological Physics, 2008. **27**(2): pp. 221-227.